

Behaviour of Precast Prestressed Hollow Core Slabs with and without FRP Strengthening

J. Suman Dhara

A Thesis Submitted to
Indian Institute of Technology Hyderabad
In Partial Fulfillment of the Requirements for
The Degree of Master of Technology

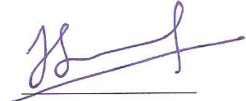


Department of Civil Engineering

June 2015

Declaration

I declare that this written submission represents my ideas in my own words, and where ideas or words of others have been included, I have adequately cited and referenced the original sources. I also declare that I have adhered to all principles of academic honesty and integrity and have not misrepresented or fabricated or falsified any idea/data/fact/source in my submission. I understand that any violation of the above will be a cause for disciplinary action by the Institute and can also evoke penal action from the sources that have thus not been properly cited, or from whom proper permission has not been taken when needed.



(Signature)

J. Suman Dhara


(J. Suman Dhara)

CE13M1006

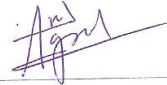
(Roll No.)

Approval Sheet

This Thesis entitled Behaviour of Precast Prestressed Hollow Core Slabs with and without FRP Strengthening by J. Suman Dhara is approved for the degree of Master of Technology from IIT Hyderabad



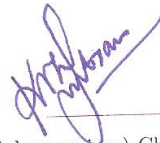
(Dr. Viswanath Chinthapenta) Examiner
Dept. of Mechanical and Aerospace Engineering
IITH



(Dr. Anil Agarwal) Examiner
Dept. of Civil Engineering
IITH



(Dr. Suriya Prakash) Adviser
Dept. of Civil Eng
IITH



(Prof. K.V.L. Subramaniam) Chairman
Dept. of Civil Engineering
IITH

Acknowledgements

I would like to express my gratitude to all those who helped me to finish this research project. First and foremost I would like to thank God, the almighty, for giving me strength and courage to do research. I would like to express my deepest thanks to my parents and siblings for their love, endless support and lively encouragement. I express my sincere gratitude to my supervisor Dr. Suriya Prakash for his inspiration, valuable guidance, timely suggestions and constant encouragement during each and every phase of this work. Finally, I would like to thank all my friends and colleagues Sammer, Pradeep, Samukham surya, Santosh, Raj, Shashi, Vijayan, Tarutal, Rasheed & many more for supporting me to make this project a great success.

Abstract

Hollow core slabs are Prestressed precast floor/roof elements which have longitudinal cores running along the span and are primarily used floor slab elements in building construction. Structural efficiency and increased flexural capacity of prestressed precast hollow core (PPHC) slabs allows larger spans to be built leading to cost savings. Strengthening of these slabs may be required for several reasons to maintain their structural integrity. The main reasons include, material degradation, increased dead or live loads, architectural modifications, installation of heavy machinery and openings in slabs.

The objectives of this research project is to understand the flexure and flexural- shear behaviour, failure mechanisms of PPHCS with and without Fiber-Reinforced Polymers (FRP) strengthening. The use of FRPs as externally bonded (EB) and near surface mounted (NSM) reinforcement for strengthening of precast prestressed hollow core slabs is evaluated experimentally.

FRP reinforcement used in this investigation include glass fiber-reinforced polymer reinforcing bars and strips. The behavior and effectiveness of FRP used for the various strengthening configurations are examined. The structural performance and modes of failure of the tested beams are presented and discussed. Experimental variables include different FRP strengthening ratios, prestressing ratio, and shear span to depth (a/d) ratio. Test results shows increase in the flexural capacity due to GFRP strengthening. Test results also revealed that the FRP strengthening ratio plays a major role in changing the failure modes and the efficiency of GFRP strengthening. Experimental results show that the flexural load carrying capacity of precast prestressed hollow core slabs was increased in the range of 14 to 36% depending on the strengthening scheme used. Analytical predictions using strain compatibility method were carried out and validated against test results. Numerical investigations were also carried out by using a finite element analysis (FEA) software package - ABAQUS. Interesting transition from flexural to flexural shear failure was noted in the behavior of the slabs as the strengthening ratio increased, there by changing the failure mode. Fair correlation was observed between the experimental and analytical results.

Contents

Declaration	ii
Approval Sheet	iii
Acknowledgements	iv
Abstract	v
1 Introduction	4
1.1 General	4
1.2 Research Motivation	6
1.3 Research Objectives	7
1.4 Scope of Work	7
1.5 Research Methodology	8
2 Literature review	9
2.1 General	9
2.2 Behaviour of Reinforced/Prestressed concrete in flexure and shear	9
2.3 Behavior of Hollow Core Slab	11
2.4 History of Fiber Reinforced Polymer Composites	13
2.5 Behaviour of Externally bonded FRP Strengthened Concrete	14
2.5.1 Flexural Strengthening	14
2.5.2 Shear Strengthening	16
2.6 Behaviour of NSM FRP Strengthened Concrete	18
2.6.1 Flexural Strengthening	18
2.6.2 Shear strengthening	20
2.6.3 NSM Bond behaviour	21
3 Experimental Program	23
3.1 General	23
3.2 Test Series I	23
3.3 Test Series II	26
3.4 Specimen Properties and Characteristics	28
3.5 Material Properties	28
3.5.1 Concrete	28
3.5.2 Internal reinforcement - pretensioned steel tendons	29
3.5.3 External reinforcement - Glass fiber reinforced polymer (GFRP)	29
3.6 Strengthening Procedure	30

3.6.1	EB method	30
3.6.2	NSM method	34
3.7	Test Setup	36
3.8	Loading Procedure	36
3.9	Instrumentation	38
4	Test Results and Discussion	40
4.1	General	40
4.2	Series I	40
4.2.1	Test Results, Mode of failure for Slab - I-C-150-7.5-0-0.36-0	40
4.2.2	Test Results, Mode of failure for Slab - I-S-150-7.5-EB-0.36-0.548	41
4.2.3	Test Results, Mode of failure for Slab - I-S-150-7.5-EB-0.36-0.947	43
4.2.4	Test Results, Mode of failure for Slab - I-S-150-7.5-NSM-0.36-0.564	43
4.2.5	Test Results, Mode of failure for Slab - I-S-150-7.5-NSM-0.36-0.94	44
4.2.6	Load-deflection relationships	46
4.2.7	Load-strain relationships	50
4.2.8	Cracking behaviour	54
4.2.9	Summary of key findings - Series I	56
4.3	Series II	59
4.3.1	Test Results, Mode of failure for Slab - II-C-250-5.4-0-0-0	59
4.3.2	Test Results, Mode of failure for Slab - II-S-250-5.4-EB-0.372-0.549	60
4.3.3	Test Results, Mode of failure for Slab - II-S-250-5.4-EB-0.372-1.647	61
4.3.4	Test Results, Mode of failure for Slab - II-S-250-5.4-NSM-0.372-0.62	63
4.3.5	Load-deflection relationships	64
4.3.6	Cracking behaviour	68
4.3.7	Summary of key findings - Series II	70
5	Analytical and Finite Element Study	73
5.1	General	73
5.2	Analytical Study	73
5.2.1	Material Properties	73
5.2.2	Cracking moment	76
5.2.3	Ultimate Flexural Load Capacity of PPHC slab	76
5.2.4	Shear Capacity Prediction of PPHC slab	77
5.2.5	Deflection Prediction of PPHC slab	79
5.2.6	Comparison between Predicted and Experimental Results	80
5.3	Finite Element Study	87
5.3.1	Material Properties and Element Type	87
5.3.2	Interactions	95
5.3.3	Geometry and Boundary Conditions	96
5.3.4	Type of Analysis	96
5.3.5	Verification of the Model	97

6	Conclusions	100
6.0.6	Summary of key findings - Series I	101
6.0.7	Summary of key findings - Series II	103
6.0.8	Concluding Remarks	106
6.0.9	Further Work	109
	References	110

List of Figures

2.1	Failure modes	12
2.2	Comparison of Load-Deflection curve with and without FRP strengthening	14
2.3	Different NSM systems	20
2.4	NSM Debonding failure modes	22
3.1	Nominal Hollow Core Slab Cross Section - Series I	24
3.2	Test Parameter Schematic - Series I	25
3.3	Nominal Hollow Core Slab Cross Section - Series II	26
3.4	Test Parameter Schematic - Series I	27
3.5	End block, Anchor and Hydraulic Prestressing Setup	29
3.6	Surface Preparation and Epoxy Resin Preparation	31
3.7	Application of EB GFRP fabric - Flexural Strengthening	32
3.8	Application of U-wrap - Shear Strengthening	33
3.9	Specimen Preparation - NSM strengthening	34
3.10	Application of GFRP bar - NSM strengthening	35
3.11	Test Setup Schematic - Series I	36
3.12	Test Setup Schematic - Series II	37
3.13	Test-Setup	37
3.14	Instrumentation- LVDT, Strain Guage Position Schematic	38
3.15	Instrumentation- LVDT & strain guage locations & DAQ	39
4.1	Mode of failure - I-C-150-7.5-0-0.36-0 (control)	41
4.2	Mode of failure - I-S-150-7.5-EB-0.36-0.548	42
4.3	Mode of failure - I-S-150-7.5-EB-0.36-0.947	43
4.4	Mode of failure - I-S-150-7.5-NSM-0.36-0.564	44
4.5	Mode of failure - I-S-150-7.5-NSM-0.36-0.94	45
4.6	Series I - Load vs. Mid-span Deflection	46
4.7	Series I - Load vs. Mid-span Tendon Strain	50
4.8	Series I - Load vs. Mid-span Tendon Strain	53
4.9	Crack Pattern at Failure - Series I	55
4.10	Mode of failure - II-C-250-5.4-0-0-0 (control)	59
4.11	Mode of failure - II-S-250-5.4-EB-0.372-0.549	60
4.12	Mode of failure - II-S-250-5.4-EB-0.372-1.647	62
4.13	Mode of failure - II-S-250-5.4-EB-0.372-1.647	63

4.14	Series II - Load vs. Mid-span Deflection	65
4.15	Crack Pattern at Failure - Series II	69
5.1	Parabolic stress-strain curve of concrete	74
5.2	Strain compatibility of concrete section strengthened by FRP composite	75
5.3	Numerical integration of curvature at different locations	80
5.4	Predicted and experimental load vs deflection - I-C-150-7.5-0-0.36-0	83
5.5	Predicted and experimental load vs deflection - I-S-150-7.5-EB-0.36-0.548	84
5.6	Predicted and experimental load vs deflection - I-S-150-7.5-EB-0.36-0.947	84
5.7	Predicted and experimental load vs deflection - I-S-150-7.5-NSM-0.36-0.564	85
5.8	Predicted and experimental load vs deflection - I-S-150-7.5-NSM-0.36-0.94	85
5.9	Predicted and experimental load vs deflection for slabs having same strengthening ratio	86
5.10	Predicted and experimental load vs deflection for slabs having same strengthening ratio	86
5.11	Compression Stress-Strain curve - M 53.1 Grade	89
5.12	Definition - Inelastic, Elastic strains	90
5.13	Definition - Inelastic, Elastic strains	90
5.14	Definition - Cracking, Elastic strains	91
5.15	Element C3D8 - Abaqus 6.13	91
5.16	Stress-Strain Curve - Prestressing Steel	94
5.17	Modelled Cross section - II-C-250-5.4-0-0-0 (control)	96
5.18	Isometric View of Assembly	97
5.19	Isometric View of Meshed Assembly	98
5.20	Load vs displacement (Experimental vs FEM) - C-250-5.4	99
5.21	Ultimate Failure and Damage - II-C-250-5.4-0-0-0	99

List of Tables

3.1	Nominal Specimen Properties	28
3.2	Properties of Sika Wrap 430G	30
4.1	Experimental results - Series I	49
4.2	Service load for all the slabs - series I	51
4.3	Yield load for all the slabs - series I	52
4.4	Experimental results - Series II	67
5.1	Comparison between the predicted and the experimental results	82
5.2	Default parameters of CDP model under compound stress	88
5.3	Concrete Compression damage	92
5.4	Concrete tension damage	93

Chapter 1

Introduction

1.1 General

The precast concrete industry is in requirement of new products and building systems to satisfy the needs and demands of our modern society: shortage of labour force, structural efficiency, fire resistance, speed of construction, quality of execution, and last but not least sustainable construction. One of the most remarkable and successful developments in this context is the development of Precast systems including Prestressed Hollow Core Slab (PPHCS). It provides an answer to most of the present market demands and challenges faced by the building industry. Key advantages include structural efficiency, low material consumption, highly automated and environmentally friendly production process, high concrete strength, slender floor thickness, and possibilities for reuse and recycling at the end of the life cycle. Strengthening of these slabs may be required for several reasons to maintain their structural integrity. The main reasons for strengthening include: material degradation, increased dead or live loads, architectural modifications, installation of heavy machinery, reinforcement corrosion, incorporate the changes in codal provisions, and provisions of openings in slab. These structural deficiencies must be addressed to ensure safety and integrity. In the Indian context, according to SAII (Supreme Audit Institution of India) nearly (39%) 49,007 bridges were found to be structurally deficient or functionally obsolete. Most of these deficient bridges are reinforced or prestressed concrete structures and are in urgent need of repair and strengthening. Moreover, several buildings also need strengthening to extend their service life.

The use of Fiber Reinforced Polymers (FRPs) has emerged as one of the most promising technologies in the field of strengthening, due to their well-established ad-

vantages relative to conventional materials and it has become more customary to strengthen concrete structures by bonding advanced non-corrodible composite materials, such as Carbon Fiber Reinforced Polymer (CFRP), Glass Fiber Reinforced Polymer (GFRP) to their surfaces. FRP Strengthening provides the construction industry with the opportunity to meet the goals of reducing maintenance and life cycle cost of structures. It can be efficiently used for repair, rehabilitation, replacement and new construction of structures. American Concrete Institute (ACI 440.2R-08) is a well recognized institute to publish design guidelines on this strengthening technique.

The use of FRP as externally bonded reinforcing is a promising new technology for rehabilitation of deteriorated structural members, strengthening of under-designed concrete elements and for upgrading of concrete structures to meet new service demands. GFRP has excellent properties of high strength to weight ratio, directional strength, corrosive resistance, weather resistance, non-magnetic characteristics and dimensional stability with low thermal conductivity. GFRP based rehabilitation consists of the external bonding fabric sheet onto the surface of the structural element to be repaired/retrofitted. Externally bonded FRP sheets and strips are currently the most commonly used techniques for flexural and shear strengthening of concrete beams and slabs. Past experimental research focused on the Flexural and shear-strengthening of reinforced and prestressed concrete beams using externally bonded FRP laminates [1, Triantafillou et al] [2, Rahimi et al] [3, Belarbi et al] [4, Murphy et al] . According to these researchers main problem was that the failure of members strengthened with externally bonded FRP sheets and strips could be brittle due to debonding and/or peeling of the FRP reinforcements especially in the high flexural and shear stress regions.

More recently, near-surface mounted (NSM) FRP reinforcement has gained attention as another alternative to minimize debonding problems associated with external bonded FRP reinforcement. NSM technique consists of inserting the FRP reinforcing bars or strips into grooves precut into the concrete cover of structural member and the FRP reinforcement is bonded by filling the groove using high-strength epoxy adhesive. Assuring the proper bond conditions for the NSM bars or strips into the groove is the crucial phase of this strengthening technique, in addition no preparation work is needed other than grooving. Published design guidelines and experimental studies predominantly focus on unaltered conventional precast prestressed hollow core slabs

[5] [6]. As no alike application was investigated as to the author's knowledge, on prestressed hollow core slabs, there is need for a comprehensive understanding of the behaviour of EB and NSM FRP strengthened hollow core elements.

There is need for a comprehensive understanding of the behaviour of FRP strengthened Hollow core slab elements to so that appropriate design provisions can be developed. Published design guidelines and experimental studies predominantly focus on unaltered conventional precast prestressed beams. An experimental program has been conducted in this study to contribute to the knowledge about the performance of strengthened hollow-core slabs. Results from this study will help in refinement of the recommended code practices, and in exploring new applications for the FRP strengthened elements.

1.2 Research Motivation

In the recent years, Precast concrete industry is gaining popularity in India. One of the most striking and successful developments in this context is the precast prestressed hollow core slabs. Material degradation, increased dead or live loads, architectural modifications, installation of heavy machinery, code revisions, openings in slab, pose a serious threat to structural integrity of PPHCS. The use of Fiber reinforced polymer (FRP) as externally bonded reinforcement and near surface reinforcement is a promising new technology for rehabilitation of deteriorated structural members, strengthening of under-designed concrete elements and for upgrading of concrete structures to meet new service demands (Bakis et al [1], El-Hacha et al [2]). Previous works have shown that strengthened specimens responded with an increase in stiffness, ductility and increase in both shear and flexural capacity. However, there is currently a lack of research in the area of PPHCS strengthened with externally bonded and near surface mounted FRP reinforcements. Use of NSM FRP bar reinforcements is novel and existing knowledge on strengthening using NSM FRP bars is much more limited than that on the externally bonded FRPs. No provisions exist in the current guidelines on the FRP strengthening of concrete structures such as ACI-440 [7].

1.3 Research Objectives

The objectives of this study is to understand the flexural and flexural-shear behaviour, failure mechanisms of PPHCS in conjunction with FRP strengthening schemes. The key objective of this research is to assess the behavior of prestressed precast hollow core slabs strengthened with EB GFRP sheets and NSM GFRP bar reinforcement. Experimental variables include different FRP flexural strengthening ratios, prestressing ratio, and shear span to depth (a/d) ratio. Comparison of strengthening efficiency between EB laminates against the NSM FRP bars is carried out. Analytical predictions using strain compatibility method are carried out. Numerical investigations are performed using a finite element analysis (FEA) software package - ABAQUS. The specific objectives included the following:

1. Critically understand the flexural, flexural-shear response and failure mechanisms of PPHCS with respect to change in a/d ratio and prestressing ratio.
2. Evaluate the efficiency of various FRP strengthening configurations to enhance the flexural, flexural-shear performance.
3. Compare the experimental test results with analytical and finite element studies. Numerical study involves finite element simulation of tested slabs using ABAQUS (nonlinear finite element modelling software package). Analytical studies involves moment –curvature behaviour at the sectional level and load-displacement behaviour at the element level.

1.4 Scope of Work

Behaviour of PPHCS with and without FRP strengthening under flexure is investigated. The scope of this the research work is limited to (i) test a series of control, EB GFRP and NSM GFRP bar strengthened full-scale PPHC slabs. Two levels of prestressing ratios are considered. FRP strengthened slabs were tested under four point bending configuration to understand the flexure and flexure-shear behaviour and their failure mechanisms. (ii) evaluate the efficiency of various FRP strengthening configurations to enhance the performance of PPHCS. Parameters considered in the experimental program include the thickness of slabs, a/d ratio and FRP configurations. (iii) compare the experimental results of the tested slabs with the analytical

predictions (iv) create a finite element model (FEM) and validate them for further parametric studies.

1.5 Research Methodology

The present work comprises of three stages to achieve the aforementioned research objectives involving experimental and analytical studies.

The **first** stage involves a comprehensive literature review. A literature review was conducted to obtain recent information regarding similar studies conducted elsewhere. Focused on strengthening of reinforced/prestressed concrete slabs and beams by fiber reinforced polymer composites, effect of EB and NSM FRP systems, and the effect of FRP strengthening configurations.

In **second** stage of the research, an experimental test program was developed which includes testing of nine full-scale precast prestressed hollow core specimens. These tests were organised into two series to address the aforementioned objectives.

In **third** stage an analytical and finite element study was carried out. Analytical study included developing moment-curvature behaviour at the sectional level and load-displacement behaviour at the element level. A finite element model of PPHC slabs with and without strengthening is constructed using ABAQUS software. The developed model is validated against the obtained experimental results.

Chapter 2

Literature review

2.1 General

A state-of-the-art literature review is carried out to accumulate information regarding the recent advancements on the various design concepts needed to direct this study. Main design parameters that controls the behaviour of EB and NSM strengthened concrete sections are: (i) size and shape of section; mechanical properties of concrete; (ii) mechanical properties of internal/external reinforcement; (iii) reinforcement ratio and its distribution along the cross section; (iv) efficiency of the concrete/reinforcement bond. This literature review aspire to explain the aforementioned design concepts and their role to address the research objectives stated in chapter 1. However, this review is not exhaustive and the need for brevity prevents all topics from being fully addressed.

2.2 Behaviour of Reinforced/Prestressed concrete in flexure and shear

Reinforced concrete(RC) sections are predominantly subjected to bending moment and shear force. According to MacGregor et al. [8] the elastic beam theory is not used in the design of reinforced concrete beams, because the compressive stress–strain relationship for concrete becomes nonlinear at higher strain values and more importantly concrete cracks at low tensile stresses, making it necessary to provide steel reinforcement to carry the tensile force. Generally RC sections are analysed by using stress-block concept in conjunction with moment equilibrium and moment–curvature relationships will be used to describe and discuss the flexural behavior of a variety of beam sections. Flexural behaviour of RC sections until failure can be divided into three stages: pre-cracking, yielding of longitudinal bars and secondary concrete

crushing. Role of internal reinforcement ratio is negligible before tensile cracking of concrete. After cracking, the stiffness of a section reduces and gross moment of inertia reduces to cracked moment of inertia. Energy is released with each additional crack formation that causes reduction in stiffness leading to increased deflections. At this instance, tensile stresses are transferred from concrete to stiffer element such as internal steel reinforcement. As tensile strength of steel is much higher, it provides reserve stiffness for the transformed section, allowing a member to sustain an increase in load carrying capacity. Conventionally, perfect bond exists between steel reinforcement and concrete, nevertheless bond strength [9, Rosenboom A] is crucial to resist large shear forces generated at the interfaces in case of many externally-applied reinforcements.

Prestressed concrete(PC) is a method for overcoming concrete's natural weakness in tension by application of pre-load to the member so that cracking and deflection are recoverable to a higher degree. PC raise overall structural performance in terms of pre-cracking stiffness, increased load carrying capacity, reduced deflections, and improved durability. In contrast to RC, the serviceability state for PC is within pre-cracking of concrete. As soon as the tensile stress exceeds the tensile strength of the concrete, PC behaves in a similar fashion to RC. Due to numerous advantages of PC, it is widely used to produce precast elements such as beams, floor/roof members.

In reality members are subjected to shear stresses in addition to flexural stresses, which may result in (brittle failure) diagonal cracks, unless appropriate amounts of properly detailed web and longitudinal reinforcement have been provided. Shear stress can be decomposed into equivalent principal tensile and principal compressive stress. A crack will form in concrete when the principal tensile stress at some location reaches the cracking strength of concrete. The direction of principal tensile stress governs the cracks. For members subjected to pure flexure, the principal tensile stresses are parallel to the longitudinal axis leading to perpendicular crack where as members subjected to shear stresses, the principal tensile stress directions are inclined to longitudinal axis of the member leading to diagonal cracks. Vertical component of inclined prestressing force reduces the shear in the member. A flexural-shear crack develops along the shear span as an extension of previously existing flexural cracks, when the flexural capacity is sufficiently large. According to Collins et al. [10] diagonal cracking will first occur either as web-shear cracking near the support or as flexure-shear cracking near the quarter-point of the span. ACI code [11] gives guidelines for predicting web-shear cracking and flexural-shear cracking reasonably. More rational theories such as modified compression field theory ca and softened truss model can predict

the response in shear of reinforced/prestressed member [10, collins et al.]. (Hsu et al.) After diagonal cracking, the tensile stresses in the concrete are substantially reduced , where compression field theory assumes that principal tensile stress is zero, more superior modified Compression field theory accounts for the contribution of the tensile stresses in the concrete between the cracks.

2.3 Behavior of Hollow Core Slab

As aforementioned in chapter 1, Prestressed Hollow Core slabs are usually used as simply supported one-way slabs with no negative and torsional moments. Although PPHC slabs have been used widely, the design methods of these slabs are based on the procedures for solid reinforced concrete beams, in spite of the differences of geometry(with voids) and reinforcement(without shear reinforcement). The possible failure mechanisms were summarized by Walren and Mercx(1993), Pajari(1989) [12] in the following ways as shown in Figure 2.1:

Bending failure mechanisms

1. Flexural tensile cracking of concrete
2. Flexural tension failure of strands
3. Flexural compression failure of concrete
4. Flexural tensile cracking of top fiber after the releasing of pre-stressed strands
5. Serviceability issues

Shear failure mechanisms

1. Anchorage failure of strands
2. Flexural shear cracking of concrete
3. Shear tension failure of web
4. Shear compression failure of web

Schematic of failure modes is shown in FIg. 2.1.

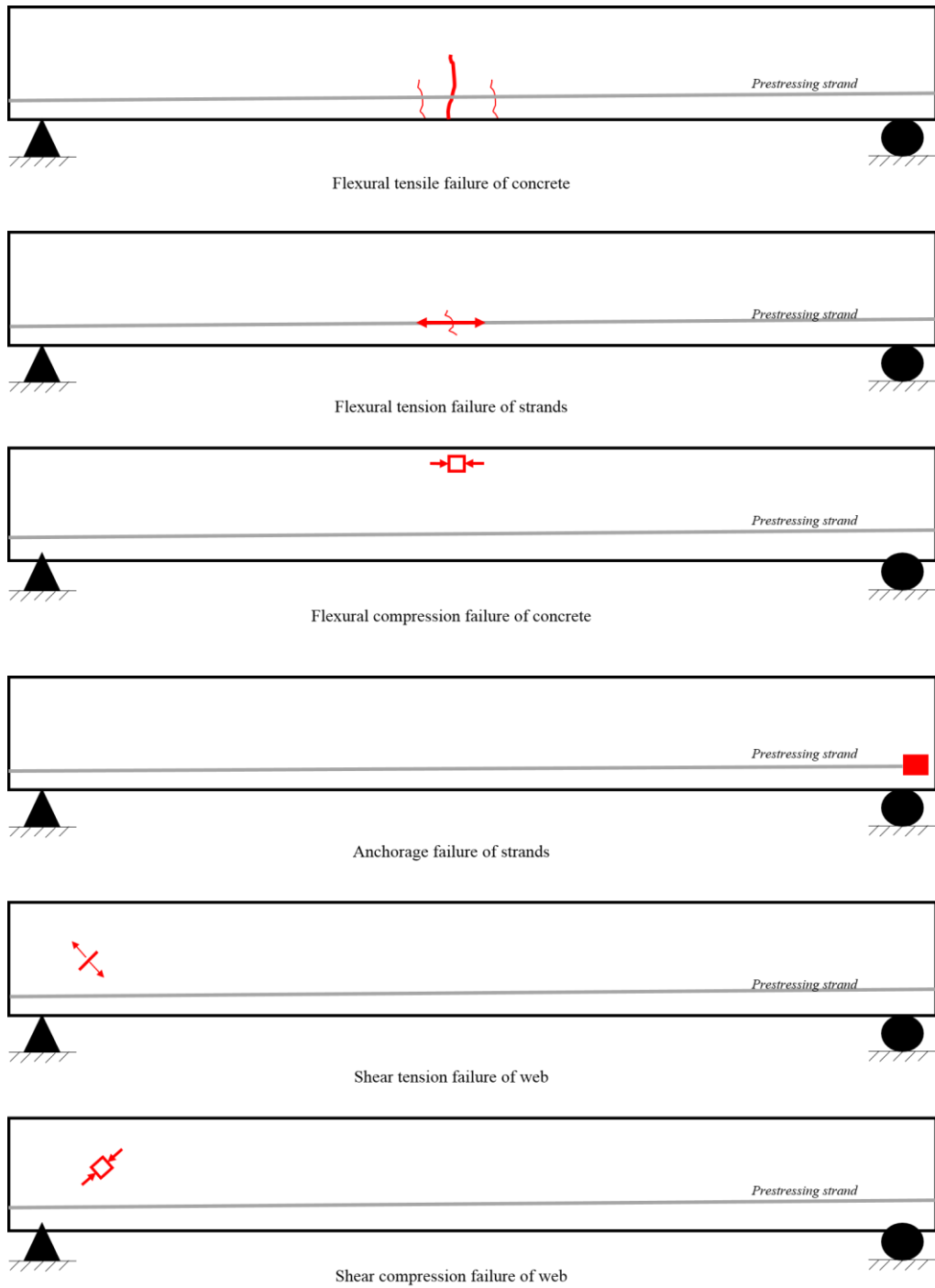


Figure 2.1: Failure modes

2.4 History of Fiber Reinforced Polymer Composites

Concrete structures need to be upgraded for several reasons mainly: degradation over time due to environmental aging, fatigue, need for upgrading to meet more stringent design requirements and increased live/dead loads etc. In the past two decades, structural repair and strengthening using Fiber Reinforced Polymer (FRP) composites have received considerable emphasis around the world. They have gained widespread use as strengthening materials for RC/PC structures in applications where conventional strengthening techniques like epoxy-bonding steel plates, concrete-steel jacketing may be problematic in terms of equipment, chemical corrosion, increase in cross section and dead load, greater installation time and energy. Thorough review of strengthening methods by Bakis et al (2002) [13] attests many potential applications of FRP composite materials in construction, one of the illustrious strengthening and retrofit solution is EB FRP System. This strengthening involves external bonding of fiber reinforced polymer composite to the areas of interest to gain in strength and performance. GangaRao et al (2007) [14] mentioned that strengthening reinforced concrete with FRP laminates is suitable for: repairing deteriorated beams and slabs to restore their strength and stiffness; limiting crack width under increased service loads; enhancing the flexural and shear strength of in-service members; providing confinement for concrete columns and designing new structural elements with depth limitations. More recently, near-surface mounted (NSM) FRP reinforcement has attracted an accelerating amount of research as well as practical application [15]. due to numerous advantages such as (i) reduced site installation, (ii) no surface preparation other than grooving, (iii) prevention of debonding failure modes in EB systems, (iv) less susceptible to corrosion due to the presence of cover, and (v) better aesthetics. The above reasons make NSM FRP strengthening better than EB FRP method.

2.5 Behaviour of Externally bonded FRP Strengthened Concrete

Material Degradation over time due to environmental aging, increased dead or live loads, architectural modifications, installation of heavy machinery, code revisions, fatigue, need for upgrading to meet more stringent design requirements and other reasons call up for a economical strengthening scheme.

State-of-the-art strengthening and retrofit techniques increasingly utilize externally bonded FRP composites, which offer unique properties in terms of strength, lightness, chemical resistance, and ease of application. Such techniques are most attractive for their fast execution and low labor costs which are considered as economical engineering solution [13, Bakis et al.].

2.5.1 Flexural Strengthening

To describe the behaviour of externally bonded FRP strengthened structural members, just for reference a comparison of load-deflection curve is made for strengthened and its counterpart. The behaviour of externally bonded (EB) strengthened member

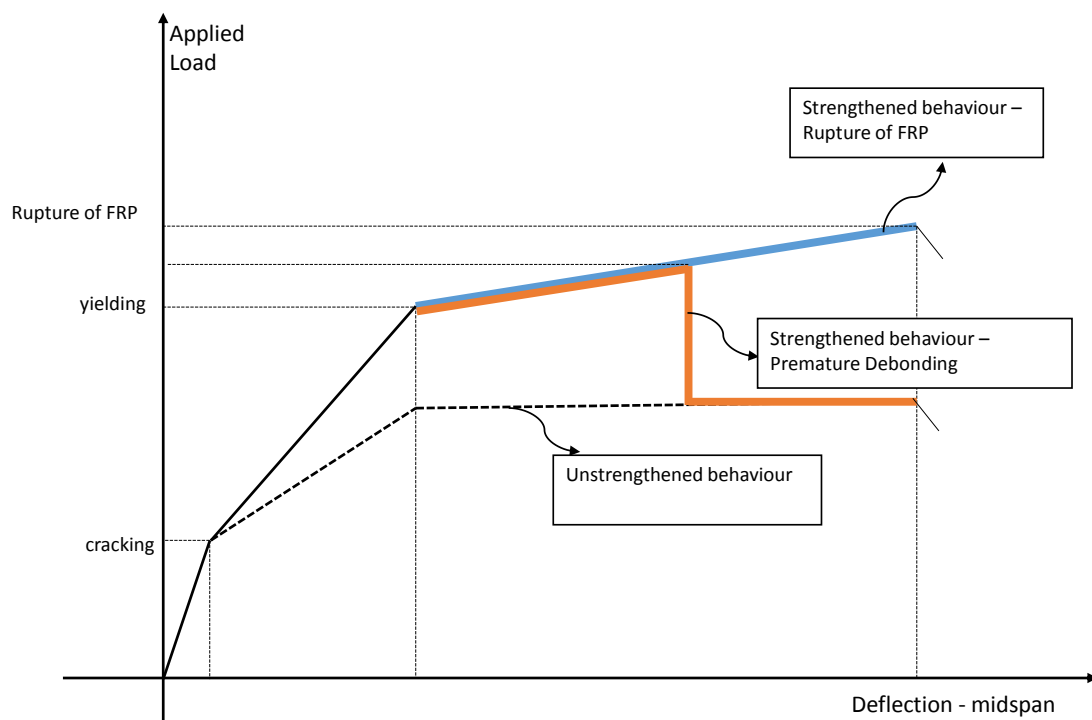


Figure 2.2: Comparison of Load-Deflection curve with and without FRP strengthening

is similar to unstrengthened counterpart until cracking of concrete. Rahimi et al. [2] determined that FRP strengthening has an no effect (same as unstrengthened section) on the precracking stiffness and cracking load and is predominantly dependent on the concrete section dimensions and the moment of inertia. After cracking, tensile stresses are effectively transferred from the concrete to the surrounding reinforcement. In this case, the reinforcement includes the internal steel as well as the externally bonded laminates via the epoxy matrix. Due to the presence of external reinforcement, post cracking stiffness increases as show in Fig.2.2. The stresses and strains increase linearly until the internal steel reinforcement begins to yield. As stated by Rahimi et al. [2], Triantafillou et al. [1], GangaRao et al. [14], two distinct modes of failure which govern the ultimate state of a strengthened specimen are: premature debonding and FRP rupture. It can be observed from Fig. 2.2 that due to high tensile stresses within the epoxy and surrounding concrete at an early stage in the loading process there is a high probability of laminate debonding [9, rosenboom]. If bond strength is adequately high the structural member may fail by rupture of FRP laminates after steel yielding as shown in Fig. 2.2. To avoid premature debonding in strengthened members ACI 440.2R-08 recommends that ultimate state should lead to one of the failure mode: rupture of the external FRP laminates, secondary concrete crushing, and primary concrete crushing. The guideline requires that adequate ductility be achieved by allowing the internal steel reinforcement to yield, followed by rupture or concrete crushing.

GangaRao et al.[16] evaluated the increase in flexural strength of reinforced concrete beams after wrapping them with carbon fabrics. Percentage increase in ultimate strength capacity of wrapped concrete beams is a function of the number of longitudinal layers of carbon fabric. For a given concrete section and number of fabric layers, increase in ultimate strength is greater for wrapped beams with a lower percentage of steel reinforcement than for those with a higher percentage of steel reinforcement. At a given load level, rebar stresses and deflections were found to be less in carbon-wrapped beams compared to rebar stresses of regular beams. Yielding of steel bars occurred at about 25 percentage higher load in wrapped beams as compared to beams without wrapping. Carbon wrapping of reinforced concrete beams resulted in a gradual plastic strain increase in steel rebars.

In addition, Glass fibre reinforced polymers, because they are more ductile and cheaper than carbon fibres, can be considered as an alternative solution to repair and strengthen concrete elements. Although glass fibre reinforced polymers (GFRPs) have a lower elastic modulus and tensile strength than carbon fibres, its high deforma-

bility, good impact and break resistance properties turn them into a good material for strengthening.

Attari et al. [17] performed experimental investigation on flexural strengthened reinforced concrete beams. The authors concluded that, in comparison with other strengthening systems, the use of FRP composite material in glass fibres alone or as a single-layered hybrid composite having a good elongation at rupture is found to improve the ductility of strengthened beams. This result refutes the generally accepted idea that FRP strengthened beams are affected by a drop in the ductility leading to a brittle and sudden failure.

Ebead et al. [18] conducted an experimental and theoretical research work on the punching shear and flexural strengthening of two-way slab system by using CFRP strips and GFRP laminates. It was concluded that CFRP strips and GFRP laminates increased strength and stiffness of two-way slabs. Results show that the flexural capacity of two-way slabs can increase to an average of 35.5% over that of the reference (unstrengthened) specimen. Small increase of the initial stiffness was achieved for flexural specimens. However, an apparent decrease in the overall ductility and energy absorption was evident due to the brittle nature of the FRP materials, in which GFRP performed well in showing ductility and energy absorption.

2.5.2 Shear Strengthening

Previous research efforts have focused mainly on FRP strengthened behaviour of RC members under axial or flexural loading. Relatively, a very less experimental and analytical work has focused on the use of FRP systems for shear strengthening of prestressed concrete members.

Murphy et al. [4] investigated the effectiveness of using externally bonded FRPs for increasing the shear strength by testing 8 full-scale prestressed concrete girders. The effectiveness of externally bonded FRP for shear strengthening was found to be significantly affected by the cross-sectional shape of the girders. Failure modes vary depending on the cross-sectional shape and shear reinforcement schemes,. Various failure modes were observed among the test specimens, including failure along the top flange, debonding of FRP, localized rupture of FRP, diagonal shear tension, web crushing, mechanical anchorage failure, and failure due to stress concentration at the loading/reaction point.

The configuration of the FRP system affects the failure mode of shear strengthened

members. Based on an extensive review of collected experimental data by Belarbi et al. [3], it was reported that the debonding is the dominant mode of failure for beams strengthened with FRP and bonded on the sides only. FRP debonding almost never occurs in beams retrofitted with complete FRP wrap and U-wraps with anchorage systems.

Recent studies by Chaallal et al. [19] revealed the fact that externally applied FRP laminates contribute more to the shear resistance of slender beams than deep beams. As the shear span-to-depth ratio decreases, the arch action of deep beams become more dominant and failure of these type beams occur due to the crushing of concrete. In this case, externally provided FRP reinforcement contributes to the increase in strength but limited to the concrete strut capacity

Needless to mention that the performance of shear strengthening of concrete structures by using externally bonded FRP laminates significantly depends on the bond behavior at interface between the FRP sheets and the concrete substrates. Shear stresses on concrete structures are transferred to FRP laminates by bond which in general is influenced by mechanical and physical properties of FRP material, concrete and adhesive. For reinforced/prestressed concrete, the distribution of bond stresses is more complex as a result of flexural and shear cracking disrupting the continuity of the FRP system [9, Rosenboom]. Bond stresses are a result of a change of the internal moments along the length of the beam and by transfer of forces across cracks. Bond failure, or debonding, usually occurs rapidly and can be initiated in several locations along the strengthened member.

The research conducted by Ibrahim et al. [20] was mainly focused on the shear-strengthening of reinforced and prestressed concrete beams using FRP. It was concluded that contribution of externally bonded FRP laminates to the shear resistance of strengthened structural members is reported to be less for members with high transverse reinforcement ratio than the ones with low transverse ratio. Triantafillou and Plevris [1] show that bonding GFRP or Aramid FRP fabrics or sheets to the sides of the RC beams improve their shear strength and ductility significantly. Kang et al. [21] conducted research to experimentally evaluate the impact of FRP amount and strip spacing on the shear behavior of prestressed concrete (PC) beams. U-shaped FRP strips with different spacing were applied externally to the test specimens in order to observe the overall behavior of the prestressed concrete I-beams and the mode of failure of the applied FRP strips. Externally applied CFRP strips in prestressed

concrete I-beams for shear-strengthening improved the overall shear capacity of the specimens, when the spacing was less than half the effective depth of the prestressed concrete beams.

Research and design guidelines confirm that externally bonded fibre reinforced polymers (FRPs) are efficiently increasing the performances of reinforced/prestressed concrete.

2.6 Behaviour of NSM FRP Strengthened Concrete

Near surface mounted FRP reinforcement has attracted an accelerating amount of research due to numerous advantages over EB FRP reinforcements stated in section 2.4. Moreover, EB FRP reinforcements can be affected by damage of concrete due to corrosion, fire, temperatures and moisture absorption. This can lead to significant reduction in the service life of the structure. NSM method was recently introduced to minimize these problems and to enhance utilization of the FRP material. It is considered as promising technique for strengthening of beams, slabs, masonry walls etc.

2.6.1 Flexural Strengthening

El-Hacha and Rizkalla(2004) [22] carried out experiments on simply supported RC T-beams strengthened in flexure with EB FRP strips and NSM FRP bars & strips. Behaviour and effectiveness of various strengthening systems was compared. Main experimental parameter was the laminate material namely CFRP and GFRP bars & strips. Test results show that load-deflection behaviour exhibited similar pre-cracking stiffness and increase in stiffness after precracking upto the yield point. After steel yielding it was observed that EB-GFRP strips were much more susceptible to debonding than identical strips embedded into the concrete. Brittle failure mode was observed in case of EB-GFRP due to premature debonding. Test results show that beam outfitted with EB-GFRP and NSM-GFRP strips experienced an increase in strength of 28 % and 85% respectively when compared with its unstrengthened counterpart.

An identical comparative study was conducted on flexural strengthening of pre-stressed bridge slabs with EB and NSM FRP bars & strips by Hassan et al (2002) [23]. Slab specimens were tested as simply supported and overhanging cantilevers. Ulti-

mate capacity, failure mechanism and cost analysis of various strengthening techniques for concrete bridges were studied. Out of all NSM FRP reinforcement was found to be feasible and cost effective for strengthening or repairing prestressed concrete girders and slabs. Strengthening using EB FRP strips provided the less increase in strength by 11% due to peeling of the strips from the concrete substrate where as using same amount of strips as NSM reinforcement enhanced the strength by almost 43% . Both EB and NSM FRP strengthening reduced the crack width by 50 to 70 % compared to the unstrengthened specimen.

De Lorenzis et al (2000) [24] investigated the effectiveness of NSM FRP rods as a strengthening system for RC structures. Four full-scale RC T-beams were tested in four point bending configuration. One beam served as control, two beams were strengthened with CFRP sandblasted rods and other beam had NSM GFRP deformed rods. All the grooves had square cross section. Beam strengthened with NSM CFRP bar and NSM GFRP deformed bar showed 44% and 26% increase in strength respectively. In comparison with NSM CFRP, beam retrofitted with NSM GFRP showed significant ductility improvement. The study concluded that NSM FRP rods can be used to enhance the flexural capacity of RC beams ranging from 25 to 45% . FRP bars can be manufactured in variety of shapes like round, square, rectangular and oval bars as well as strips Fig 2.3 [15] These different cross-sectional shapes have their own different advantages and practical applications.

Lee and cheng (2010) [25] tested eleven full scale slab overhangs strengthened in negative bending moment regions with various types of NSM reinforcement. Main parameters included: surface condition(e.g.,textured and sand coated), cross-sectional shape (e.g., round and square), material type (carbon and glass), and prestressing effect. Strength increase of 37.7% was obtained when compared to control. Maintaining same amount of axial stiffness, slab specimens strengthened by GFRP round rods showed similar flexural performance to the specimen strengthened with CFRP round rods. The prestressing applied to the NSM strips was found to have a small improvement on the load-carrying capacity, however it was delaying formation of the cracks. Effectiveness of surface treatment on NSM CFRP rods like smooth, sand coated only, ribbed, textured, spirally wound sand-coated were investigated. All of the surface treatments of CFRP NSM rods except for the smooth condition significantly increased the ultimate load carrying capacity of the slab.

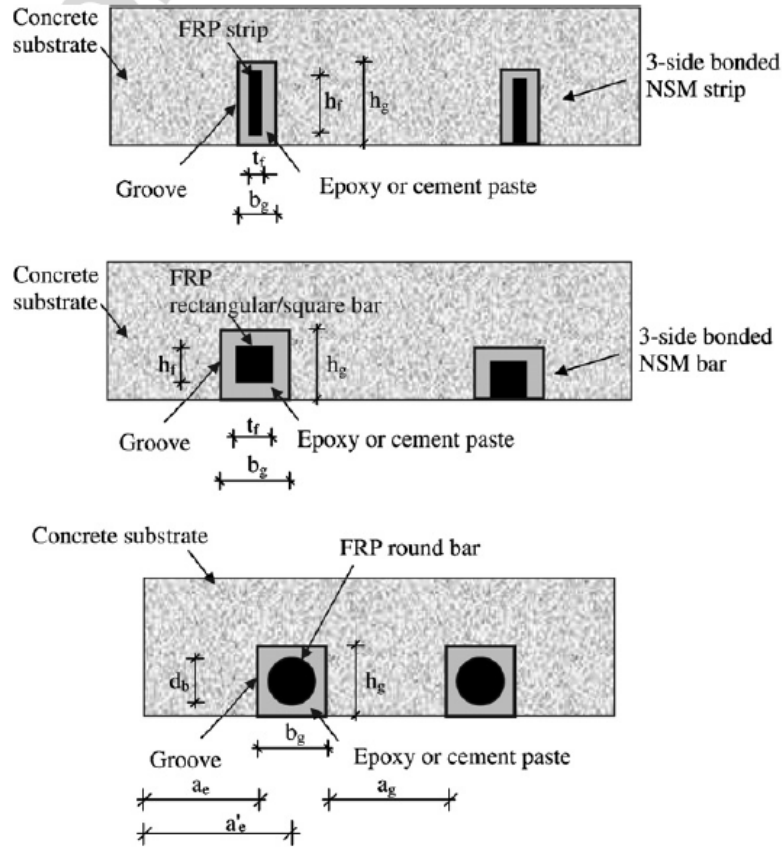


Figure 2.3: Different NSM systems

2.6.2 Shear strengthening

Shear capacity of RC/PC beams can be enhanced by effective use of NSM FRP reinforcement. For this purpose grooves are cut on the sides of the member at a desired angle to the beam axis and NSM FRP bars are inserted.

De Lorenzis and Nanni [26] tested eight full scale RC T-beams. The variables examined in the shear tests were spacing of the rods, strengthening pattern, end anchorage of the rods, and presence of internal steel shear reinforcement. In absence of internal steel stirrups, an increase in capacity as high as 106 % with respect to control beam was observed. Nevertheless significant increase in shear strength was observed with a presence of limited amount of internal shear reinforcement.

Experimental program to appraise the possibility of the application of NSM CFRP laminates for low strength RC beams was carried out by Barros and Dias [27]. Comparisons between the effectiveness of NSM CFRP strips of different inclinations and EB FRP shear reinforcement were made. Following major conclusions were made

(i) NSM technique is still viable and effective in beams of low strength concrete, (ii) NSM strengthening effectiveness decreases with the increase in the CFRP percentage, and (iii) inclined laminates were more effective than vertical laminates. The reported capacity increases ranged from 22% to 77% and were in all cases greater than beams strengthened with equal amounts of EB FRP.

2.6.3 NSM Bond behaviour

The bond between an NSM bar and the substrate material plays a crucial role in ensuring the effectiveness of the NSM technique. Bond behaviour depends on various factors like the tensile and shear strength of concrete, strength of groove filler used, groove and bar dimensions, surface configuration and groove surface roughness etc. Various bond tests were studied by several researchers and some of them are summarized below.

Hassan and Rizkalla (2004) [28] conducted experiments on reinforced concrete beams strengthened with NSM CFRP rods in three point bending configuration. The CFRP rods had limited bonded lengths. Governing failure mode for all the strengthened beams was by splitting of the concrete surface at the concrete epoxy interface. ACI 440.2R-08 [7] uses the equation proposed by Hassan and Rizkalla (2004) for evaluation of bond strength of NSM rods.

According to Hassan and Rizkalla (2004) and De Loreniz et al(2007) [15] common bond failure modes are mentioned below. Fig. 2.4 illustrates these common modes of debonding failure.

- 1. Bond failure at the bar–epoxy interface**
- 2. Bond failure at the epoxy– concrete interface**
- 3. Splitting of the epoxy cover** (splitting of the epoxy cover without cracking of concrete, cracking of the epoxy cover including fracture in the concrete along inclined planes, fracture of the concrete edge)

Lee et al (2012) [29] experimentally evaluated the bond characteristics of a wide range of embedded FRP NSM reinforcements with various surface configurations, cross-sectional shapes, material types, adhesive types, and groove sizes. A total of 109 concrete block specimens were tested under direct pull out test configuration. Test results indicated that CFRP rods experienced higher bond strength and lower

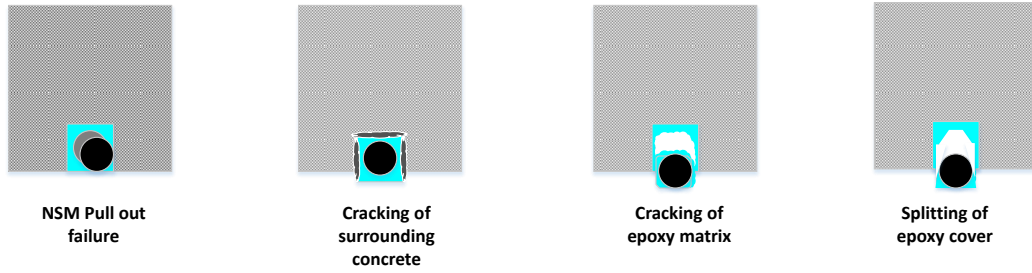


Figure 2.4: NSM Debonding failure modes

slippage when compared to GFRP rods. However, the failure modes of specimens with CFRP and GFRP rods were similar. Spirally wound and sand-coating with indentation and grooved surface were found to exhibit very good bond due to combined effect of frictional force and mechanical interlocking. Increase in groove size led to increase in bond strength with no change in failure mode.

Wahab and Soudki (2011) [30] carried out experimental study on bond behavior of RC beams strengthened with NSM nonprestressed and prestressed CFRP rods. The test variables considered are: presence of internal tension steel reinforcement (unreinforced and reinforced) use of NSM CFRP strengthening (nonprestressed and prestressed), and type of CFRP rod (spirally wound and sand blasted). Six RC beams were cast and tested under four point configuration. Two beams served as control (spirally wound and blasted), two beams had non prestressed CFRP rods with a difference in CFRP used (spirally wound and sand blasted), two beams had prestressed CFRP rods with a difference in CFRP used (spirally wound and sand blasted). The failure mode for the nonprestressed strengthened beams was by CFRP rod pullout at midspan whereas failure mode for the prestressed strengthened beams depended on the CFRP used. For the prestressed sand blasted CFRP rods failed as its nonprestressed counterpart, but beams strengthened with prestressed spirally wounded CFRP rods failed by pullout of the CFRP rod from the epoxy in the region close to support.

Chapter 3

Experimental Program

3.1 General

Experimental investigation is one of the most important and reliable ways for better understanding the behaviour of FRP strengthened PPHC Slabs. In light of the review performed in Chapter 2 on previous research endeavors, an experimental program was conducted in the structural engineering laboratory of Indian Institute of Technology Hyderabad. The test specimens considered in this investigation are categorized into two series namely Series I and Series II. Specimens were tested under four-point bending configuration to failure under monotonic loading conditions using a hydraulic actuator. Details of these two series are described below.

3.2 Test Series I

Series I prototypes are designed to evaluate the efficiency of EB and NSM strengthening configurations in low shear. Each slab has a total of 44% of voids, and is reinforced with four high-strength low-relaxation steel strands. Each specimen was designed to simulate a typical full-scale prestressed roof or floor member. All the test slabs have a shear span to depth ratio(a/d) of 7.5. This ratio, in conjunction with a relatively low level of prestressing ratio was selected to ensure flexure dominant behaviour. All the slabs had similar cross section, having width of 600 mm, depth of 150 mm as shown in fig. 3.1 Although void profiles tend to vary, they are unique to each precast manufacturer. All of the test specimens were fabricated by a local precast concrete supplier(*PRECA*). The nomenclature for the specimens follow the label format like I-C-150-7.5-0-0.36-0, I-S-150-7.5-EB-0.36-0.548, I-S-150-7.5-NSM-0.36-0.564, where roman numeral denotes the test series-I, the following letters denotes ‘C’ - Control and ‘S’ - Strengthened, next number denotes depth of

the section, EB - Externally bonded, NSM - Near Surface Mounted, and the following number denotes the percentage of prestressing ratio, and the last number denotes percentage of flexural GFRP reinforcement ratio.

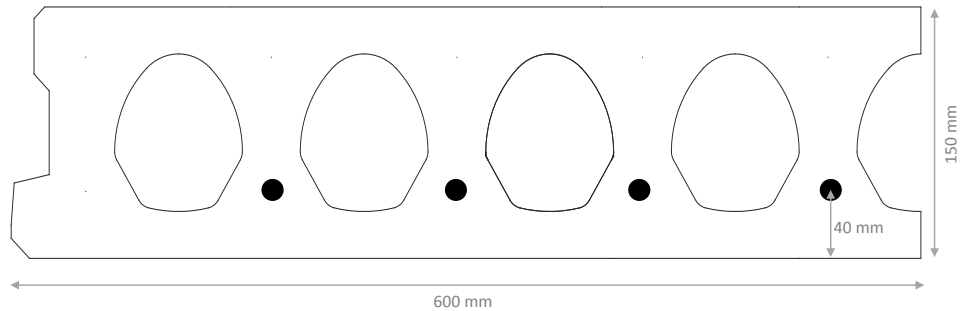


Figure 3.1: Nominal Hollow Core Slab Cross Section - Series I

This series compares the flexural response of five of the total nine specimens, namely: I-C-150-7.5-0-0.36-0, I-S-150-7.5-EB-0.36-0.548, I-S-150-7.5-EB-0.36-0.947, I-S-150-7.5-NSM-0.36-0.564, I-S-150-7.5-NSM-0.36-0.94. Two strengthening reinforcement ratios are considered: 0.0056, 0.00094. Internal reinforcement ratio of 0.0036 was constant for all the test specimens. The parameters investigated in this series include the FRP strengthening ratio, efficiency of different GFRP strengthening techniques (EB and NSM).

The test parameter schematic in Fig. 3.2 renders simplified illustration of the strengthening strategies used in series I. Prestressing ratio and strengthening ratio are indicated for comparison.

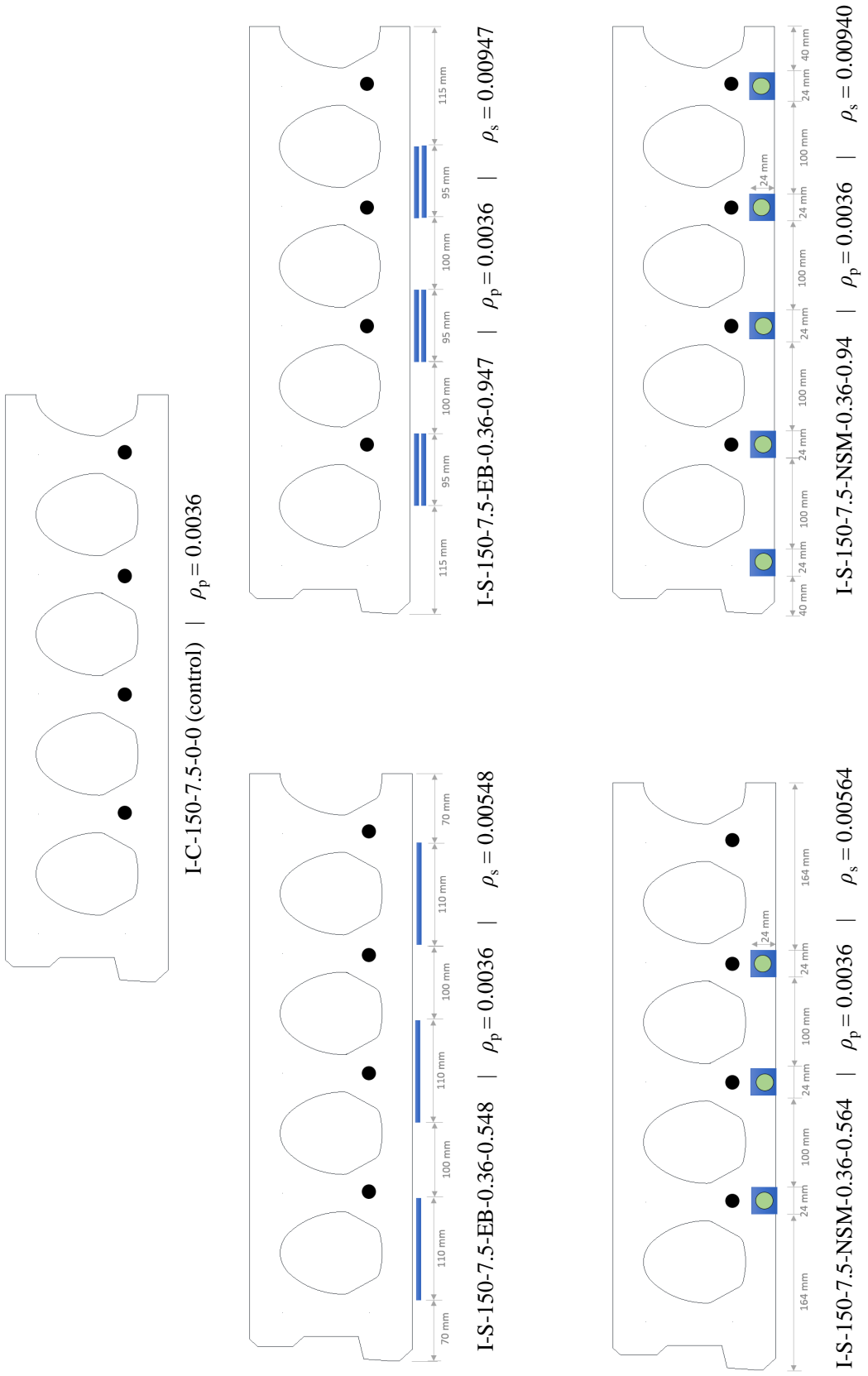


Figure 3.2: Test Parameter Schematic - Series I

3.3 Test Series II

Series II prototypes are designed to evaluate the efficiency of EB and NSM strengthening configurations in high shear. The test specimens have a constant thickness of 250 mm and width of 600 mm. Each slab has a total of 44% of voids, and is reinforced with high-strength low-relaxation steel tendons. Each specimen was designed to simulate a typical full-scale prestressed roof or floor member. All test slabs have a shear span-to depth ratio (a/d) of 5.4. This ratio was selected so that the ultimate strength of the specimens would be controlled by a flexural-shear mode of failure. Figure 3.3 shows typical cross section of series II test specimen, the voids are shaped with a mix of straight vertical sides, and a curved profile along the top and bottom of the void.

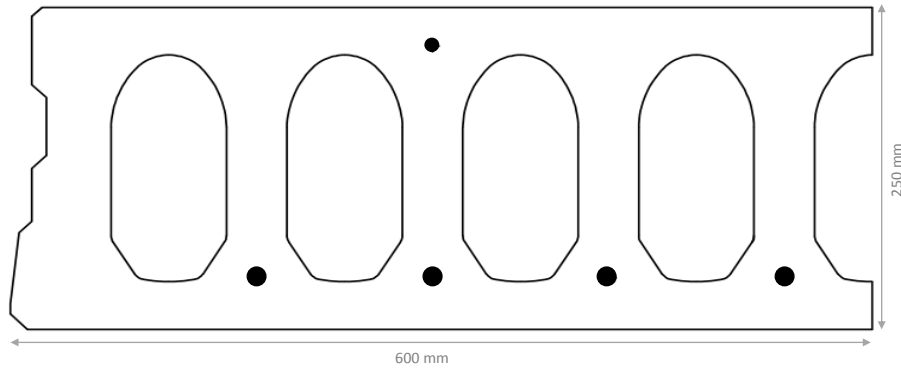
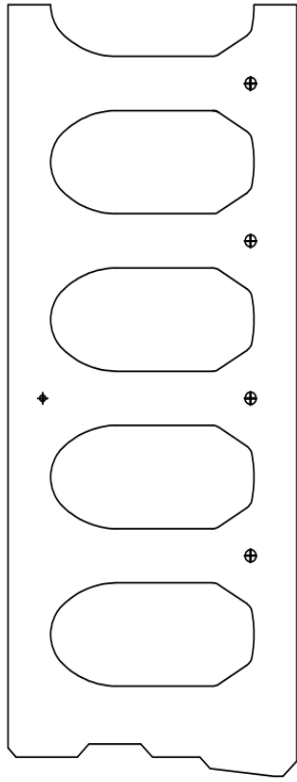
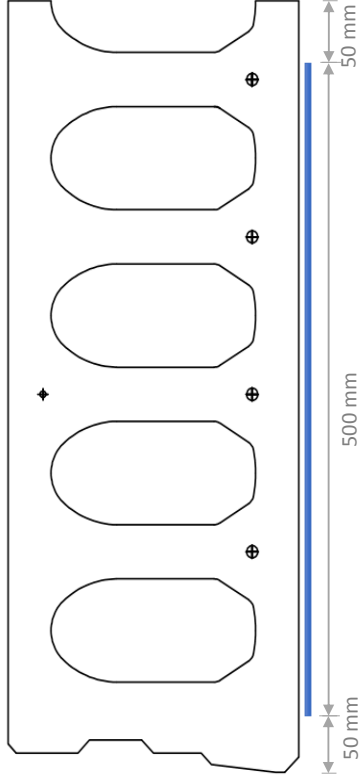


Figure 3.3: Nominal Hollow Core Slab Cross Section - Series II

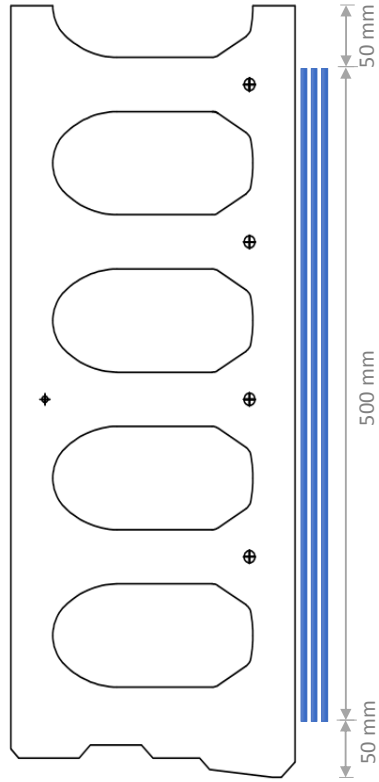
The nomenclature for the Series II specimens follow the label format like II-C-250-5.4-0-0, II-S-250-5.4-EB-0.372-0.549, II-S-250-5.4-NSM-0.372-0.62, where roman numeral denotes the test series-II, the following letters denote ‘C’ - Control and ‘S’ - Strengthened, next number denotes depth of the section, EB - Externally bonded, NSM - Near Surface Mounted, and next number denotes the percentage of prestressing ratio, last number denotes percentage of GFRP ratio. This series compares the flexural, flexure-shear response of four of the total nine specimens, namely: II-C-250-5.4-0-0, II-S-250-5.4-EB-0.372-0.549, II-S-250-5.4-EB-0.372-1.647, II-S-250-5.4-NSM-0.372-0.62. Two flexural FRP reinforcement ratios are considered: 0.00537, 0.01612. Internal reinforcement ratio of 0.00372 was constant for all the test specimens. The parameters investigated in this series include the FRP strengthening ratio, efficiency of different GFRP strengthening techniques (EB and NSM). To enhance the shear performance of the members, shear strengthening was carried out. The test parameter schematic in Fig. 3.4 renders simplified illustration of the strengthening strategies used in series II.



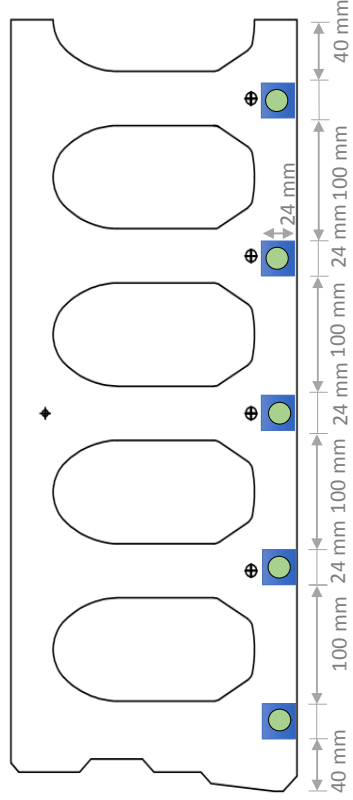
II-C-250-5.4-0-0 (control) | $\rho_p = 0.00372$



II-S-250-5.4-EB-0.372-0.549 | $\rho_p = 0.00372$ | $\rho_s = 0.00549$



II-S-250-5.4-EB-0.372-1.647 | $\rho_p = 0.00372$ | $\rho_s = 0.01647$



II-S-250-5.4-NSM-0.372-0.62 | $\rho_p = 0.00372$ | $\rho_s = 0.0062$

Figure 3.4: Test Parameter Schematic - Series I

3.4 Specimen Properties and Characteristics

Research and design guidelines confirm that EB and NSM FRPs are efficiently increasing the performances of reinforced/prestressed concrete. Acknowledging numerous advantages of GFRP over other strengthening materials, Glass Fiber Reinforced Polymer composite(GFRP) fabric for EB method and spiral wounded GFRP bars for NSM technique were used in this study. Table 3.1 summarizes the nominal specimen properties such as the area of prestressing steel, prestressing ratio, area of GFRP, and the corresponding FRP ratio.

Series I prototypes had a total length of 3000 mm, and were simply supported over a clear span of 2660 mm. Flexural strengthening was carried out by application of suitable number of GFRP layers/ NSM bars at bottom surface (positive bending).

In case of Series-II, specimens had a total length of 3,500 mm, and were simply supported over a clear span of 3,230 mm. Flexural strengthening was carried out by application of suitable number of GFRP layers/ NSM bars at bottom surface (positive bending). U-wrap having width of 250 mm with a spacing of 300 mm were applied as shown in Fig 3.8 in case of shear strengthening.

Table 3.1: Nominal Specimen Properties

	Specimen	Area of prestressing tendons (mm ²)	Prestressing ratio	Area of Flexural GFRP (mm ²)	Flexural Strengthening ratio
Series I	I-C-150-7.5-0-0.36-0	217	0.0036	-	-
	I-S-150-7.5-EB-0.36-0.548	217	0.0036	330	0.00548
	I-S-150-7.5-EB-0.36-0.947	217	0.0036	570	0.00947
	I-S-150-7.5-NSM-0.36-0.564	217	0.0036	339	0.00564
	I-S-150-7.5-NSM-0.36-0.94	217	0.0036	565	0.0094
Series II	II-C-250-5.4-0-0	394.8	0.00372	-	-
	II-S-250-5.4-EB-0.372-0.549	394.8	0.00372	500	0.00549
	II-S-250-5.4-EB-0.372-1.647	394.8	0.00372	1500	0.01647
	II-S-250-5.4-NSM-0.372-0.62	394.8	0.00372	565	0.0062

3.5 Material Properties

3.5.1 Concrete

All specimens were cast using normal weight, ready-mix concrete with a target compressive strength of 50 MPa at 28 days. Six standard cubes(150 x 150 x 150 mm)

of which 3 were tested for 28 days where average compressive strength was found to be 53.6 MPa and 3 were tested on the day of testing. The unit weight of concrete was taken as 2400 kg/m³. The design concrete strength for the slabs produced by the manufacturers was 45 MPa at 7 days and 53.1 MPa at 28 days. Crushed limestone aggregates used in the concrete mix with a nominal maximum size of 10 mm. Strength of concrete on the test date was used for the FEM analysis.

3.5.2 Internal reinforcement - pretensioned steel tendons

The type of strands used in the tested specimens was seven-wire low-relaxation strands with a design value of tensile strength of 1860 MPa and modulus of elasticity of 196.5 GPa. Only two strand sizes were utilized, 9.5-mm and 12.7-mm diameter, in the specimens of this experimental program. The tendons were anchored from one end of the 90 m precast bed and stressed from the other end. The end block and prestressing tendon setup can be seen from Fig 3.5. Top and bottom prestressing strands were pulled by hydraulic jack with 60 kN and 120 kN force respectively(Fig 3.5). Prestress in top and bottom prestressing strands after losses was about 875.84 MPa & 972.64 MPa respectively. The stress-strain curve for prestressing steel can be approximated from the Ramberg-Osgood model.



Figure 3.5: End block, Anchor and Hydraulic Prestressing Setup

3.5.3 External reinforcement - Glass fiber reinforced polymer (GFRP)

The GFRP sheet used for EB was SIKA WRAP 430G. These sheets were supplied in a roll package having 500 mm width, 0.358 mm thickness and 100-meter length. Sika Wrap 430G is a unidirectional glass fiber fabric. The epoxy resin used to bond the GFRP sheet to the concrete was Sikadur-330. The adhesive is a two-component epoxy resin. It is primarily used for the structural repair of cracks and delaminations in concrete, masonry, or timber; for bonding steel or FRP to concrete; and for anchoring bolts, dowels, and rebar into concrete, masonry, or stone. The properties of Sika Wrap 430G are given in Tables 3.2. Dry fiber properties include, the tensile

strength of 2300 MPa, tensile E-Modulus of 76 GPa. Laminate thickness is 1 mm (impregnated with Sikadur-330) per layer having tensile strength of 348 MPa, tensile E-Modulus of 14 GPa.

Spirally wound GFRP bars of 12 mm diameter were used as NSM reinforcement, having tensile strength of 700 MPa, tensile E-modulus of 49 GPa. The epoxy resin used to bond the GFRP sheet to the concrete was Sikadur-30 LP. The adhesive is a two-component epoxy resin which is specially designed for use at high temperatures (HDT - 82^o).

Table 3.2: Properties of Sika Wrap 430G

Longitudinal Modulus, E ₁₁ (GPa)	14
Transverse Modulus, E ₂₂ (GPa), E ₃₃ = E ₂₂ (GPa)	8.86
In-plane Shear Modulus, G ₁₂ (GPa)	4.56
Longitudinal Tensile Strength, (MPa)	348
Transverse Tensile Strength, (MPa)	17.98
Longitudinal compressive Strength, (MPa)	395.05
Transverse compressive Strength, (MPa)	98.57
In-plane Shear Strength, (MPa)	49.85

3.6 Strengthening Procedure

The PPHC slab specimens were required to be strengthened along the tension side, the same side as the prestressing tendons located. To ease the bottom surface strengthening process, each slab was delicately flipped using forklift. Care was taken not to create any dynamic motion while the slabs were inverted as this additional stress combined with the pre-camber may induce unintentional cracking.

3.6.1 EB method

The surface preparation for EB method include: grinding the uneven edges, grinding the edges to have 10cm radius for effective bonding of FRP, flushing with high strength grout for evenness as shown in Fig 3.6. The two components of epoxy Sikadur 330 were then mixed in a ratio of 1:4 as shown in fig 3.6. The mixed Sikadur 330 epoxy resin was placed directly onto the prepared surface as shown in Fig 3.6. The CFRP sheet was cut to the desire length and Sika GFRP sheet was placed on the resin coating in the required direction where fibers were aligned longitudinally, as shown in Fig 3.7. Irregularities or air pockets were worked out by using a special laminated roller patented by Sika. For the test specimens requiring more than one layer of GFRP sheet, additional Sikadur 330 epoxy layer was applied, then a second

layer of CFRP was applied on this prepared surface. After successful application of required number of layers, a sealer coat of Sikadur 330 was applied.

U-wrap configuration was selected for shear strengthening of hollow core slabs, wrapping of GFRP sheets was carried out where a U - wrap was applied starting from the one side of slab as shown in Fig 3.8 . Care was taken to align the edges of U-wrap perpendicular to the longitudinal axis of the slab.



Figure 3.6: Surface Preparation and Epoxy Resin Preparation



GFRP Roll Package



Epoxy Application



Use of Roller to remove entrapped air



Strengthened specimen

Figure 3.7: Application of EB GFRP fabric - Flexural Strengthening



Epoxy Application



Use of Roller to remove entrapped air



Shear Strengthening U wrap



Strengthened Specimen

Figure 3.8: Application of U-wrap - Shear Strengthening

3.6.2 NSM method

In accordance with NSM layout specifications given by ACI 440.2R-08 (2008), for circular NSM bars, the minimum dimensions of grooves should be 1.5 times the bar diameter. De Lorenzis and Nanni (2002) [24], Lee et al (2012) [29] concluded that increasing the groove size will yield an increase in average bond strength thereby a conservative groove size of 24 mm was selected. For NSM strengthening, a diamond blade concrete cutter was used to make square grooves at the bottom surface of the slabs having side dimension of 24mm for different slabs at appropriate locations as shown in Fig 3.10. After cleaning of grooves with compressed air, epoxy resin is filled half way, then FRP bar is placed in the groove and lightly pressed, which forces the epoxy resin to flow around the bar. The groove is now filled with more resin and the surface is leveled to concrete substrate



Cutting of grooves



Chipping of grooves



Final specimen – ready for NSM strengthening

Figure 3.9: Specimen Preparation - NSM strengthening



Mixing of Sikadur 30 epoxy



Half filling of grooves with epoxy



Application of GFRP bar



Surface levelled to concrete substrate



Strengthened specimen

Figure 3.10: Application of GFRP bar - NSM strengthening

3.7 Test Setup

The test setup is a four-point bending configuration, by which constant moment region along the mid-span is obtained. Figure 3.13 illustrates the components in the test setup. A 250 kN MTS hydraulic actuator was utilized to apply two monotonic concentrated loads centered over the mid-span of each test specimen. The loads were transferred to the slab specimens via a single longitudinal rigid steel loading beam, stiffened with web stiffeners for high rigidity. Two transverse I beams were used to apply distributed line load points along the full width of the slab as shown in Fig. 3.11, Fig. 3.12.

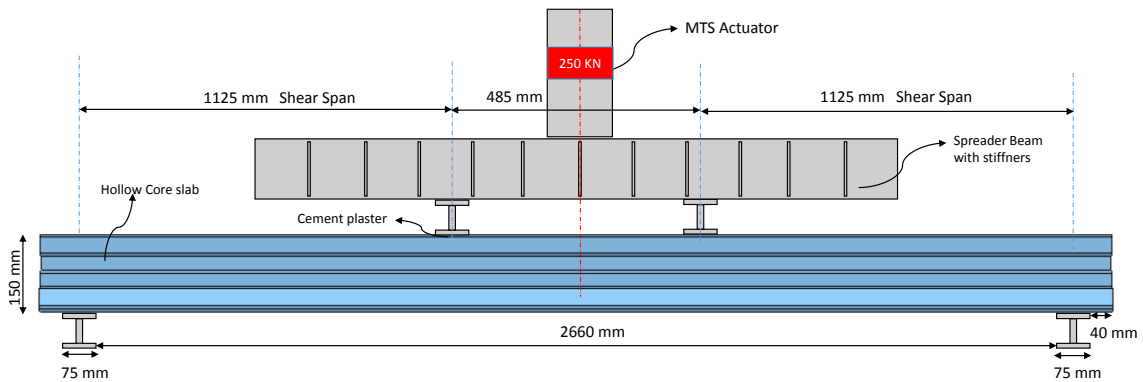


Figure 3.11: Test Setup Schematic - Series I

Superior cement mortar was used between the two transverse spreader I-beams and the slab to remove the surface irregularities for ensuring uniform contact. Care was taken to avoid stress concentrations related bearing failures while testing. The bottom reaction supports included I-beams having 65 mm top flange width, and stiffened with transverse stiffeners. These support beams were sufficiently stiffened to avoid any sudden buckling failure and for transferring the loads safely to the loading frame.

3.8 Loading Procedure

The test procedure for all test specimens was identical. A preload of 5 kN was applied for initial set of the plaster. Loading was applied monotonically at displacement stroke controlled rate of 0.02 mm/sec until first cracking. After cracking, the loading rate was increased to 0.05 mm/sec until failure. Loading was interrupted intermittently at every 10 kN to observe the failure progression, marking of cracks and take pictures.

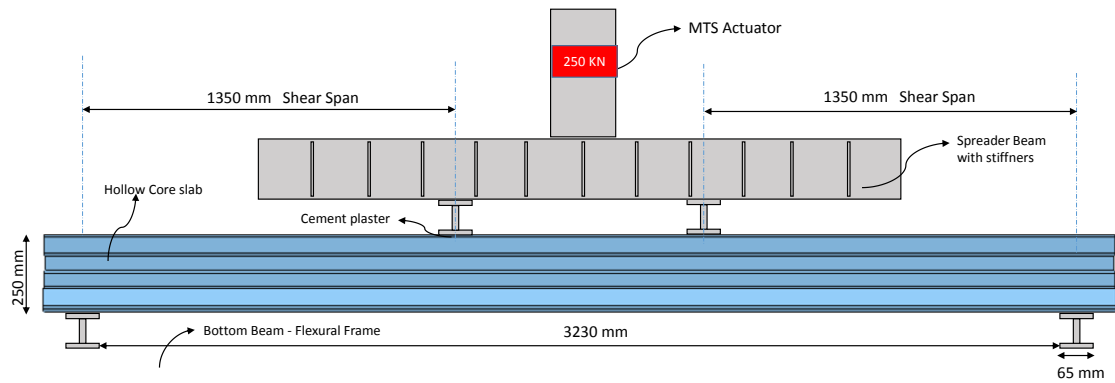


Figure 3.12: Test Setup Schematic - Series II

- A. 250 kN MTS Actuator
- B. Loading beam
- C. 3.5m hollow core slab
- D. 100mm LVDT @ $L/2$
- E. 50mm LVDT @ $L/3$
- F. Data acquisition system
- G. Support

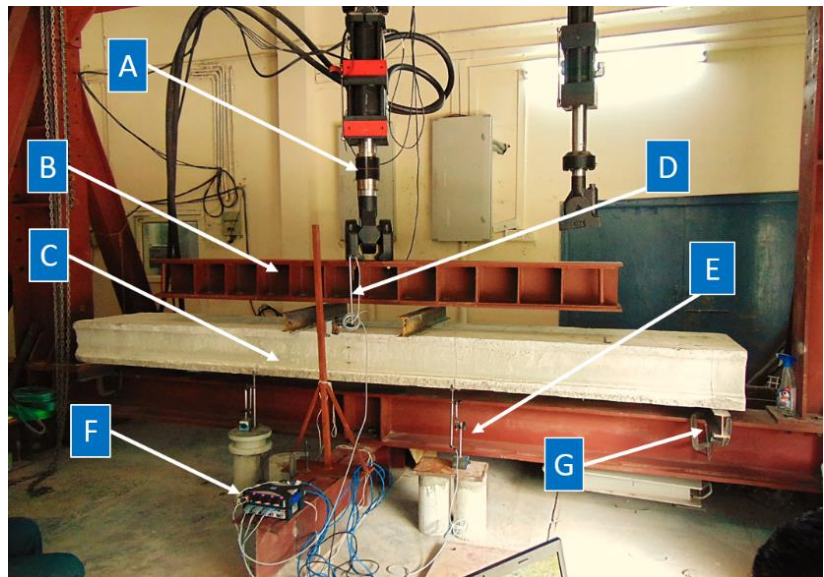


Figure 3.13: Test-Setup

3.9 Instrumentation

Each slab specimen was instrumented in the similar fashion. Instrumentation mainly involved: Linear Variable Differential Transducers (LVDT), strain gauges connected to data acquisition system. Deflections were recorded by using four LVDTs denoted D1-D4. Specific locations of LVDTs were chosen to capture the entire deflection profile. Fig 3.14 shows a typical LVDT positions prior to testing along the slab's span. Special LVDT stands were fabricated to hold the LVDTs in place till the ultimate failure. HBM data acquisition setup used in this study.

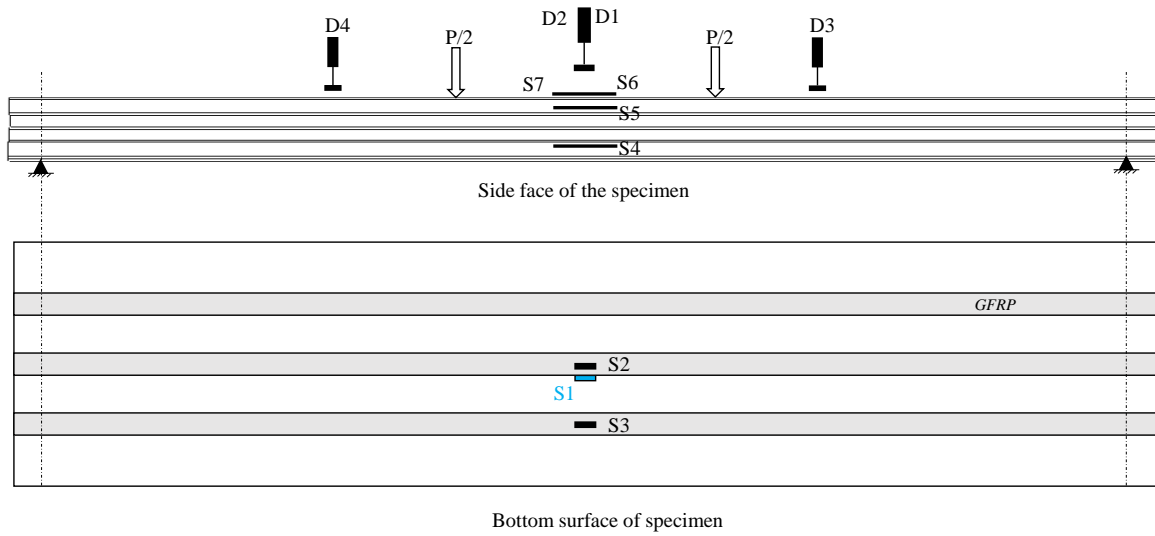
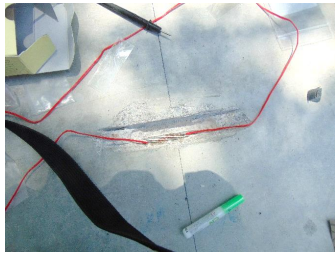
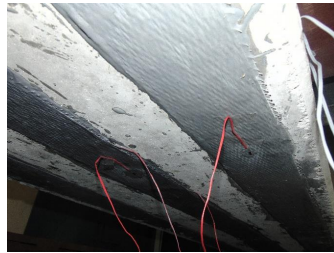


Figure 3.14: Instrumentation- LVDT, Strain Guage Position Schematic

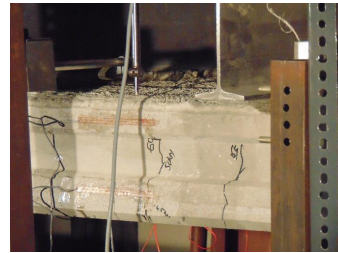
As shown in Fig 3.14 two 50 mm LVDT were positioned at one third clear span distance and two 100 mm LVDT were positioned front & back at the centre of the span to accurately capture mid-span deflection. Surface was thoroughly cleaned, one 2 mm strain gauge (S1) was installed to measure the strain on prestressing strand by drilling a rectangular hole, which was crucial in capturing the yield strain. Two 2 mm strain gauges (S2-S3) were installed to monitor the strain on bottom GFRP. Two 120 mm concrete strain gauges (S4-S5) were installed at top and bottom at the centre line on the concrete slab to capture the strain profile. Two 120 mm concrete strain gauges (S6-S7) were installed to measure the top fiber's compressive concrete strain at the mid span section as shown in Fig 3.14.



Strain gauge on prestressing strand



Strain gauges on FRP



Strain gauges on concrete



LVDT locations

Figure 3.15: Instrumentation- LVDT & strain gauge locations & DAQ

Chapter 4

Test Results and Discussion

4.1 General

Nine precast prestressed hollow core slabs were tested to evaluate the strengthened response. Different strengthening techniques were used, details as mentioned in chapter 3. The objective of the following sections is to summarize the experimental results of the tested specimens.

4.2 Series I

This section summarizes test results of five specimens categorized into series I. One slab served as control, two slab specimens were strengthened with EB-GFRP strips and two specimens were strengthened with NSM-GFRP bars. Two strengthening reinforcement ratios are considered. Refer section 3.2 and Fig. 3.2 for details and strengthening configurations used. Detailed analysis of the ultimate capacity and mode of failure of each test specimen is presented in the below sections.

4.2.1 Test Results, Mode of failure for Slab - I-C-150-7.5-0-0.36-0

C-150-7.5-0-0-0 was the control slab in series I. During the application of loading, the flexural cracks first appeared when the load reached 44 kN. Yielding of the prestressing tendons started when the load reached 73 kN. The peak load measured was 74 kN and corresponding mid-span deflection was 65.8 mm. The load deflection response is shown in Fig 4.6.

Failure progression was as follows: Flexural cracking at the bottom over constant moment region; Further crack propagation; Formation of distributed cracks along the length of the specimen; Yielding of pretensioned strands; As the section was under-

reinforced, significant ductility was observed, then test was stopped after midspan deflection reached 100 mm. Figure 4.1 illustrates the test specimen at failure.

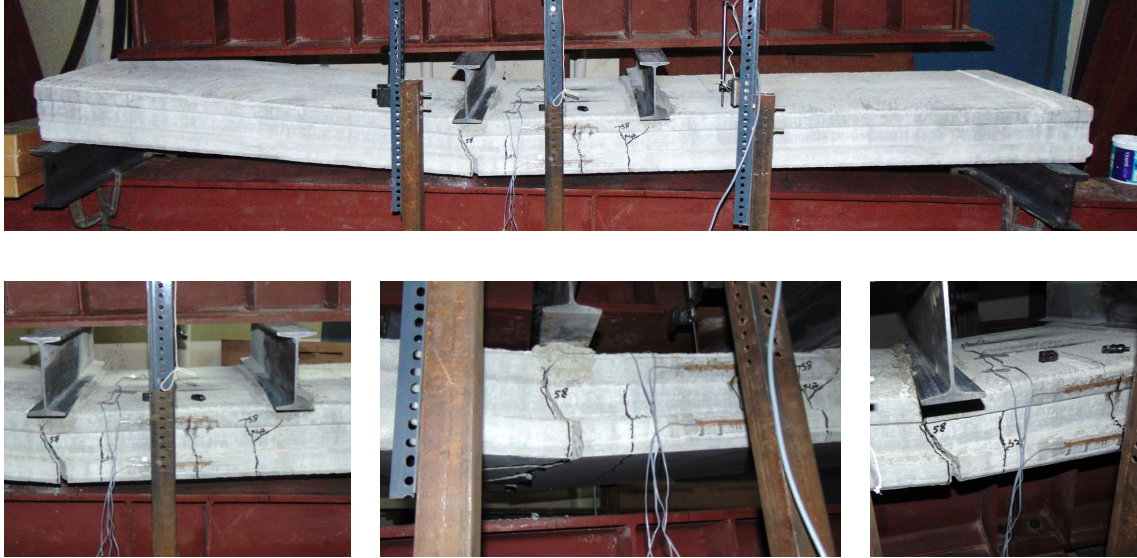


Figure 4.1: Mode of failure - I-C-150-7.5-0-0.36-0 (control)

4.2.2 Test Results, Mode of failure for Slab - I-S-150-7.5-EB-0.36-0.548

Specimen I-S-150-7.5-EB-0.36-0.548 was outfitted with three GFRP strips of 110 mm width each. During the application of loading, the flexural cracks first appeared when the load reached 45 kN. Yielding of the prestressing tendons started when the load reached 80 kN. This strengthened specimen experienced a peak load of 87.1 kN and corresponding mid-span deflection was 35 mm, compared to 74 kN for the non-strengthened control specimen, resulting in a 17.4% increase in capacity.

Failure progression involved: flexural cracking at the bottom over constant moment region; Crack propagation; Formation of more distributed cracks along the length of the specimen when compared to control specimen ; Yielding of pretensioned strands; As the specimen was heavily under-reinforced externally, it lead to bottom GFRP rupture at the peak load; Further Pretensioned tendons continued to take load, significant ductility was observed, then test was stopped after midspan deflection reached 100 mm. Figure 4.2 illustrates the test specimen at failure.



Figure 4.2: Mode of failure - I-S-150-7.5-EB-0.36-0.548

4.2.3 Test Results, Mode of failure for Slab - I-S-150-7.5-EB-0.36-0.947

Specimen I-S-150-7.5-EB-0.36-0.947 was outfitted with six GFRP strips of 95 mm width each. During the application of loading, the flexural cracks first appeared when the load reached 45 kN. Yielding of the prestressing tendons started when the load reached 63.5 kN. This strengthened specimen experienced a peak load of 78 kN and corresponding mid-span deflection was 24.58 mm, compared to 74 kN for the nonstrengthened control specimen, resulting in a 5.41% increase in capacity.

Failure progression involved: flexural cracking at the bottom over constant moment region; Crack propagation; Formation of more distributed cracks along the length of the specimen when compared to control specimen ; Premature debonding of GFRP occurred; Yielding of pretensioned strands; followed by minor concrete crushing below the loading point. Further Pretensioned tendons continued to take load, significant ductility was observed, then test was stopped after midspan deflection reached 100 mm. Figure 4.3 illustrates the test specimen at failure.



Figure 4.3: Mode of failure - I-S-150-7.5-EB-0.36-0.947

4.2.4 Test Results, Mode of failure for Slab - I-S-150-7.5-NSM-0.36-0.564

Specimen I-S-150-7.5-NSM-0.36-0.564 was outfitted with three GFRP bars of 12 mm dia each. During the application of loading, the flexural cracks first appeared when the load reached 42.4 kN. Yielding of the prestressing tendons started when the load

reached 57.9 kN. This strengthened specimen experienced a peak load of 71.8 kN and corresponding mid-span deflection was 40.3 mm, compared to 74 kN for the nonstrengthened control specimen, showing a decrease in load capacity

Failure progression involved starting from: flexural cracking at the bottom over constant moment region; Crack propagation; Formation of more distributed cracks along the length of the specimen when compared to control specimen ; Yielding of pretensioned strands; followed by minor concrete crushing below the loading point; sudden diagonal shear tension failure occurred close to the flexural capacity at a high level of flexural cracking. Lower shear capacity of this slab can be either due to concrete tensile strength variability or manufacturing defect. Figure 4.4 illustrates the test specimen at failure.



Figure 4.4: Mode of failure - I-S-150-7.5-NSM-0.36-0.564

4.2.5 Test Results, Mode of failure for Slab - I-S-150-7.5-NSM-0.36-0.94

Specimen I-S-150-7.5-NSM-0.36-0.94 was outfitted with five GFRP bars of 12 mm dia each at the bottom. During the application of loading, the flexural cracks first appeared when the load reached 44.6 kN. This strengthened specimen experienced a peak load of 109.3 kN and corresponding mid-span deflection was 26.96 mm, compared to 74 kN for the nonstrengthened control specimen, resulting in a 47.7% increase in capacity.

Failure progression involved: flexural cracking at the bottom over constant moment region; Crack propagation; Formation of more distributed cracks along the length of the specimen when compared to control specimen ; No yielding of pretensioned strands was noticed but strains were close to yielding strain; Significant flexural-shear cracks developed along the shear span of the slab as shown in Fig 4.5; followed by minor concrete crushing below the loading point; Flexural capacity was effectively improved, until the flexure-shear failure occurred. Figure 4.5 illustrates the test specimen at failure.



Figure 4.5: Mode of failure - I-S-150-7.5-NSM-0.36-0.94

4.2.6 Load-deflection relationships

Fig 4.6 shows the load versus the mid-span deflection(D1) response for all the tested slabs of series I. Table 4.1 summarize the experimental test results for all Series I specimens.

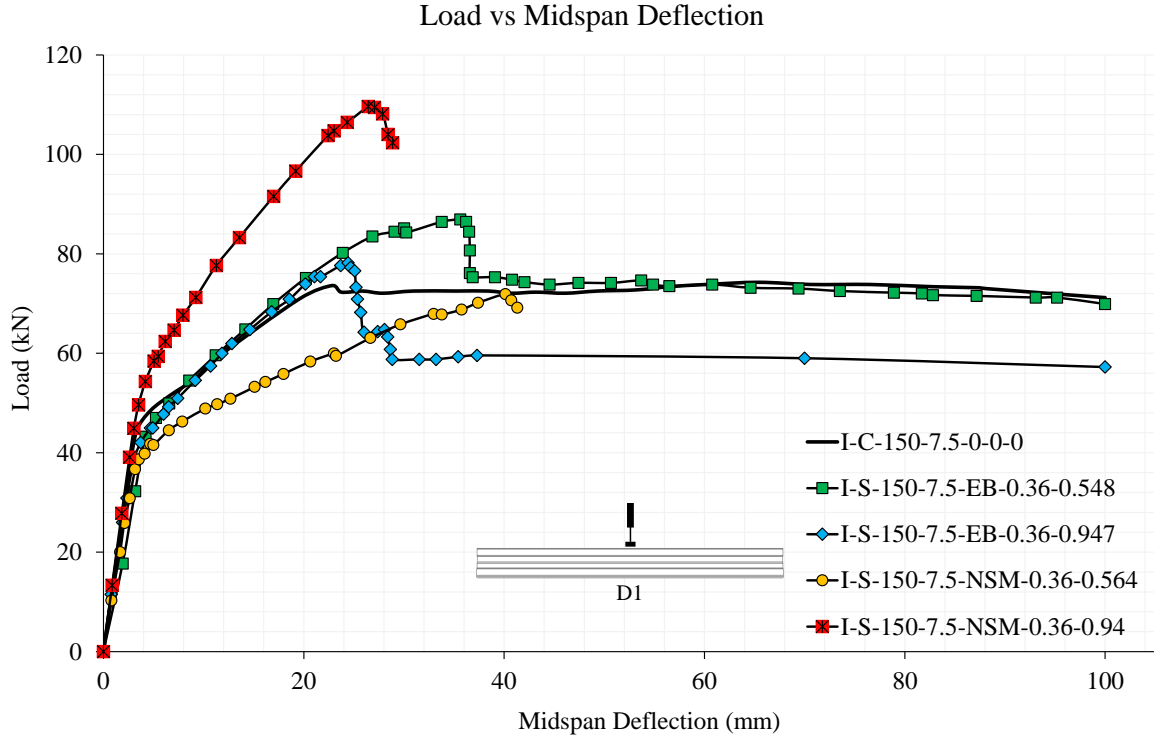


Figure 4.6: Series I - Load vs. Mid-span Deflection

Pertaining to the load-midspan deflection behaviour of control specimen (I-C-150-7.5-0-0.36-0) is same as any under-reinforced prestressed section. During initial stages of loading the section is uncracked and exhibit a linear-elastic behaviour. Concrete cracks after attaining its tensile capacity, then behaviour changes from uncracked to cracked-elastic as pointed out by change in slope of the curve(Fig 4.6). As the load is increased, pretensioned strands start to take load and the section responds elastically until the yield strength is reached. At the yielding of strands, load-deflection curve flattens, and no further increase in moment capacity is observed. Ultimately slab failed by top concrete crushing.

Prior to cracking the load-deflection behaviour of unstrengthened and strengthened specimens was near identical. For each slab, the cracking load was determined based on the change in slope of the load-deflection curve. In case of EB FRP specimens, addition of thin EB FRP laminates slightly increased the section moment of inertia

due to which cracking load was marginally increased. In case of NSM FRP specimens cracking loads slightly decreased to accommodate the redistribution of stresses caused by removing the concrete material during grooving. Pre-cracking stiffness for all the control and strengthened specimens was almost same as much of the composite action takes place after cracking. After flexural cracking, the tensile stresses are transferred from the concrete substrate to the internal and external reinforcement if any. Different strengthening techniques demonstrated substantial influence on the slabs post-cracking response until the failure. Unlike control, FRP reinforcement continued to provide the required stiffness to the system in order to sustain the increasing load. This post-cracking stiffness increase is dependent on the FRP reinforcement ratio and strengthening scheme used.

Slab (I-S-150-7.5-EB-0.36-0.548) demonstrated a considerable increase in post cracking stiffness and capacity (17.4%) until GFRP rupture, The strength gained in this slab was about 17.4% when compared to the control slab. This is attributed to GFRP laminates applied at the tension face of the slab. The ultimate deflection was reduced from 65 mm to 35 mm. Due to the application of GFRP, the stiffness of the slab increased slightly and therefore, the ultimate deflection decreased and also due to early rupture of GFRP laminate as epoxy-concrete substrate bond strength was high enough, ultimate displacement was reduced with respect to control specimen. After rupture of EB GFRP laminates, the load dropped to a load level equivalent to the yielding load of the cross section which led to yielding of strands and then after the response was same as control. Increasing the strengthening ratio, for Slab(I-S-150-7.5-EB-0.36-0.947) almost similar increase in post cracking stiffness was noted with a capacity enhancement of only 5.06% which was due to premature debonding of GFRP laminates causing the system to weaken by sudden release of energy.

In case of NSM FRP slab(I-S-150-7.5-NSM-0.36-0.564), reduction in capacity and deformability was noticed, which could be attributed to its brittle shear tension failure mode. This slab showed lower post-cracking stiffness among all the tested slabs of series I this can be attributed to unexpected lower shear capacity compared to the flexural capacity of control, either due to large variability in concrete tensile strength or manufacturing defect. when the NSM GFRP area was increased by 66.6%, slab(I-S-150-7.5-NSM-0.36-0.94), post-cracking response exhibited the highest stiffness improvement among all the tested slabs, despite its flexural-shear failure mode. This signifies that the extremely advantageous effect of increasing the NSM GFRP area when good bond is secured, should always be directed by flexural strengthening lim-

its considerations precluding any abrupt changes in the failure mode. However, the higher improved stiffness of the NSM technique over EB technique makes it more appealing for use in serviceability governed applications (Table 4.2).

In comparing the slab(I-S-150-7.5-EB-0.36-0.947) and slab(I-S-150-7.5-NSM-0.36-0.94), the strength increase using almost same EB GFRP area as NSM GFRP was approximately 1.4 times that obtained using externally bonded laminates, reflecting the highest strengthening efficiency obtained by NSM technique. Even NSM technique resulted in optimum bond strength than EB technique. Thus NSM strengthening technique using GFRP bars is more effective in strength governed applications than the EB GFRP laminates.

Table 4.1: Experimental results - Series I

<i>Parameter</i>	I-C-150-7.5-0-0.36-0	I-S-150-7.5-EB-0.36-0.548	I-S-150-7.5-EB-0.36-0.947	I-S-150-7.5-NSM-0.36-0.564	I-S-150-7.5-NSM-0.36-0.94
Flexural strengthening ratio	-	0.00548	0.00947	0.00564	0.0094
First crack load (KN)	44	45	45	42.4	44.6
First crack displacement (mm)	3.57	4.72	4.8	4.9	3
Yielding load (KN)	73	80.8	63.5	57.9	NO
Yielding displacement (mm)	23	36.5	28.3	20.43	NO
Peak load (KN)	74.24	87.19	78	71.8	109.3
Peak displacement (mm)	65.8	34.95	24.58	40.3	26.96
Failure Mode	Yielding, Flexure failure	Yielding, Rupture of GFRP.	Debonding of GFRP, Yielding, Flexure Failure	Yielding, Diagonal shear crack sudden collapse	No yielding, Flexure-shear crack

4.2.7 Load-strain relationships

This section summarizes the strains in prestensioned strands and FRP. The tensile strains were measured using strain gauges attached on the surface of the reinforcements as mentioned in section 3.9. As mentioned above, midspan location was chosen to measure strain in prestensioned tendons. Fig 4.7 illustrate the load-midspan tendon strain for series I specimens. The initial precracking stage indicates that majority of the load-carrying resistance is given by concrete tensile capacity and initial prestress force inside the concrete. Having the same characteristics of load-deflection behaviour, the load-tensile strain is also linear upto cracking of concrete. This applies for strengthened specimens as well. After cracking of prestressed concrete section, the load is more rapidly transferred to the internal prestressed steel tendons which is indicated by the abrupt increase in tensile strain in tendons (Fig 4.7). Stiffening effect of the tendons offers additional load-carrying capacity to the section, thereby positive increase in slope is observed (Fig 4.7). As the load reaches the yielding stage, the slope of the load-tendon strain curve attains a plateau, with no further increase in load-carrying capacity, this holds good for unstrengthened specimens but may not be true for FRP strengthened specimens.

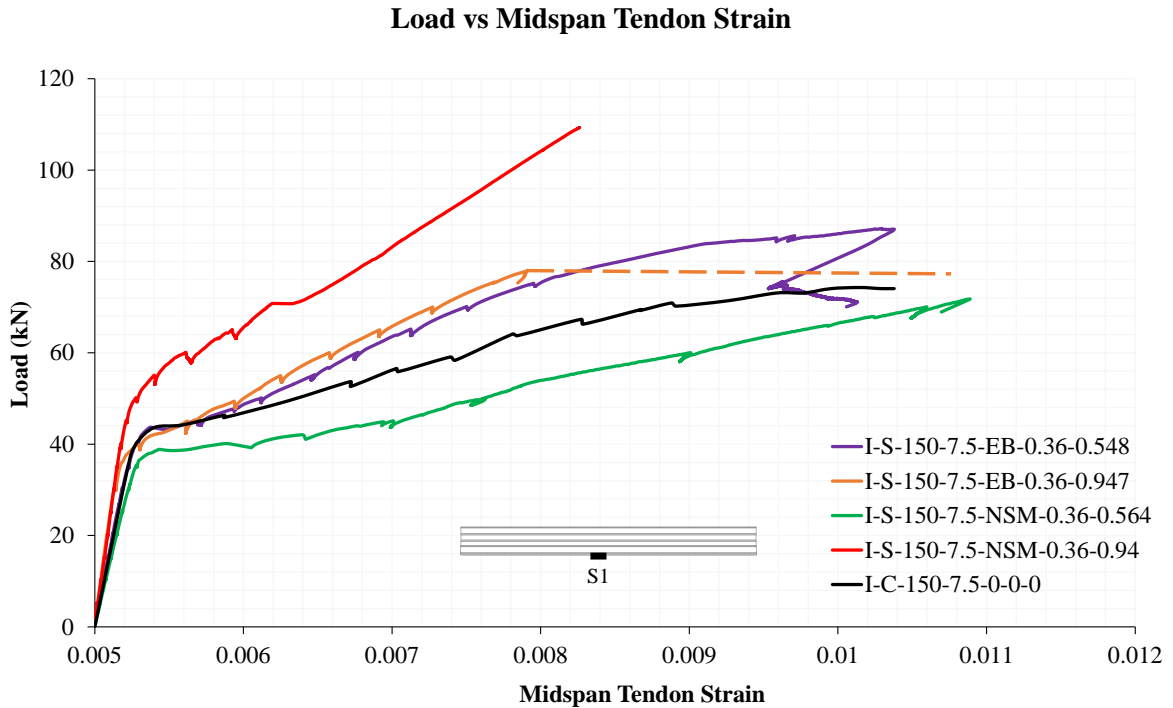


Figure 4.7: Series I - Load vs. Mid-span Tendon Strain

The ACI 440.2R-08 suggests that existing internal steel reinforcement should be prevented from yielding under service load levels. This is to avoid any inelastic deformations at service stage. The code limits the stresses in steel tendons to 82% of yield strength or to limit the compressive stress in the concrete to 45% of the compressive strength at service stage. As per ACI 440.2R-08, serviceability strain was determined from the maximum allowable stress in the prestressed steel which was found to be $\varepsilon_{ps,s} = 0.007064$. All of the strengthened specimens showed service load greater than the experimental cracking load (Fig 4.7). Corresponding to serviceability strain, service loads for different slabs determined from the experimental data are shown in Table 4.2.

Table 4.2: Service load for all the slabs - series I

Specimen code	Service load (kN)
I-C-150-7.5-0-0.36-0	55.84
I-S-150-7.5-EB-0.36-0.548	63.9
I-S-150-7.5-EB-0.36-0.947	66.26
I-S-150-7.5-NSM-0.36-0.564	44.5
I-S-150-7.5-NSM-0.36-0.94	83.31

By addition of externally bonded FRP, the service load increased by 18.6% with respect to control, by further increasing the EB FRP strengthening ratio increased the service load by 3.6 %. It is evident that increasing the strengthening reinforcement ratio does not provide a substantial enhancement to the capacity at the serviceability state thereby strengthening limit governs. In case of NSM FRP specimens, the service load was increased by 49.1 %, however for slab (I-S-150-7.5-NSM-0.36-0.564) there was decrease in service load which can be due to larger variability of concrete tensile strength and modulus. Slab(I-S-150-7.5-NSM-0.36-0.94) demonstrated highest enhancement in service load of 49.1%. Overall service loads can be significantly improved by FRP strengthening.

Yielding of prestressed tendons is marked by an increase in deflection of the member, or strain within the material, with no corresponding increase in load-carrying capacity which generates load plateau in the load-tensile strain curve. As pointed out in the previous sections, strengthened specimens exhibit a load-sharing mechanism between the internal steel reinforcement and the FRP reinforcement. Table 4.3 illustrates yield load for different specimens. By addition of externally bonded FRP ($\rho_{frp} = 0.00548$), the yield load increased by 16.19% with respect to control, by further increasing the EB FRP strengthening ratio to 0.0947 increased the yield load by only 5.07 % with respect to control, which can be due to abrupt debonding of external

FRP laminate, thereby sudden transfer of load from FRP to prestressed strand making it to yield quickly. Generally strain gauges are fragile and sensitive, at debonding due to sudden transfer of load to strand made the strain gauge to loose its potential in case of slab (I-S-150-7.5-EB-0.36-0.947), yield load for this slab is indicated by dashed line in Fig 4.7. In case of NSM FRP slab (I-S-150-7.5-NSM-0.36-0.564), yielding of prestressed tendons occurred at lower load level, which can be due to change of failure mode to shear failure. For slab (I-S-150-7.5-NSM-0.36-0.94) no yielding was noticed, which can be again due to change of failure mode to flexure-shear failure. By FRP strengthening, yielding can be delayed due to the reserve stiffness of the internal steel reinforcement due to load carrying contribution of FRP. Overall strengthened specimens experienced a noticeable enhancement in post-cracking stiffness, and correspondingly a significant increase in their respective yield loads.

Table 4.3: Yield load for all the slabs - series I

Specimen code	Yield load
I-C-150-7.5-0-0.36-0	74.04
I-S-150-7.5-EB-0.36-0.548	86.03
I-S-150-7.5-EB-0.36-0.947	77.8
I-S-150-7.5-NSM-0.36-0.564	66.41
I-S-150-7.5-NSM-0.36-0.94	No

Tensile strains in the EB-GFRP laminates and NSM-GFRP bars were measured using 5 mm electrical strain gauges. Fig 4.8 illustrates the load-midspan FRP strain for all strengthened specimens of series-I. Regrettably these strain gauges are highly susceptible to the damage and loose their potential when tensile cracks form in the vicinity of the gauges. Most of these strain gauges got damaged at or near failure, only the obtained strain data is plotted against load in Fig 4.8. It is evident that till tensile cracking of concrete, FRP does not contribute towards the load carrying mechanism (similar precracking stiffness). After cracking there is abrupt increase in strains in FRP and positive increase of stiffness(Slope) which indicates the load-sharing behaviour of FRP. For EB slabs increasing the strengthening reinforcement ratio decreases the strain in FRP laminates but there exist a strengthening limit, prior to which debonding may occur. In case of NSM slabs increasing the strengthening ratio certainly decreased the strains but may change the failure mode. So caution is necessary in designing the strengthening scheme.

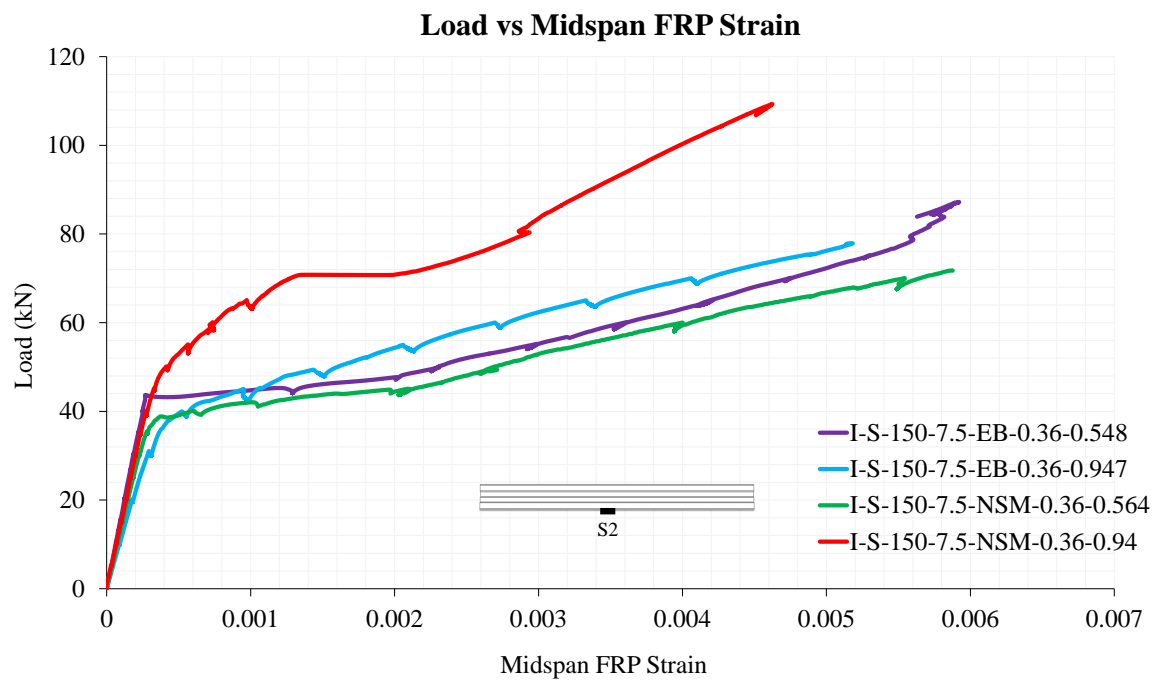


Figure 4.8: Series I - Load vs. Mid-span Tendon Strain

4.2.8 Cracking behaviour

Concrete is weak in tension due to its inherent very less tensile capacity (almost 10% of compression capacity). When applied load generates a tensile stress greater than tensile strength of the section, the concrete cracks. This load is called as cracking load. After which load-carrying mechanism is shared by internal prestressed strands and external reinforcement if present. Redistribution of load leads to the development of additional cracks and propagation of the existing cracks.

Control slab(I-C-150-7.5-0-0.36-0) exhibited typical flexural cracking behaviour. Initially a single crack formed at the cracking load. After which prestressed strands started contributed for load increase till the yield load was reached. At this point, new cracks formed with even spacing in the constant moment region. As the applied load neared to ultimate load, existing cracks started propagating towards neutral axis continued to widen. This occurred till the ultimate load is reached as shown in Fig 4.9.

Initial formation of cracks were similar at the cracking load for all the strengthened slabs. By application of EB GFRP laminates to the bottom surface of the slab effectively reduced the width of the cracks by redistributing the tensile stresses. As shown in Fig 4.9, greater number of cracks developed for the slabs strengthened with EB GFRP strips and NSM GFRP bars irrespective of strengthening ratios used. Along the constant moment region, larger cracks were evenly spaced. crack widths decreased while the number of cracks increased for all the strengthened specimens. These cracks where not limited only to constant moment zone but also developed along the shear span. Cracks were typically within a distance of $2d$ from the loading points. At certain load level, existing flexural cracks turned into flexure-shear cracks along the shear span of the strengthened specimens. Slab(I-S-150-7.5-EB-0.36-0.548) and (I-S-150-7.5-EB-0.36-0.947) ultimately failed by flexural crack propagating upwards where minor concrete crushing occurred below the load point. In case of slab(I-S-150-7.5-NSM-0.36-0.564) sudden shear tension crack occurred at failure. Slab (I-S-150-7.5-NSM-0.36-0.94) also exhibited the same pattern of cracking as that of its counterpart (slab I-S-150-7.5-EB-0.36-0.947) but ultimately flexure-shear crack occurred at failure. This indicates that increasing the NSM GFRP ratio effectively redistributed the stresses to the shear span by formation of more cracks. NSM FRP strengthened specimens exhibited high level of flexural cracking, indicating that the flexural strengthening limit was marginally violated.



Figure 4.9: Crack Pattern at Failure - Series I

4.2.9 Summary of key findings - Series I

Capacity and Mode of Failure

- The use of EB GFRP strengthening technique effectively enhanced the capacity of PPHC slabs by as much as 17.4%. This improvement in ultimate capacity lessened with increasing reinforcement ratio as premature debonding may govern the failure.
- As EB FRP strengthening ratio is increased, unfavourable debonding of laminates may occur which can be prevented through conscientious design of the system in terms of flexural strengthening limits.
- Having identical strengthening reinforcement ratio, the use of NSM GFRP strengthening technique showed highest enhancement in capacity of PPHC slabs by as much as 47.7%. when compared to EB GFRP technique.
- NSM technique resulted in optimum bond strength than EB technique revealing full composite action between the NSM GFRP bars and concrete.
- Increasing the strengthening reinforcement ratio can change the mode of failure form a ductile response to less ductile response.

Load-Strain Relationships

- The EB and NSM technique accommodated for the load-sharing mechanism between the internal prestressing reinforcement and FRP reinforcement thereby contributing towards load enhancement.
- In accordance with ACI 440.2R-05, all of the strengthened slabs showed service load enhancement from which having NSM technique demonstrated highest improvement in service load by as much as 49.1% making the NSM technique more attractive in serviceability governed applications.
- All of the strengthened showed service load greater than the experimental cracking load.

- By FRP strengthening, yielding can be delayed due to the reserve stiffness of the internal steel reinforcement due to load carrying contribution of FRP. Overall strengthened specimens experienced a noticeable enhancement in post-cracking stiffness, and correspondingly a significant increase in their respective yield loads.

Load-Deflection Relationships

- Strengthening of PPHC slabs with EB GFRP strips and NSM GFRP bars improved the overall load deflection response.
- Prior to cracking the load-deflection behaviour of unstrengthened and strengthened specimens was near identical. In case of EB FRP specimens, addition of thin EB FRP laminates slightly increased the section moment of inertia thereby cracking load was marginally increased. In case of NSM FRP specimens cracking loads slightly decreased to accommodate the redistribution of stresses caused by removing the concrete material during grooving.
- Pre-cracking stiffness for all the control and strengthened specimens was almost same. Different strengthening techniques demonstrated substantial influence on the slabs post-cracking response until the failure.
- Strengthening by EB GFRP strips showed decrease in ultimate deformability which is much pronounced in NSM GFRP bar strengthening technique indicating that, EB technique is much better in terms of overall ductility.
- In NSM FRP strengthened PPHC slabs, post-cracking response exhibited the highest stiffness improvement among all the tested slabs, despite its flexural-shear failure mode. This signifies that the extremely advantageous effect of increasing the NSM GFRP area when good bond is secured, should always be directed by flexural strengthening limits considerations precluding any abrupt changes in the failure mode.
- NSM strengthening technique using GFRP bars is more effective in strength governed applications than the EB GFRP laminates.

Cracking Behaviour

- Greater number of cracks developed for the slabs strengthened with EB GFRP strips and NSM GFRP bars irrespective of strengthening ratios used.
- Along the constant moment region, larger cracks were evenly spaced. crack widths decreased while the number of cracks increased for all the strengthened specimens. These cracks where not limited only to constant moment zone but also developed along the shear span.
- At certain load level, existing flexural cracks turned into flexure-shear cracks along the shear span of all the strengthened specimens.
- NSM FRP strengthened specimens exhibited high level of flexural cracking, indicating that the flexural strengthening limit was marginally violated.

4.3 Series II

4.3.1 Test Results, Mode of failure for Slab - II-C-250-5.4-0-0-0

As aforementioned this specimen was the control slab. The total span of this slab was 3,500 mm; the slab was loaded by two line loads 600 mm apart as shown schematically Fig 3.12. Control test specimen was subjected to four-point bending under simply-supported conditions, and was tested until ultimate failure was achieved. During the application of loading, the flexural cracks first appeared when the load reached 129 kN. Yielding of the prestressing tendons started when the load reached 160 kN. The peak load measured was 187 kN and corresponding mid-span deflection was 38.2 mm when the test was stopped.



Figure 4.10: Mode of failure - II-C-250-5.4-0-0-0 (control)

Failure progression involved: Flexural cracking at the bottom over the constant moment region; Crack propagation and distribution of cracks along the length of the specimen; Yielding of strands; Development of diagonal cracks as extensions of previously existing flexural cracks (flexure-shear cracking); Sudden compression failure below the loading point occurred as shown in Fig 4.10.

Inference: As the prestressing ratio was relatively on higher side, increased shear stresses at the tip of the crack led to development of diagonal cracks as extensions of previously existing flexural cracks (flexure-shear cracking). Due to the reduction of uncracked concrete section, lack of aggregate interlock as smaller size aggregates

were used, lack of shear reinforcement due to casting processes of hollow core slab, as there is little scope for redistribution of shear stresses after flexural-shear diagonal cracking, a sudden and violent flexure-shear diagonal tension failure accompanied by shear compression failure below the loading point was displayed as shown in Fig 4.10.

4.3.2 Test Results, Mode of failure for Slab - II-S-250-5.4-EB-0.372-0.549

This slab was strengthened using one sheet of GFRP at the bottom surface of the slab as shown in Fig 3.7, 500 mm width, 1 mm thickness and 3.5 meter length. It was shear strengthened with U-wrap having 250mm width, 300mm spacing longitudinally as shown in Fig 3.8. This test specimen was subjected to four-point bending under simply-supported conditions, and was tested until ultimate failure was achieved. During the application of loading, the flexural cracks first appeared when the load reached 130 kN. The presence of GFRP did not affect the pre-cracking stiffness and cracking load as expected. After cracking, internal prestressing reinforcement as well as external GFRP laminate started taking tensile stresses as anticipated, thereby stiffness increase was observed. Since the section was under-reinforced externally, as only one layer of GFRP laminate was applied as an external reinforcement, GFRP rupture took place when load reached 163 kN. After GFRP rupture, sudden drop of load was observed due to redistribution of stresses. Later on internal reinforcement i.e. prestressing strands continued to contribute for increase in load-carrying capacity.



Figure 4.11: Mode of failure - II-S-250-5.4-EB-0.372-0.549

Yielding of the prestressing tendons started when the load reached 167 kN. The

peak load measured was 178 kN and corresponding mid-span deflection was 49 mm. ACI 440.2R-08 (2008) recommends that strengthened specimens exhibit a ductile flexural response at the ultimate state, namely crushing of the concrete in compression.

Failure progression involved: Flexural cracking at the bottom over constant moment region; Further crack propagation, formation of distributed cracks along the length of the specimen; Bottom GFRP rupture; Yielding of strands; De-bonding of U-wraps; Development of diagonal cracks as extensions of previously existing flexural cracks (flexure-shear cracking); Sudden compression failure below the loading point occurred as shown in Fig 6.

Inferences: After cracking internal prestressing reinforcement as well as external GFRP laminate contributed for increase in load-carrying capacity. Further Pretensioned tendons continued to take load; Yielding of pretensioned strands. By premature debonding of U-wraps, shear strengthening was not fully utilized, increased shear stresses at the tip of the crack led to development of diagonal cracks as extensions of previously existing flexural cracks (flexure-shear cracking). There was little scope for redistribution of shear stresses after flexural-shear cracking due to the reduction in contribution by uncracked concrete section in shear, lack of aggregate interlock as smaller size aggregates were used and due to lack of shear reinforcement in casting processes of hollow core slab. The above factors led to a brittle flexure-shear diagonal tension failure accompanied by shear compression failure below the loading point as shown in Fig 4.12.

4.3.3 Test Results, Mode of failure for Slab - II-S-250-5.4-EB-0.372-1.647

This slab was strengthened using three sheets of GFRP laminate at the bottom surface of the slab as shown in Fig 3.7, 500 mm width, 1 mm thickness and 3.5 meter length. It was shear strengthened with U-wrap having 250mm width, 300mm spacing longitudinally as shown in Fig 3.8. This test specimen was subjected to four-point bending under simply-supported conditions, and was tested until ultimate failure was achieved. During the application of loading, the flexural cracks first appeared when the load reached around 130 kN. The presence of GFRP did not affect the pre-cracking stiffness and cracking load as expected. After cracking internal prestressing reinforcement as well as external GFRP laminate started taking tensile stresses as anticipated, thereby stiffness increase was observed. Yielding of the prestressing tendons started when the load reached around 209 kN. Premature debonding of GFRP laminate was observed when the load reached 229 kN and at a displacement of 30 mm. Later on internal reinforcement i.e pretensioned strands continued to contribute to load resistance upto ultimate failure. Sudden flexure-shear diagonal crack occurred at peak

load of 234.3 kN corresponding to a displacement of 40.7 mm.



Figure 4.12: Mode of failure - II-S-250-5.4-EB-0.372-1.647

Failure progression was as follows: few flexural cracks at the constant moment region; Crack propagation, formation of distributed flexural cracks along the length of the specimen; flexure-shear diagonal tension cracking; Diagonal cracks developed at a distance $2d$ to $4d$ distance (shear span) from the face of the support, which led to the cracking and debonding of U-wraps; One of the diagonal cracks widened into a principal diagonal tension crack and extended to the top compression fibre of the slab as shown in Fig 4.12. Pure flexural cracks did not propagate to the level of neutral axis as there is a change of failure mode. As the loading increased further, debonding of the bottom GFRP occurred at a previously formed flexure-shear diagonal crack. This resulted in further propagation leading to sudden and violent failure as shown in Fig 4.12.

Inferences: Due to increase in FRP external strengthening ratio from 0.00537 to 0.01647, the mode of failure after yielding of prestressing strands changed to shear dominated failure. With further loading, load levels reached the flexure-shear capacity of the member leading to flexure-shear diagonal tension cracking. This further led to destruction of bond between the prestressing steel and the surrounding concrete at the support. Thereafter, more diagonal cracks developed at a distance $2d$ to $4d$ distance (shear span) from the face of the support. This severe cracking which led to the debonding of U-wraps. One of the diagonal cracks widened into a principal diagonal tension crack and extended to the top compression fibers of the slab as

shown in Fig 4.12 at the shear span. This can be considered as diagonal-tension failure where favorable influence of the vertical normal stresses caused by the reactive force at support is exhausted. It is worth mentioning that flexural cracks did not propagate to the neutral axis as there is a change of failure mode. As the loading increased further, debonding of the bottom GFRP took place. Previously formed flexure-shear diagonal crack started propagating up to the top shear-compression zone and thereby leading to sudden failure with a major flexure-shear crack as shown in Fig 4.12.

4.3.4 Test Results, Mode of failure for Slab - II-S-250-5.4-NSM-0.372-0.62

Specimen II-S-250-5.4-NSM-0.372-0.62 was outfitted with five GFRP bars of 12 mm dia each. It was shear strengthened with U-wrap having 250mm width, 300mm spacing longitudinally as shown in Fig 3.8. During the application of loading, the flexural cracks first appeared when the load reached around 130 kN. The presence of NSM GFRP did not affect the pre-cracking stiffness and cracking load as expected. After which NSM GFRP bars and pretensioned strands contributed for load increases. Sudden and violent flexure-shear diagonal crack occurred at peak load of 166 kN corresponding to a displacement of 20 mm.



Figure 4.13: Mode of failure - II-S-250-5.4-EB-0.372-1.647

Failure progression involved: Flexural cracking at the bottom over constant moment region; Crack propagation, formation of distributed cracks along the length of

the specimen; No yielding of Pretensioned strands; Development of diagonal cracks as extensions of previously existing flexural cracks (flexure-shear cracking); One of the diagonal cracks widened into a principal diagonal tension crack and extended to the top compression fibre of the slab; Sudden compression failure below the loading point occurred as shown in Fig 4.13.

Inferences: After cracking internal prestressing reinforcement as well as external GFRP laminate contributed for increase in load-carrying capacity; No yielding of Pretensioned tendons was noticed; By premature debonding of U-wraps, shear strengthening was not fully utilized, increased shear stresses at the tip of the crack led to development of diagonal cracks as extensions of previously existing flexural cracks (flexure-shear cracking). There was little scope for redistribution of shear stresses after flexural-shear cracking due to the reduction in contribution by uncracked concrete section in shear, lack of aggregate interlock as smaller size aggregates were used and due to lack of shear reinforcement in casting processes of hollow core slab. The above factors led to a brittle flexure-shear diagonal tension failure accompanied by shear compression failure below the loading point as shown in Fig 4.13.

4.3.5 Load-deflection relationships

Fig 4.6 shows the load versus the mid-span deflection(D1) response for all the tested slabs of series II. Table 4.4 summarize the experimental test results for all Series II specimens.

Pertaining to the load-midspan deflection behaviour of control specimen (I-C-150-7.5-0-0.36-0) is same as any under-reinforced prestressed section. During initial stages of loading the section is uncracked and exhibit a linear-elastic behaviour. Concrete cracks after attaining its tensile capacity, then behaviour changes from uncracked to cracked-elastic as pointed out by change in slope of the curve(Fig 4.14). As the load is increased, pretensioned strands start to take load and the section responds elastically until the yield strength is reached. At the yielding of strands, load-deflection curve flattens, and no further increase in moment capacity is observed. Ultimately slab failed by top concrete crushing.

Prior to cracking the load-deflection behaviour of unstrengthened and strengthened specimens was near identical. For each slab, the cracking load was determined based on the change in slope of the load-deflection curve. In case of EB FRP specimens, addition of thin EB FRP laminates slightly increased the section moment of inertia due to which cracking load was marginally increased. In case of NSM FRP

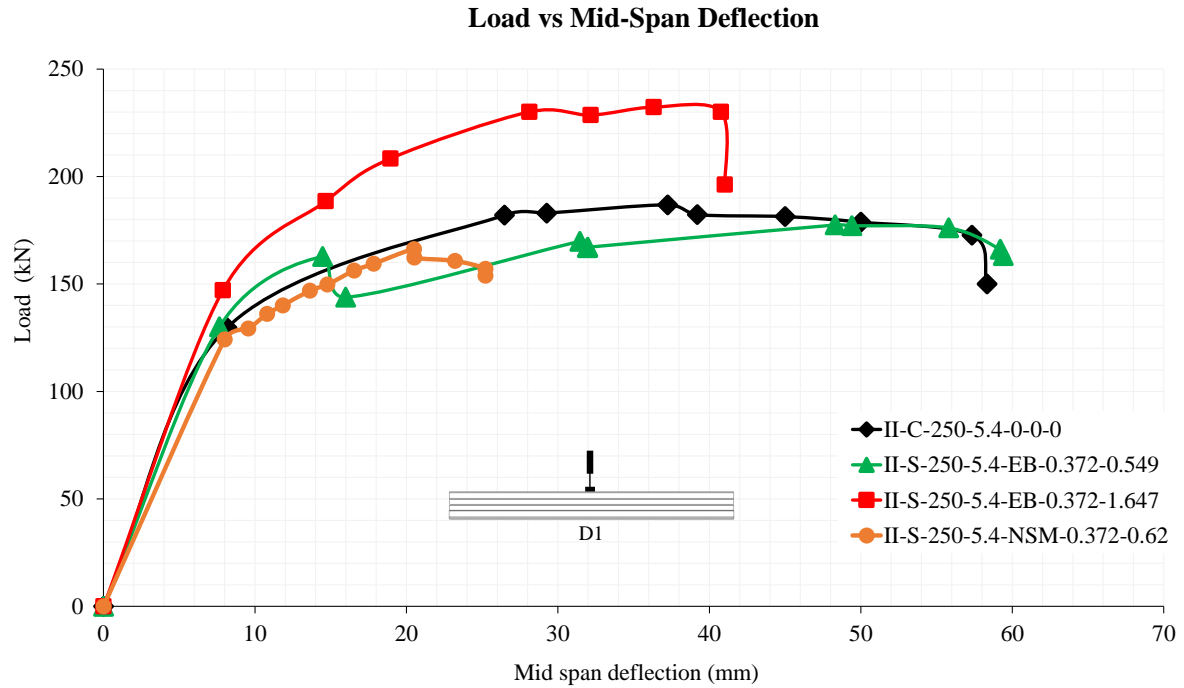


Figure 4.14: Series II - Load vs. Mid-span Deflection

specimens cracking load remained as control. Pre-cracking stiffness for all the control and strengthened specimens was almost same as much of the composite action takes place after cracking. After flexural cracking, the tensile stresses are transferred from the concrete substrate to the internal and external reinforcement if any. Different strengthening techniques demonstrated substantial influence on the slabs post-cracking response until the failure. Unlike control, FRP reinforcement continued to provide the required stiffness to the system in order to sustain the increasing load. This post-cracking stiffness increase is dependent on the FRP reinforcement ratio and strengthening scheme used.

Slab (II-S-250-5.4-EB-0.372-0.549) demonstrated a considerable increase in post cracking stiffness but slight decrease in capacity, since the section was under-reinforced externally, as only one layer of GFRP laminate was applied as an external reinforcement, GFRP rupture took place. After GFRP rupture, sudden drop of load was observed due to redistribution of stresses. Later on internal reinforcement i.e. pre-stressing strands continued to contribute for increase in load-carrying capacity. The ultimate deflection was increased from 36 mm to 48 mm with respect to control specimen. The addition of one layer of GFRP laminate increased the deflection ductility by 8.6%. Increasing the strengthening ratio, for Slab(II-S-250-5.4-EB-0.372-1.647) significant increase in post cracking stiffness was noted with a capacity enhance-

ment of 25.3%. Addition of three layers of GFRP laminates showed the highest post cracking stiffness improvement among all the tested slabs of series II. The ultimate deflection was increased from 36 mm to 40.79 mm with respect to control specimen. Slight increase in deflection ductility was observed. Overall deflection ductility was increased for EB strengthened slabs subjected to high shear, due to the presence of U-wraps (shear strengthening) which makes this technique more suitable for seismic applications

In case of NSM FRP slab(II-S-250-5.4-NSM-0.372-0.62), reduction in capacity and deformability was noticed, which could be attributed to its brittle flexure-shear failure mode. This slab showed similar post-cracking stiffness as the control slab. Flexure-shear failure capacity of this slab being lower than that of control might be due to either due to large variability in concrete tensile strength or manufacturing defect. In case of high shear, the higher improved stiffness of the EB technique over NSM technique makes it more appealing for use in serviceability governed applications.

Table 4.4: Experimental results - Series II

<i>Parameter</i>	II-C-250-5.4-0-0-0	II-S-250-5.4-EB-0.372-0.549	II-S-250-5.4-EB-0.372-1.647	II-S-250-5.4-NSM-0.372-0.62
Flexural strengthening ratio	-	0.00537	0.01612	0.0062
Shear strengthening ratio	-	0.01028	0.01028	0.01028
First crack load KN	129	130	130	130
First crack displacement mm	6.9	7	7	8
Yielding load KN	181.8	169.4	206.3	NO
Yielding displacement mm	25.8	31.39	29	NO
Peak load KN	186.9	178.2	234.3	167
Peak displacement mm	36.32	47.9	40.79	20
Ultimate load KN	173.5	173.6	231.9	167
Ultimate displacement mm	57.3	57.4	41.7	20
Deflection ductility	1.40	1.52	1.406	-
Failure Modes	Flexure-shear Failure	Rupture of GFRP, Flexure-shear crack	Debonding of GFRP, minor diagonal shear crack & Flexure-shear crack	Flexure-shear failure

4.3.6 Cracking behaviour

Initial formation of cracks were similar at the cracking load for all the strengthened slabs. By application of EB GFRP laminates to the bottom surface of the slab effectively reduced the width of the cracks by redistributing the tensile stresses. As shown in Fig 4.15, greater number of cracks developed for the slabs strengthened with EB GFRP strips and NSM GFRP bars irrespective of strengthening ratios used.

Along the constant moment region, larger cracks were evenly spaced. crack widths decreased while the number of cracks increased for all the strengthened specimens. These cracks where not limited only to constant moment zone but also developed along the shear span. Cracks were typically within a distance of $2d$ from the loading points. At certain load level, existing flexural cracks turned into flexure-shear cracks along the shear span of the strengthened specimens.



Figure 4.15: Crack Pattern at Failure - Series II

4.3.7 Summary of key findings - Series II

Capacity and Mode of Failure

- The use of EB GFRP strengthening technique effectively enhanced the flexure-shear capacity of PPHC slabs by as much as 25.3% without any compromise in deflection ductility.
- As EB FRP strengthening ratio is increased, unfavourable debonding of laminates may occur which can be prevented through conscientious design of the system in terms of flexural strengthening limits.
- NSM technique resulted in optimum bond strength than EB technique revealing full composite action between the NSM GFRP bars and concrete.
- Increasing the strengthening reinforcement ratio can change the mode of failure from a ductile response to less ductile response.
- Shear strengthening with U-wrap layers acted as an anchorage and prevented premature debonding failure mode.

Load-Deflection Relationships

- Strengthening of PPHC slabs with EB GFRP strips and NSM GFRP bars improved the overall load deflection response.
- Prior to cracking the load-deflection behaviour of unstrengthened and strengthened specimens was near identical. In case of EB FRP specimens, addition of thin EB FRP laminates slightly increased the section moment of inertia thereby cracking load was marginally increased. In case of NSM FRP specimens cracking loads slightly decreased to accommodate the redistribution of stresses caused by removing the concrete material during grooving.
- Pre-cracking stiffness for all the control and strengthened specimens was almost same. Different strengthening techniques demonstrated substantial influence on

the slabs post-cracking response until the failure.

- By FRP strengthening, yielding can be delayed due to the reserve stiffness of the internal steel reinforcement due to load carrying contribution of FRP. Overall strengthened specimens experienced a noticeable enhancement in post-cracking stiffness, and correspondingly a significant increase in their respective yield loads.
- Strengthening by EB GFRP strips showed decrease in ultimate deformability which is much pronounced in NSM GFRP bar strengthening technique indicating that, EB technique is much better in terms of overall ductility.
- Addition of flexural laminates increased the deflection ductility for lower strengthening ratios as their failure modes were not significantly altered.
- Flexural GFRP strengthening (high ratio) effectively enhanced the capacity up to 26%. Post-cracking stiffness also increased significantly due to the beneficial effect of anchorage effect provided by U-wrapping.
- Low FRP ratio resulted in earlier debonding followed by rupture of FRP sheet and did not produce significant increase in the ultimate capacity. Marginal improvement in post-cracking stiffness was observed. However, it degraded to the stiffness of control slab after rupture of FRP sheets.
- High FRP ratio resulted in good improvement in ultimate strength, post-cracking stiffness. However, there was decrease in displacement at failure indicating reduction in ductility due to FRP strengthening.
- In high shear conditions, shear strengthening improved the deflection ductility of PPHC slabs
- NSM strengthening changed the failure from flexure dominant to more shear dominant behaviour. Due to change in the failure mode, NSM slabs failed in a brittle manner leading to no increase in strength. Future work should focus on improving the efficiency of NSM strengthening on behaviour of hollow core slabs

at low a/d ratios.

- For lower a/d ratio (shear dominant), EB GFRP strengthening in terms of flexure and shear strengthening increased the capacity of PPHC slabs as well as improved the deflection ductility making it more attractive for strength and seismic governed applications

Cracking Behaviour

- Greater number of cracks developed for the slabs strengthened with EB GFRP strips and NSM GFRP bars irrespective of strengthening ratios used.
- Along the constant moment region, larger cracks were evenly spaced. crack widths decreased while the number of cracks increased for all the strengthened specimens. These cracks were not limited only to constant moment zone but also developed along the shear span.
- At certain load level, existing flexural cracks turned into flexure-shear cracks along the shear span of all the strengthened specimens.
- GFRP strengthening by EB strips and NSM bars resulted in uniform distribution of cracks relative to control PHC slab which failed by few major cracks.
- EB GFRP strengthened specimens exhibited high level of flexural cracking, making the ultimate flexure shear failure mode more ductile.

Chapter 5

Analytical and Finite Element Study

5.1 General

Analytical study was carried out using strain compatibility approach and in accordance with ACI 318-05 [11], ACI 440.2R-08 [7]. Comparison with experimental and predicted values was made. Numerical investigations were performed by using a finite element analysis (FEA) software package - ABAQUS. Details of these studies are mentioned in the following sections.

5.2 Analytical Study

In this section, the analytical model is briefly explained. Flexural analysis of PPHC slabs was carried out, which consists of section analysis based on strain compatibility approach to predict the ultimate capacity. This section summarizes the calculations for cracking moment, failure load for the control and strengthened slabs. Shear capacity predictions are calculated based on ACI 318-05 specifications. Finally, predicted response is compared with experimental test results.

5.2.1 Material Properties

Concrete

Concrete was modeled using parabolic stress-strain relationship in compression as shown in Fig 5.1. concrete compressive force is approximated by Whitney equivalent rectangular stress block method using the parameters α and β . These stress block parameters were calculated such that the magnitude and location of the resultant

compressive force did not change. Equations of α and β are given in Eq.5.1, 5.2 respectively. Peak compressive concrete strain ε'_c was taken as 0.002, maximum compressive concrete strain ε_{cu} was taken as 0.0035.

$$\alpha = \frac{1}{\beta} \left(\frac{\varepsilon_c}{\varepsilon'_c} - \frac{1}{3} \left(\frac{\varepsilon_c}{\varepsilon'_c} \right)^2 \right) \quad (5.1)$$

$$\beta = \frac{4 - \frac{\varepsilon_c}{\varepsilon'_c}}{6 - \frac{2\varepsilon_c}{\varepsilon'_c}} \quad (5.2)$$

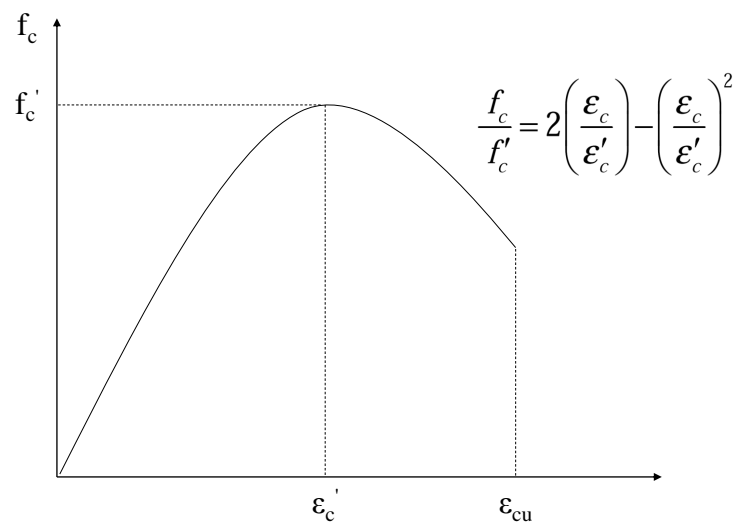


Figure 5.1: Parabolic stress-strain curve of concrete

Prestressed strand

The tensile properties of low relaxation steel strands were based on the coupon testing. The tensile strength, yield stress and modulus of elasticity used in the analytical calculations were 1860 MPa, 1680 MPa and 195 GPa.

GFRP laminates

Linear elastic stress-strain behaviour of the GFRP laminates (sheet & bars) was obtained by coupon testing. A tensile modulus of GFRP sheet and GFRP bar was 14 GPa and 49 GPa respectively. An ultimate tensile strain of 0.017 for GFRP sheet and 0.016 for GFRP bar was used in analytical calculations.

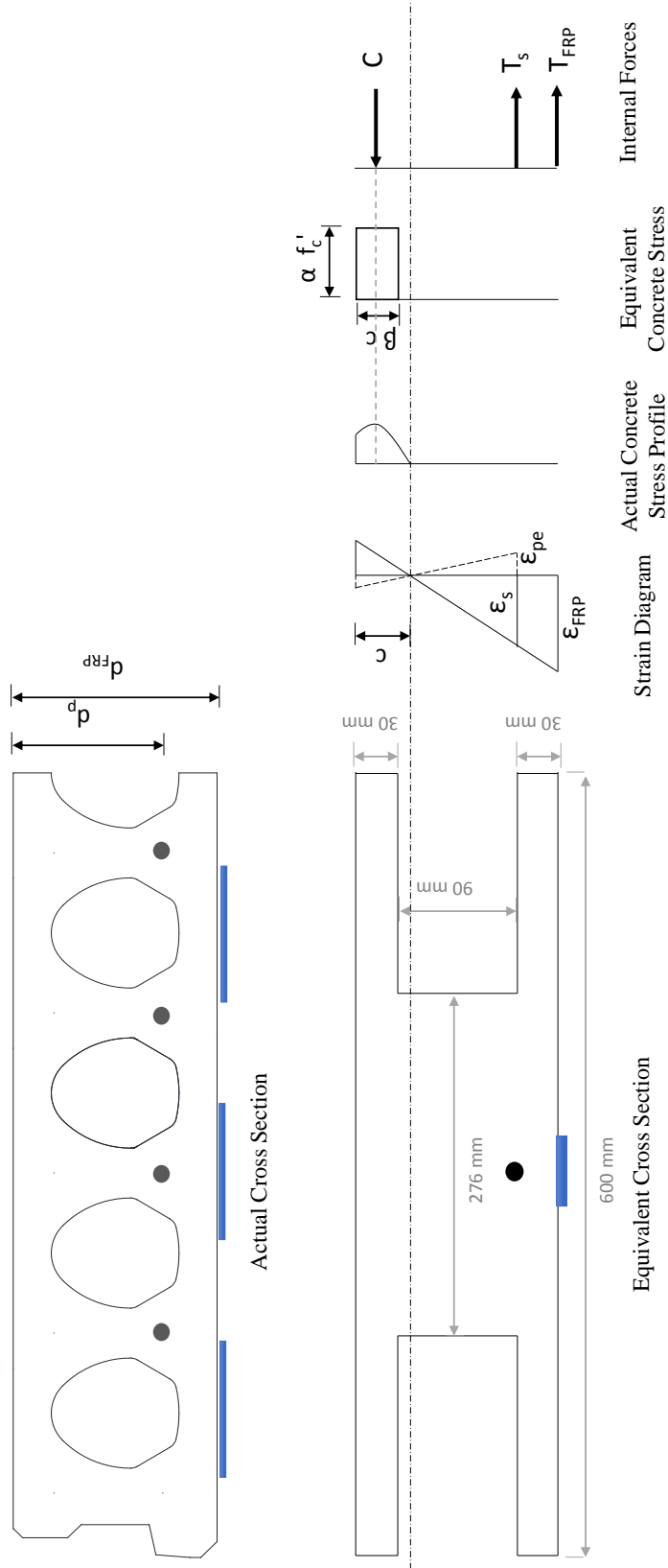


Figure 5.2: Strain compatibility of concrete section strengthened by FRP composite

5.2.2 Cracking moment

The cracking moment (M_{cr}) is calculated based on the gross moment of inertia and gross cross section area. Tensile strength (f_{cr}) of concrete is assumed to be given by Eq.5.4 and equal to the maximum tensile concrete stress. External reinforcement contribution towards cracking moment is neglected for simplification as no significant change is observed.

$$f_{cr} = 0.7\sqrt{f_{ck}} \quad (5.3)$$

$$M_{cr} = f_{cr}I/y_b + P_e e + P_e I/y_b A \quad (5.4)$$

where P_e is the effective prestressing force after all losses, I is gross moment of inertia, A is gross cross section area, y_b distance from the centroid to the extreme tension fiber.

5.2.3 Ultimate Flexural Load Capacity of PPHC slab

Flexural capacities of unstrengthened and strengthened PPHC slabs are calculated as per ACI 318-05 [11], ACI 440.2R-08 [7]. Governing failure modes like compressive concrete crushing before yielding of steel, rupture of tensile FRP, debonding of FRP are taken into account. An iterative analytical method to analyse the response of FRP strengthened slab specimens is established based on strain compatibility and equilibrium. Elastic-perfectly plastic stress-strain relationship was used for prestressing steel and linear elastic relationship was used for GFRP sheet & bar using the data provided in section 3.4. Mid-span section was chosen for calculations.

Based on the strain compatibility and equilibrium of internal forces, total flexural response of the section can be obtained by following the below steps:

- Assume concrete compressive strain ε_c thereby calculate α and β .
- Assume certain neutral axis depth, c .
- Calculate strains at level of prestressed strands ε_{ps} and FRP laminates ε_f from below equations.

$$\varepsilon_{ps} = \varepsilon_{pe} + \varepsilon_{ce} + \varepsilon_s \quad (5.5)$$

$$\varepsilon_s = \varepsilon_c \frac{d_p - c}{c} \quad (5.6)$$

$$\varepsilon_{frp} = \varepsilon_c \frac{d_f - c}{c} \quad (5.7)$$

$$\varepsilon_{fd} = 0.41 \sqrt{\frac{f'_c}{nE_f t_f}} \quad (5.8)$$

where,

ε_c = concrete strain at extreme compressive fiber

ε_{ps} = total strain in prestressed strand

ε_{pe} = effective strain in prestressed strand after losses

ε_{ce} = strain in concrete at the level of prestressed strand due to prestressing force

ε_s = strain in prestressed strand resulted from strain compatibility due to external moment

ε_{frp} = strain in FRP reinforcement resulting from strain compatibility

ε_{fd} = debonding strain in FRP reinforcement

- Determine the internal forces in the compression (C) and the tension regions ($T = T_s + T_{frp}$) based on the strains obtained, using constitutive relationships respectively.
- Check the equilibrium of the section by equating, $T - C = 0$ and simultaneously iterating the assumed value of neutral axis depth (c) till equilibrium of forces is satisfied.
- Calculate the moment, by multiplying the total internal compressive force (C) with its corresponding lever arm.
- Curvature can be calculated as, $\phi = \varepsilon_c / c$
- Finally, flexural failure moments corresponding to compressive concrete crushing (M_{fc}), tensile GFRP rupture (M_{ft}) and debonding of GFRP (M_{fd}) can be calculated.

5.2.4 Shear Capacity Prediction of PPHC slab

Shear strength of concrete members without web reinforcement is difficult to predict and the experimental results corroborate this by demonstrating a wide scatter. PPHC slabs likewise fall into this class with added complexity due to broad array of void

shapes in the cross section and the stresses developed at the voids during manufacturing process. These stresses tend to reduce the shear strength of the webs in PPHC slabs. Two predominant shear failures which are possible in PPHC slabs are due to the development of either flexural shear cracks or the web shear cracks depending on the shear span to depth ratio (a/d) in the loading arrangement. ACI 318 [11] code equations were used in this study for computation of flexural-shear and web-shear strength. Equations where the effect of prestressing steel is taken into consideration for the calculation of flexural-shear capacity (V_{ci}) are given below.

$$V_{ci} = V_{fs} + V_{ds} + V_d \quad (5.9)$$

For four point loading configuration, diagonal cracks can develop as extensions of previously existing flexural cracks. These flexural-shear cracks initiates in the region of high moment combined with significant shear. Generally taken as $d/2$ distance away from the point load. In this region, diagonal shear crack developed will coincide with the principal tension plane in concrete and extends into the flexural compression zone. The cracking moment (M_{cr}) is then given as

$$M_{cr} = \frac{I}{y_b} \left(\frac{\sqrt{f'_c}}{2} + f_{pe} - f_d \right) \quad (5.10)$$

$$V_{fs} = \frac{V_i M_{cr}}{M_{max}} \quad (5.11)$$

$$V_{ds} = 0.05 \sqrt{f'_c} b_w d_p \quad (5.12)$$

where,

V_{fs} = shear force that exists where flexural shear cracks are developed;

V_{ds} = additional shear force required to initiate the diagonal segment of the shear crack;

V_d = shear force at the section due to unfactored dead loads only;

V_i = factored shear force at the considered section due to externally applied load

M_{max} = factored moment at the considered section due to externally applied load;

f_{pe} = compressive stress in concrete at the bottom due to effective prestressing force only;

f_d = stress due to unfactored dead load at the bottom;

$$V_{ci} = 0.05 \sqrt{f'_c} b_w d_p + \frac{V_i M_{cr}}{M_{max}} + V_d \geq 0.17 \sqrt{f'_c} b_w d \quad (5.13)$$

In high shear zone(web region), principal tensile stress directions are inclined to the longitudinal axis of the member, hence diagonal shear cracks develop in the web when the principal tensile stress exceeds the tensile strength of concrete. These diagonal cracks initiate in the web of the PPHC slabs where the thickness of web is minimum, located close to the neutral axis and then propagates diagonally as the load is increased. The web shear capacity (V_{cw}) of prestressed member is given as

$$V_{cw} = (0.29\sqrt{f'_c} + 0.3f_{pc})b_wd_p + V_p \quad (5.14)$$

where f_{pc} is the effective prestress at the centroid of the slab. As the prestressing strands are horizontal for PPHC slab, beneficial vertical component of prestressing force is non-existent ($V_p = 0$).

Expression 5.13 is a function of applied load (P -test), which implies that values of V_{ci} , V_i and M_{max} can be calculated only when applied load (P -test) is known. Spreadsheet was developed including a criterion for failure whenever shear force ($V_i + V_d$) becomes equal to shear resistance $V_c = \min(V_{cw}, V_{ci})$ at any point between the load and the face of support. Load (P -test) was iterated until first failure point was identified when $V_c = (V_i + V_d)$ and the corresponding load (P -test) value is taken as the predicted failure load. Shear strength is the lesser of flexure-shear and web shear capacity.

5.2.5 Deflection Prediction of PPHC slab

Deflection was calculated analytical for various unstrengthened and strengthened PPHC slabs using numerical integration of curvature at many sections along the span according to below equations. To accommodate for any abrupt curvature change, numerical integration was performed at five sections along the half span of the slab. In this regards, the selected sections were at the support, location between the support and the cracking moment, location where applied moment equals cracking moment, location of the concentrated load and location at mid-span as shown in Fig 5.3

$$\Delta = \sum_{k=1}^n \left(\frac{\phi_k x_k + \phi_{k+1} x_{k+1}}{2} \right) \Delta x_k \quad (5.15)$$

where,

Δ = mid-span deflection;

ϕ_k = curvature corresponding to a distance x_k from the support;

ϕ_{k+1} = curvature corresponding to a distance x_{k+1} from the support;

Δx_k = length of segment, $(x_{k+1} - x_i)$;

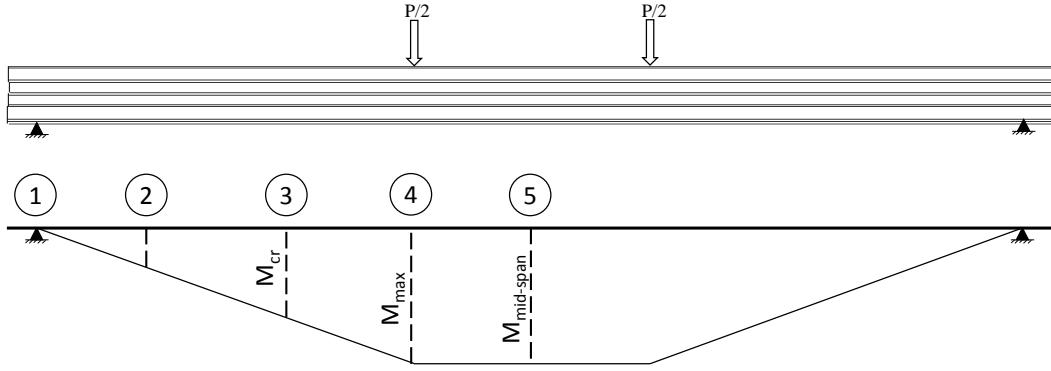


Figure 5.3: Numerical integration of curvature at different locations

The moment corresponding to the chosen load level is first determined at each selected section and equilibrium of internal tensile and compressive forces is established in an iterative procedure to determine top fibers compressive concrete strain (ε_c), corresponding neutral axis depth (c). The sectional curvature (ϕ) at the chosen load level is calculated using the Eq 5.16. Mid span deflection is then calculated using the Eq 5.15.

$$\phi = \frac{\varepsilon_c}{c} \quad (5.16)$$

5.2.6 Comparison between Predicted and Experimental Results

5.2.6.1 Capacity and mode of failure

Analytical prediction of capacity and mode of failure, was carried out as explained in the previous sections. For each slab, the predicted failure mode is the one resulting in the least analytical capacity (P_u). Analytical Cracking load (P_{cr}), failure load (P_u), failure modes are compared with experimental test results, shown in Table 5.1. The table shows excellent correlations between the analytical and experimental capacities and failure modes. In series I, for slab (I-S-150-7.5-EB-0.36-0.548) predicted failure mode was debonding of GFRP but due to very less difference between the predicted debonding load and rupture load, actual observed failure mode was rupture of GFRP. For slab (I-S-150-7.5-NSM-0.36-0.564) failure mode prediction(flexure-shear) is not same as actual observed failure mode (shear tension failure) which can be either due to variability of concrete tensile strength or manufacturing defect. For rest of the slabs fair prediction of capacities and failure modes is observed.

In case of series II, for control slab(II-C-250-5.4-0-0-0) predicted failure mode(i.e flexure-shear failure) is same as actual experimental failure mode. For slab (II-S-250-

5.4-EB-0.372-0.549) predicted failure mode is matching with experimental failure mode, however the flexure-shear capacity predicted by ACI equations is lower than experimental failure load. For slab (II-S-250-5.4-EB-0.372-1.647) predicted failure mode was flexure-shear but actual experimental failure mode is diagonal shear failure mode, however the web-shear capacity predicted by ACI equations is significantly higher than experimental web-shear load. Indicating that the ACI code equations needs to be modified in order to predict the ultimate load capacity accurately and capture the correct failure mode.

Table 5.1: Comparison between the predicted and the experimental results

<i>Specimen</i>	<i>Analytical Results</i>							<i>Experimental Results</i>			Pu (exp) / Pu(analy.)
	P_{cr} (KN)	P_{fc} (KN)	P_{fa} (KN)	P_{ft} (KN)	P_s (KN)	P_u (KN)	<i>Mode of failure</i>	P_{cr} (KN)	P_u (KN)	<i>Mode of failure</i>	
I-C-150-7.5-0-0.36-0	42.69	73.05	-	-	102.3	73.05	Flexural failure	44	74.24	Flexural failure	1.016
I-S-150-7.5-EB-0.36-0.548	42.69	87.63	84.70	86.08	102.3	84.7	De-bonding of GFRP	45	87.19	Rupture of GFRP	1.029
I-S-150-7.5-EB-0.36-0.947	42.69	95.501	93.11	95.03	102.3	93.11	De-bonding of GFRP	45	78	De-bonding of GFRP	0.837
I-S-150-7.5-NSM-0.36-0.564	42.69	110.64	116.12	120.79	102.3	102.3	Flexure-shear	42	71.8	Shear failure	0.701
I-S-150-7.5-NSM-0.36-0.94	42.69	119.23	138.98	145.92	102.3	102.3	Flexure-shear	44	109.3	Flexure-shear	1.068

Series I

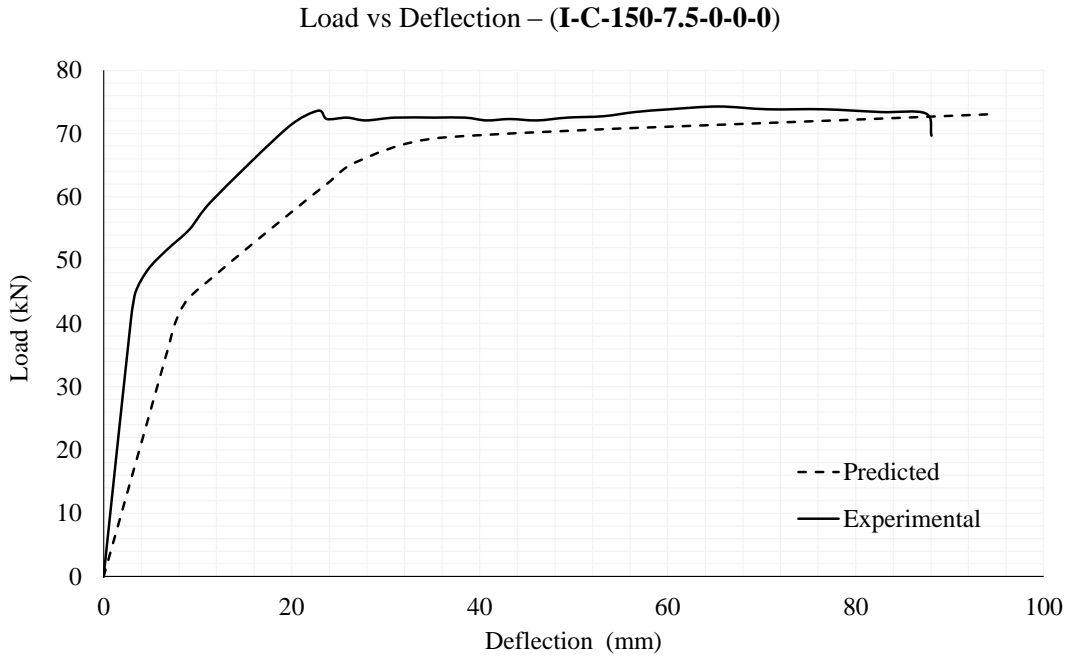


Figure 5.4: Predicted and experimental load vs deflection - I-C-150-7.5-0-0.36-0

5.2.6.2 Deflections

Comparison between the predicted and experimental load-deflection response of slabs is shown in figures (Fig 5.4 - 5.10). Good correlation was observed between the analytical and experimental load deflection response of the slabs. Entire load deflection behaviour was predicted fairly, however precracking stiffness was lower than the experimental which can be due to either underestimated concrete elastic modulus in the analysis or may be due to limited number of sections considered for numerical curvature integration process.

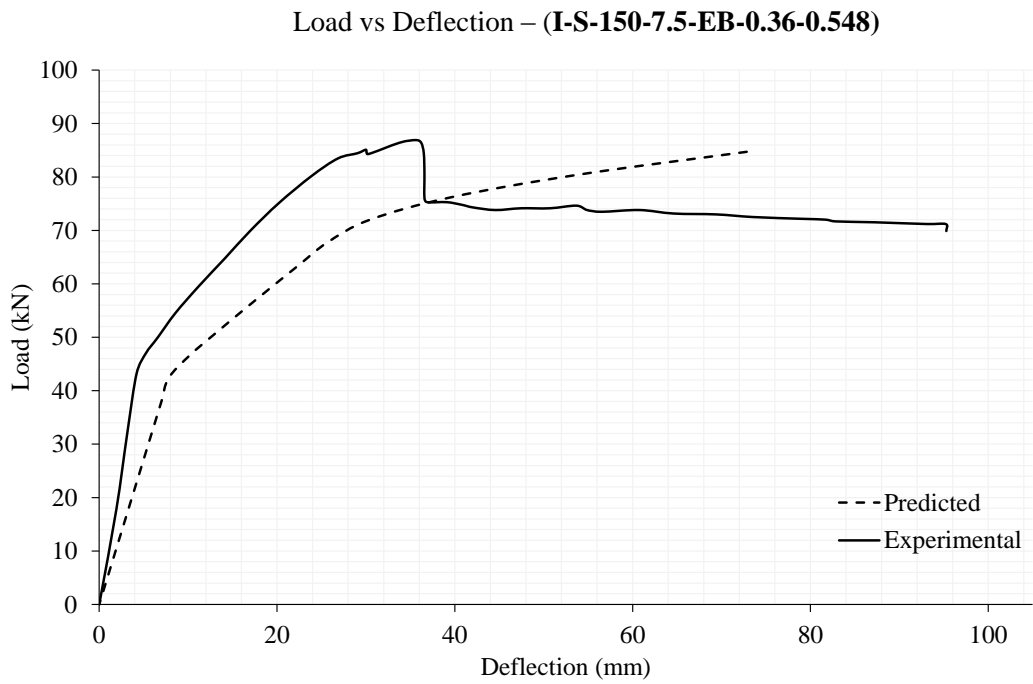


Figure 5.5: Predicted and experimental load vs deflection - I-S-150-7.5-EB-0.36-0.548

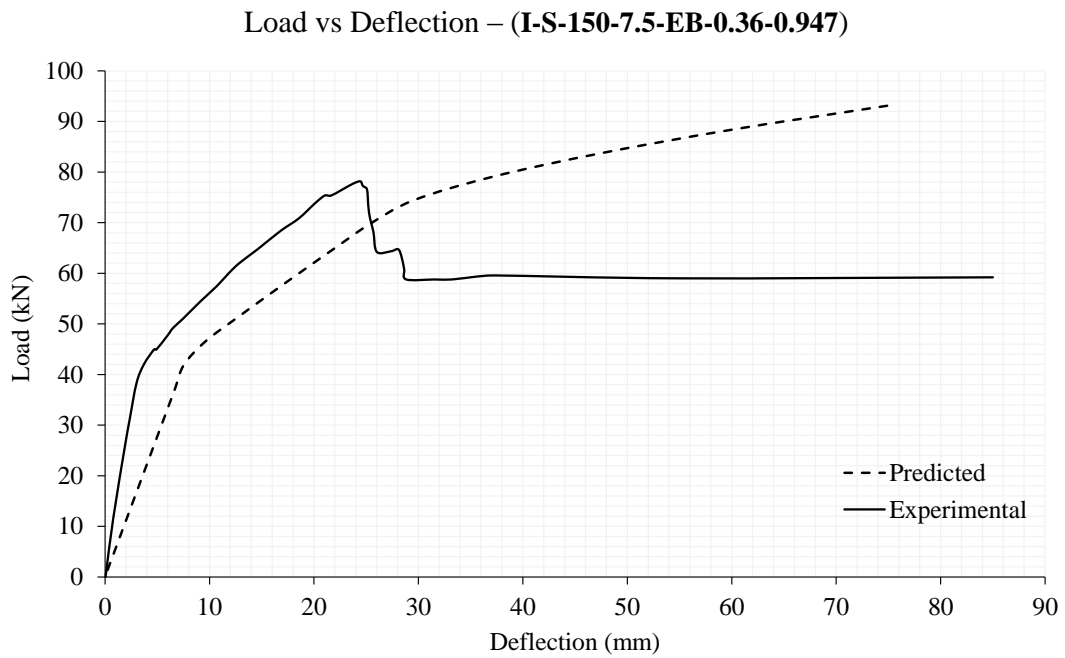


Figure 5.6: Predicted and experimental load vs deflection - I-S-150-7.5-EB-0.36-0.947

Load vs Deflection – (I-S-150-7.5-NSM-0.36-0.564)

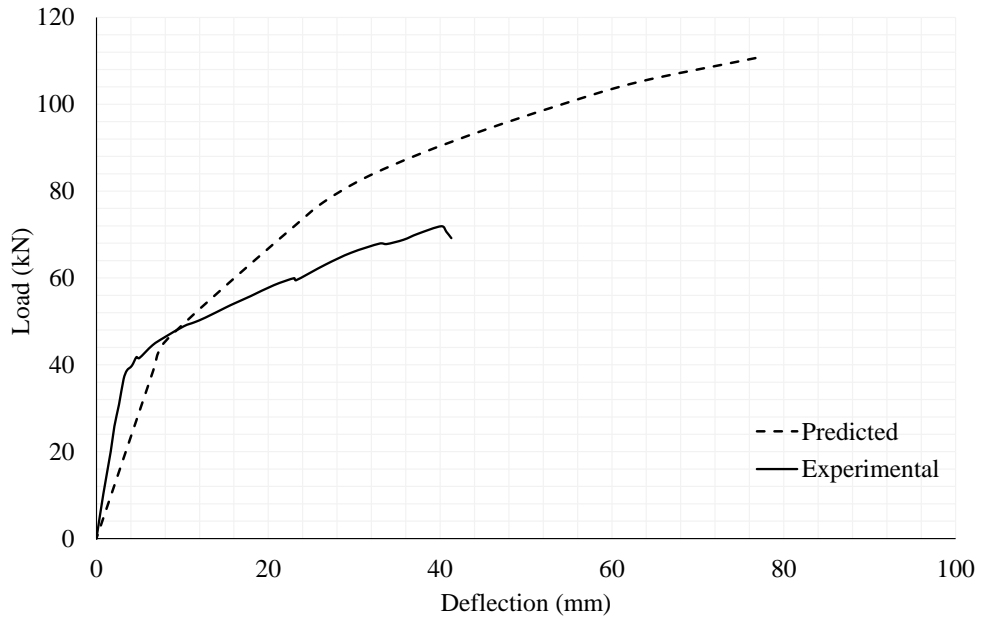


Figure 5.7: Predicted and experimental load vs deflection - I-S-150-7.5-NSM-0.36-0.564

Load vs Deflection – (I-S-150-7.5-NSM-0.36-0.94)

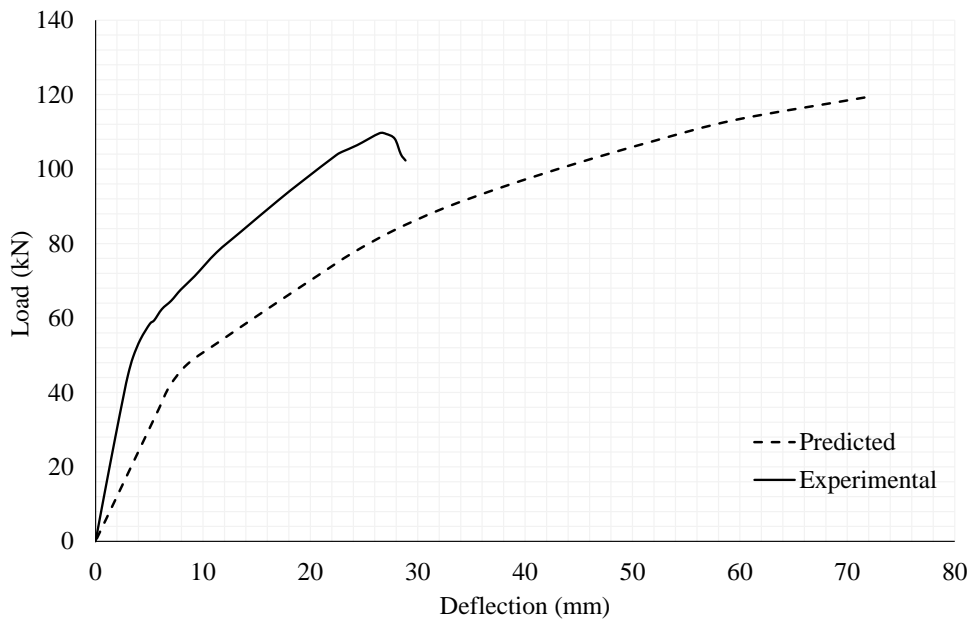


Figure 5.8: Predicted and experimental load vs deflection - I-S-150-7.5-NSM-0.36-0.94

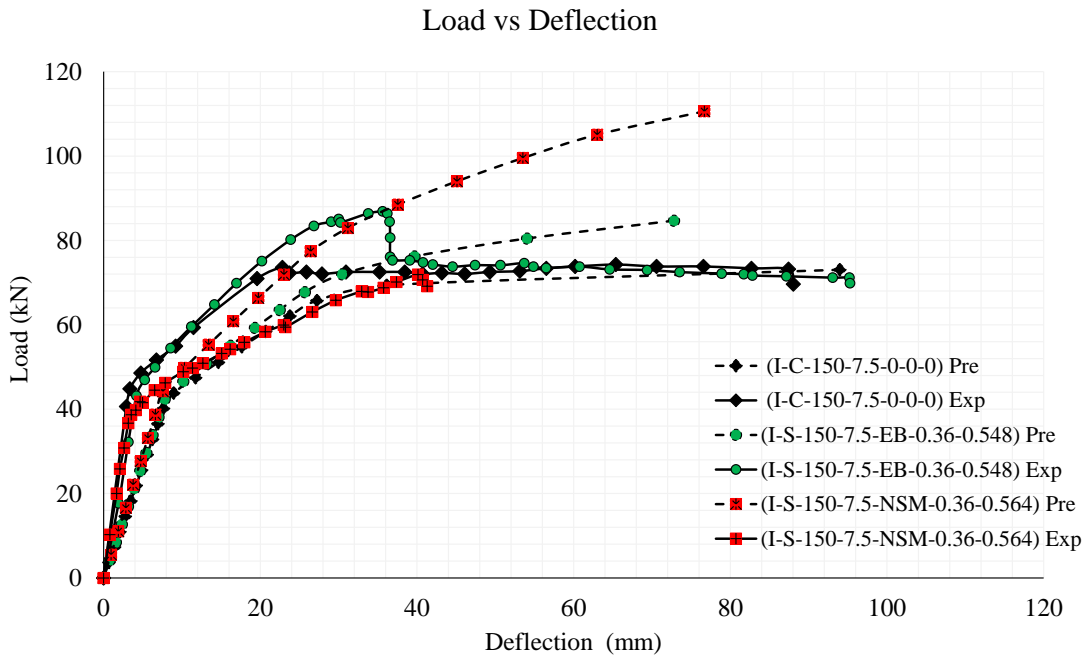


Figure 5.9: Predicted and experimental load vs deflection for slabs having same strengthening ratio

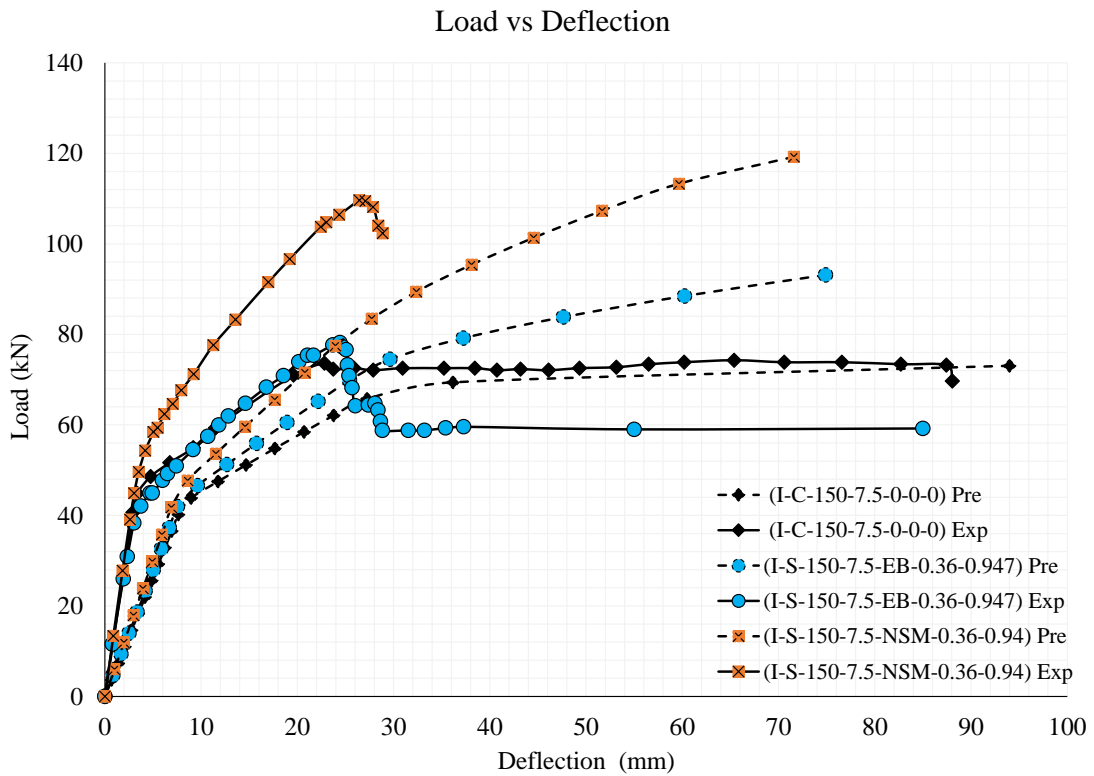


Figure 5.10: Predicted and experimental load vs deflection for slabs having same strengthening ratio

5.3 Finite Element Study

Finite element modelling (FEM) is a utilitarian and economic tool to study the complex behaviour of structural elements such as flexure-shear resistance of PPHC slabs. As a result, this part of the research program was dedicated to the nonlinear analysis using three-dimensional FEM to simulate the laboratory tests. The finite element software package ABAQUS 6.13 Simulia, was used in this study. Using the provided structural features in that package, a model for PHC slabs was constructed and used to analyse the behaviour. This chapter presents details of procedures followed in constructing the FEM model. This includes discussion of type of elements used for simulation of different components of the PHC slabs, constitutive model for each element, meshing, boundary conditions, steps in analysis and how the solution was controlled. Finally, the model was verified against the experimental test results.

5.3.1 Material Properties and Element Type

Concrete

Complex material properties of concrete pose a challenge for computer simulations in the field of concrete structures. As opposed to steel, concrete when subjected to compression exhibits nonlinearity very early. The two main concrete failure mechanisms are cracking under tension and crushing under compression. Concrete Damaged Plasticity Model was used to represent high strength concrete in this study. Young's Modulus of 28542.46071 MPa and poisson's ratio of 0.2 were used. The CDP (Concrete Damaged Plasticity) model used in the ABAQUS software is a modification of the Drucker-Prager strength hypothesis. The unquestionable advantage of the CDP model is the fact that it is based on parameters having an explicit physical interpretation. The exact role of the above parameters and the mathematical methods used to describe the development of the boundary surface in the three-dimensional space of stresses are explained in the ABAQUS user's manual. In CDP model, other parameters describing the performance of concrete are determined for uniaxial stress, where as model's parameters characterizing its performance under compound stress was taken from the literature [31] as shown in Table 5.2. The concrete damaged plasticity (CDP) model uses stress/strain relationships to correlate parameters for relative concrete damage for both tension and compression. In a simple plasticity model after yielding has occurred, if force is removed, the residual plastic strain is found by a rebound function of the modulus of elasticity. Damage parameters of the CDP model modify this rebound function to include damage effects. The CDP

model also accounts for cyclic loading effects where a recovery factor can be specified to account for the amount of total inverse loading strength available after damage has occurred.

Table 5.2: Default parameters of CDP model under compound stress

Parameter	Value
Dilation angle	36.31
eccentricity	0.1
fb0/fc0	1.16
k	0.67
viscosity parameter	0

5.3.1.1 Stress-strain curve for uniaxial compression

The stress-strain relation for a given concrete can be most accurately described on the basis of uniaxial compression tests carried out in laboratory. Thorenfeldt's stress-strain model was used to generate the uniaxial stress-strain relationship for high strength concrete in this study, seen in Fig. 5.11 . Deducting the elastic part ε_c^{el} from the total strains ε_c thereby inelastic strains ε_c^{in} are obtained, as shown in Eq 5.17 . Corresponding definitions of useful variables are shown in Fig 5.14.

$$\varepsilon_c^{in} = \varepsilon_c - \varepsilon_c^{el} \quad (5.17)$$

$$\varepsilon_c^{el} = \frac{\sigma_c}{E_0}$$

The Inputed Compression stress-strain curve and the corresponding damage curve are presented Table 5.3. Compression damage parameter can be calculated using Eq. 5.18.

$$d_c = \frac{\sigma_{cu} - \sigma_c}{\sigma_{cu}} \quad (5.18)$$

5.3.1.2 Stress-strain curve for uniaxial tension

The tensile strength of concrete under uniaxial stress is difficult to obtain from direct tension test, thereby indirect methods such as splitting or beam bending test are used. Since tension stiffening may considerably affect the results of the analysis, uniaxial tension stress-strain curve data for high strength concrete was generated using reliable equations proposed by Wang and Hsu [32] can be seen Fig 5.12. Selim Pul [33] conducted experimental investigation on tensile behaviour of high strength concrete. In his study, the uniaxial tensile, split tensile and flexural tensile tests were conducted and the relationships between the respective tensile strengths were

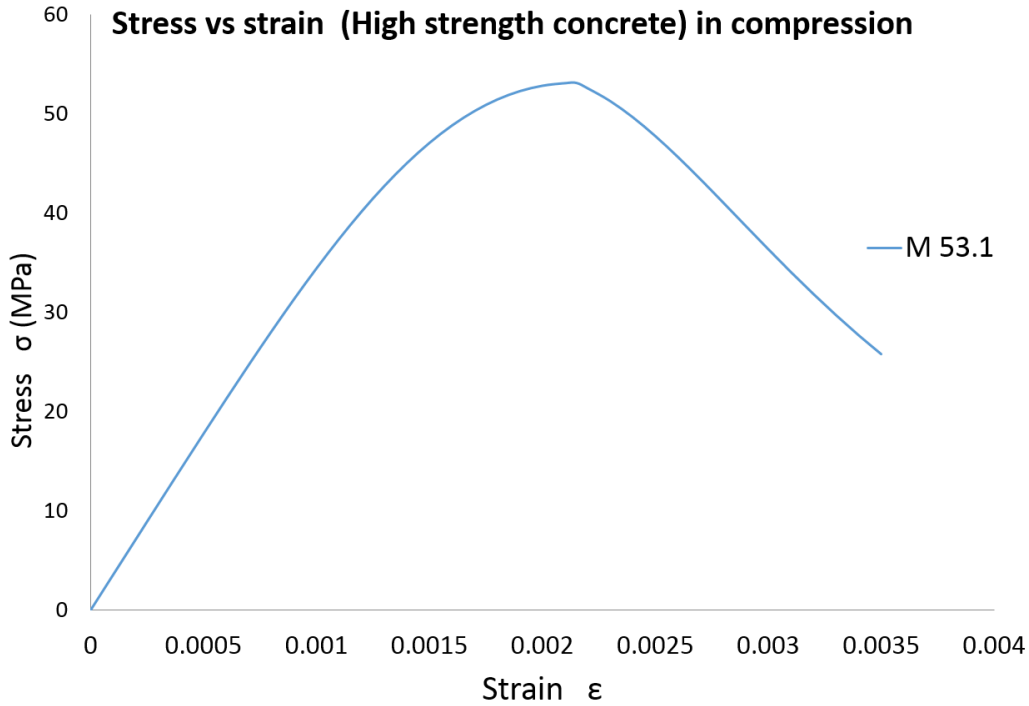


Figure 5.11: Compression Stress-Strain curve - M 53.1 Grade

proposed. Uniaxial tensile strength as a function of 28days concrete compressive strength was proposed [33] as seen from Eq. 5.19.

$$f_t = 0.026f_c^{1.223} \quad (5.19)$$

5.3.1.3 Element Type

The concrete was simulated using an element type called C3D8R: An Continuum stress/displacement, three dimensional, 8-node linear brick, reduced integration, hour-glass control. It is a three dimensional solid element that is capable of taking into account the nonlinear elasto-plastic characteristics of concrete. This element can be composed of a single homogeneous material or, in Abaqus/Standard, can include several layers of different materials for the analysis of laminated composite solids. The solid (or continuum) brick elements in Abaqus can be used for linear analysis and for complex nonlinear analyses involving contact, plasticity, and large deformations. They are available for stress, heat transfer, acoustic, coupled thermal-stress, coupled pore fluid-stress, piezoelectric, and coupled thermal-electrical analyses. The geometry of the element is defined by eight corner nodes with three translational degrees of freedom (UX, UY, and UZ) at each node as shown in Fig 5.15.

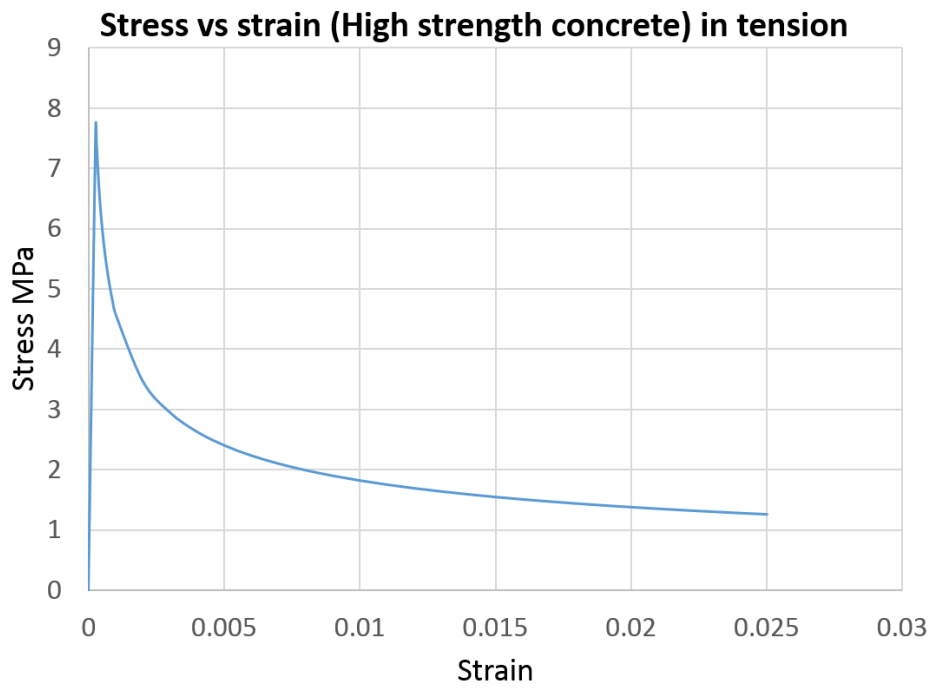


Figure 5.12: Definition - Inelastic, Elastic strains

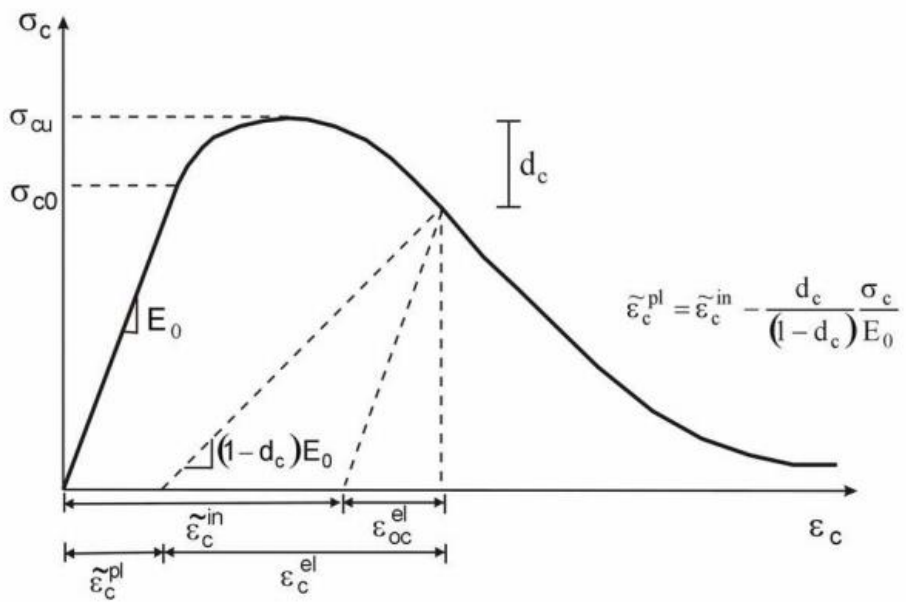


Figure 5.13: Definition - Inelastic, Elastic strains

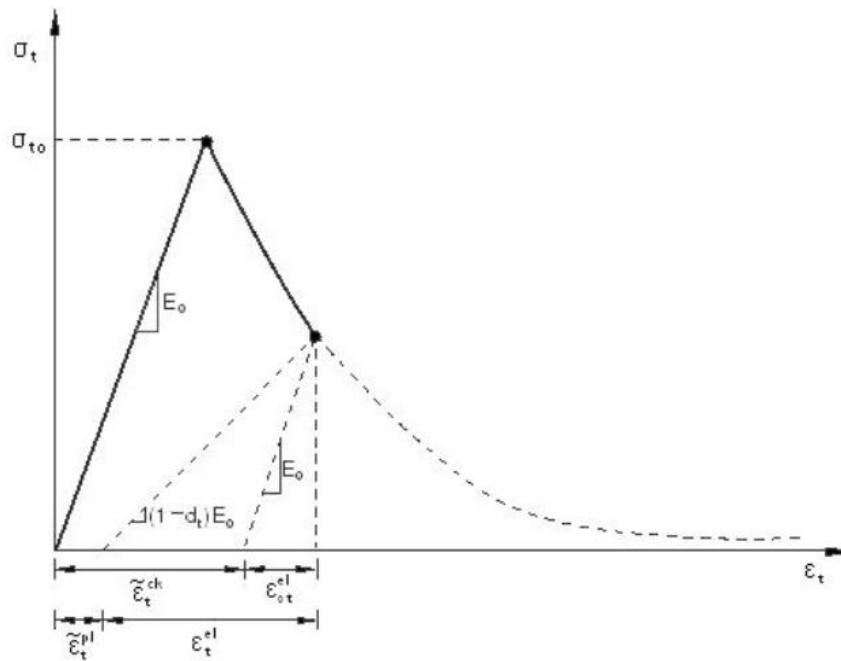
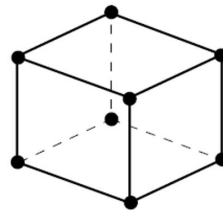
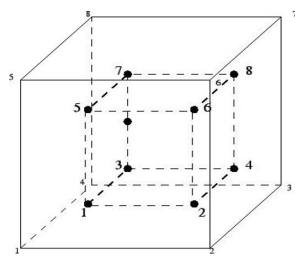


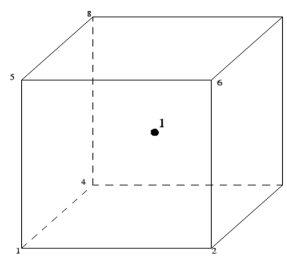
Figure 5.14: Definition - Cracking, Elastic strains



(a) Linear element
(8-node brick, C3D8)



(b) Full Integration



(b) Reduced Integration

Figure 5.15: Element C3D8 - Abaqus 6.13

Table 5.3: Concrete Compression damage

Yield stress	Inelastic strain	Damage parameter	Inelastic strain
0	0	0	0
8.556599126	0	0	0
11.39607121	7.327E-07	0	7.327E-07
17.00821158	4.10843E-06	0	4.10843E-06
22.43827523	1.38633E-05	0	1.38633E-05
27.53637074	3.52489E-05	0	3.52489E-05
32.12267895	7.45652E-05	0	7.45652E-05
36.01287302	0.00013827	0	0.00013827
39.05033558	0.000231851	0	0.000231851
41.13663891	0.000358756	0	0.000358756
42.25055203	0.00051973	0	0.00051973
42.45806113	0.00061246	0	0.00061246
42.47979332	0.000661698	3.34532E-16	0.000661698
42.04851027	0.000726809	0.010152664	0.000726809
41.01643587	0.000862968	0.034448318	0.000862968
39.71418722	0.001008593	0.065104039	0.001008593
38.19357084	0.001161868	0.100900267	0.001161868
36.50806648	0.001320921	0.140578058	0.001320921
34.7095052	0.001483934	0.182917277	0.001483934
32.84548959	0.001649241	0.226797331	0.001649241
30.95768246	0.001815381	0.271237451	0.001815381
29.08093276	0.001981134	0.315417273	0.001981134
27.24310364	0.002145524	0.358680881	0.002145524
25.46541898	0.002307806	0.400528652	0.002307806
23.76314212	0.002467446	0.440601277	0.002467446
22.14642572	0.002624088	0.478659758	0.002624088
20.62120985	0.002777525	0.514564261	0.002777525

Table 5.4: Concrete tension damage

Yield stress	Cracking strain	Damage parameter	Cracking strain
7.731312769	0	0	0
7.421803871	4.00E-05	0.040033162	4.00E-05
6.615062912	0.000168238	0.144380378	0.000168238
5.624675541	0.000402937	0.27248118	0.000402937
5.013280222	0.000624357	0.351561582	0.000624357
4.585196744	0.000839355	0.406931671	0.000839355
3.474929333	0.001878254	0.550538254	0.001878254
2.633503979	0.003907734	0.659371693	0.003907734
2.408629348	0.004915612	0.688457909	0.004915612
2.105323118	0.006926239	0.727688792	0.006926239
1.995822804	0.007930075	0.741852016	0.007930075
1.825399702	0.009936046	0.763895246	0.009936046
1.697014202	0.011940544	0.780501158	0.011940544
1.595536564	0.0139441	0.793626696	0.0139441
1.512550844	0.015947007	0.804360412	0.015947007
1.442942328	0.017949446	0.813363866	0.017949446
1.383394285	0.019951532	0.821066056	0.019951532
1.33164635	0.021953345	0.827759348	0.021953345
1.28609627	0.023954941	0.833650984	0.023954941
1.26526639	0.024955671	0.836345207	0.024955671

Internal Reinforcement - Prestressing strands

5.3.1.4 Material Properties

linear isotropic material properties include Young's Modulus of 196500 MPa and poisson's ratio of 0.3 for prestressing strands. The prestressing strands do not have identifiable yielding point like in case of regular mild steel and no strain hardening exist before rupture. Accurate representation of stress-strain response of prestressing strand can be obtained using the Ramberg -Osgood Model as shown in Fig 5.16.

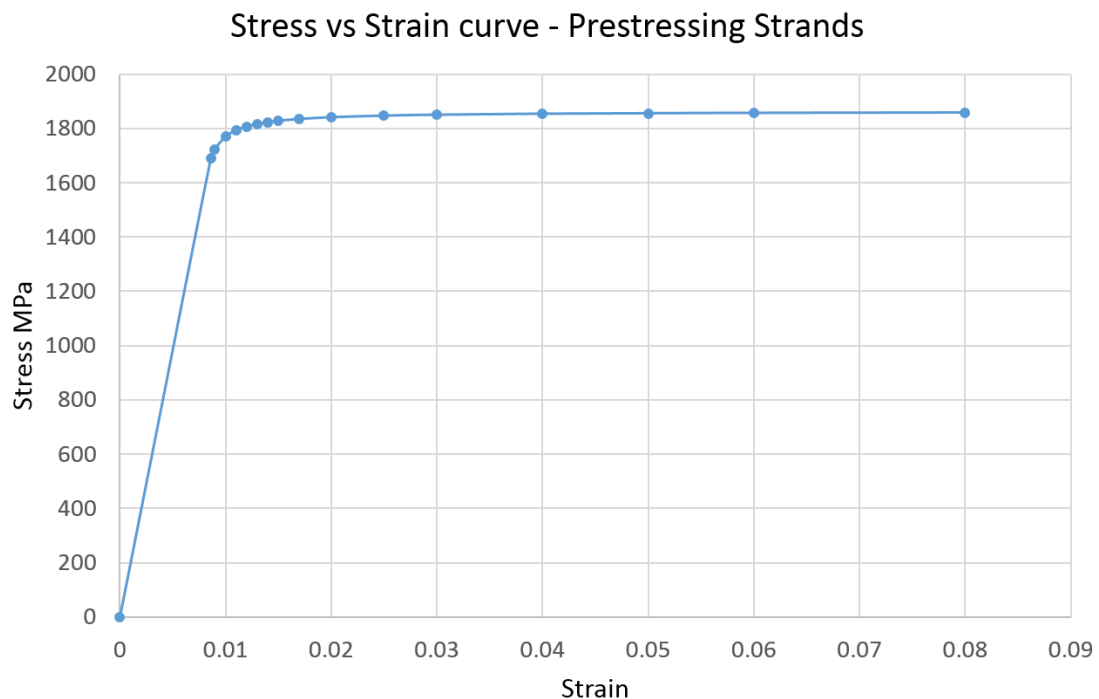


Figure 5.16: Stress-Strain Curve - Prestressing Steel

5.3.1.5 Element type

The prestressing strands of the PHC slabs were modeled using an element type called T3D2: A 2-node linear 3-D truss. This is a 3-D truss element that is capable of resisting axial compression and tension forces but not moment. It has characteristics of plasticity, large deflection, and large strain deformations.

5.3.1.6 Initial Stress State

The most utilitarian feature of the T3D2 element with respect to PPHC slabs was the initial stress state capability that could be specified by the user to simulate the prestressing force. This was accomplished by the using *Initial Condition, name=stress. The stress had to be specified in the direction of the local axis that extends along length of the element; that is, in x-direction. A initial stress of 875.84 MPa and 972.64 MPa was given as input for bottom and top prestressing strands respectively. This stress was transferred to the surrounding concrete elements by the end of first analysis step.

5.3.1.7 Steel Bearing Plates

Loading and support plates were modeled using C3D8R: An Continuum stress/displacement,three dimensional, 8-node linear brick, reduced integration. Linear-elastic material properties were given, requiring modulus of elasticity and Poisson's ratio, which were inputted as 200 GPa and 0.3, respectively.

5.3.2 Interactions

For Internal reinforcement(Prestressing strands) "Embedded region" constraint was defined, to describe the perfect bond between concrete and prestressing strands. An embedded region constraint allows you to embed a region of the model within a "host" region of the model or within the whole model, in this scenario host is concrete. Abaqus searches for the geometric relationships between nodes of the embedded elements and the host elements. If a node of an embedded element lies within a host element, the translational degrees of freedom at the node are eliminated and the node becomes an "embedded node." The translational degrees of freedom of the embedded node are constrained to the interpolated values of the corresponding degrees of freedom of the host element.

A surface-based tie constraint was used to define the interaction between the steel bearing plates and concrete. A surface-based tie constraint can be used to make the translational and rotational motion as well as all other active degrees of freedom equal for a pair of surfaces. Abaqus uses the undeformed configuration of the model to determine which slave nodes are tied to the master surface. By default, all slave nodes that lie within a given distance of the master surface are tied. The default distance is based on the typical element size of the master surface. A rigid body constraint was used for steel bearing plates which allows us to constrain the motion of regions of the assembly to the motion of a reference point. Further two concentrated loads were applied at the respective reference points on two steel loading plates as shown in

Fig 5.18. The relative positions of the regions that are part of the rigid body remain constant throughout the analysis.

5.3.3 Geometry and Boundary Conditions

Cross section of the test specimen was exactly reproduced for simulation as shown in Fig 5.17. Cross section of the model was bedded on X-Y plane and Z-axis was set along longitudinal direction of the slab. Isometric view of whole assembly including hollow core slab, steel bearing plates, embedded prestressing strands with respective interactions in place can be viewed from Fig 5.18. Meshed assembly is displayed in Fig 5.19 below.

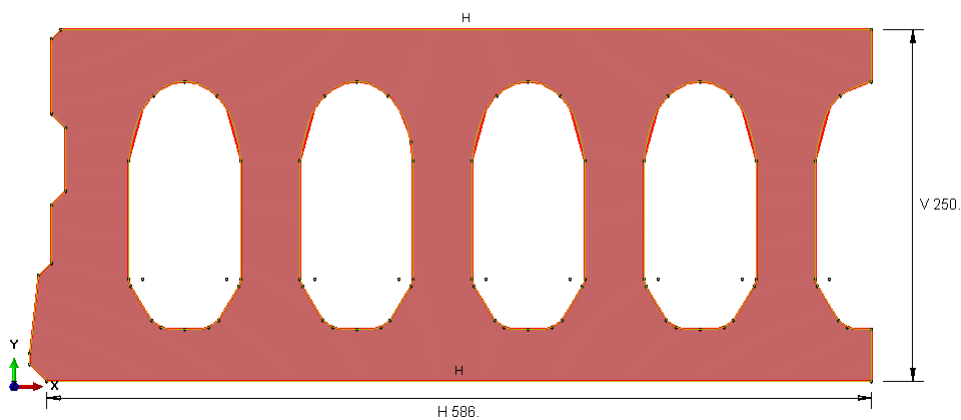


Figure 5.17: Modelled Cross section - II-C-250-5.4-0-0-0 (control)

5.3.4 Type of Analysis

The nonlinear multi-step analysis was performed in this study. The intent of the first loading step was to transfer the prestressing effect from the stressed strands to the surrounding concrete section, following the actual fabrication sequence of PPHC slab. This first loading step eventually causes the camber along length of the slab. In fact, all results obtained from the first load step were not required for the analysis and were offset from final results. The next second step involved application of two equal displacements on steel loading plate at the respective reference points to represent the experimental displacement control mode. Dynamic Explicit analysis with semi-automatic mass scaling was used in both the steps. Explicit dynamic scheme is a mathematical technique for integrating the equations of motion through time. Unknown values are obtained from information already known. A bounded solution is obtained only when the time increment is less than the stable time incre-

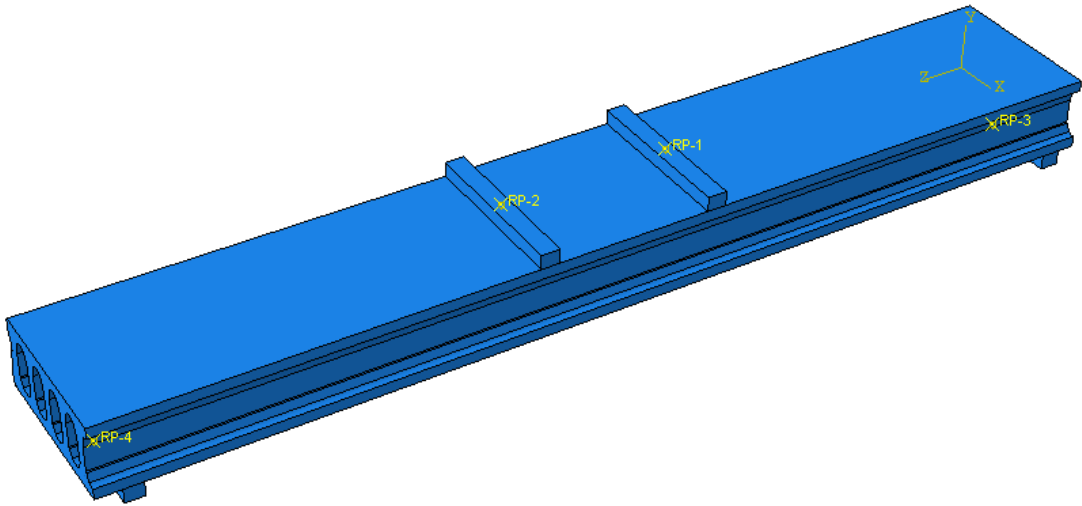


Figure 5.18: Isometric View of Assembly

ment. Quasi-static analysis can be achieved by using mass scaling which involves, artificially increasing the mass to a small degree, which increases the stable time increment, eventually increases the speed of the simulation.

5.3.5 Verification of the Model

The FEM which has been introduced with details in the previous sections was proved to simulate flexure, flexure-shear behaviour of PPHC slabs in this section by comparing the results obtained from the model against physical experimental results of chapter 4. The aim was to ensure that the elements, material models, constants, convergence criteria etc. utilized in the developed model were all suitable to simulate the subject matter of this study. Model showed reasonable consistency in simulating the flexure, flexure-shear behaviour of tested slab.

5.3.5.1 Control slab - II-C-250-5.4-0-0-0

Comparison of load-displacement curve obtained from FEM and experimental test is done to evaluate the FEM model. 28-days stress-strain curve (Fig 5.11) has been adopted for the non-linear FEM analysis. By comparing the experimental and finite element model load displacement curves respectively, following issues were noted: FEM is over predicting the pre-cracking stiffness and cracking load. Overall load-displacement curve is overpredicted by FEM model, as the early age concrete stress-strain curve has not been taken into consideration when the prestress release from the prestressed strands to the concrete takes place. FEM model underpredicts the

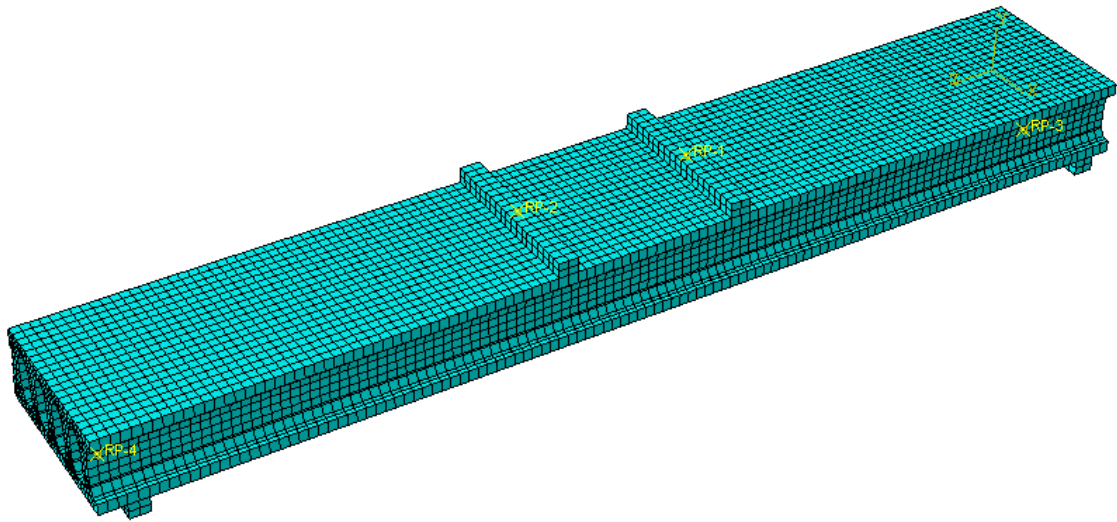


Figure 5.19: Isometric View of Meshed Assembly

displacements at peak and ultimate as shown in Fig 5.20. Ultimate failure mode for FEM model is same as experimental test i.e Flexure-shear failure, which is displayed in th Fig 5.21.

Excellent correlation with experimental failure modes including similar compression damage, tension damage and ultimate failure mode was observed. Though FEM study was carried out only for control specimen, author believes that there is a need for calibration of the model, which would be considered in future work progress.

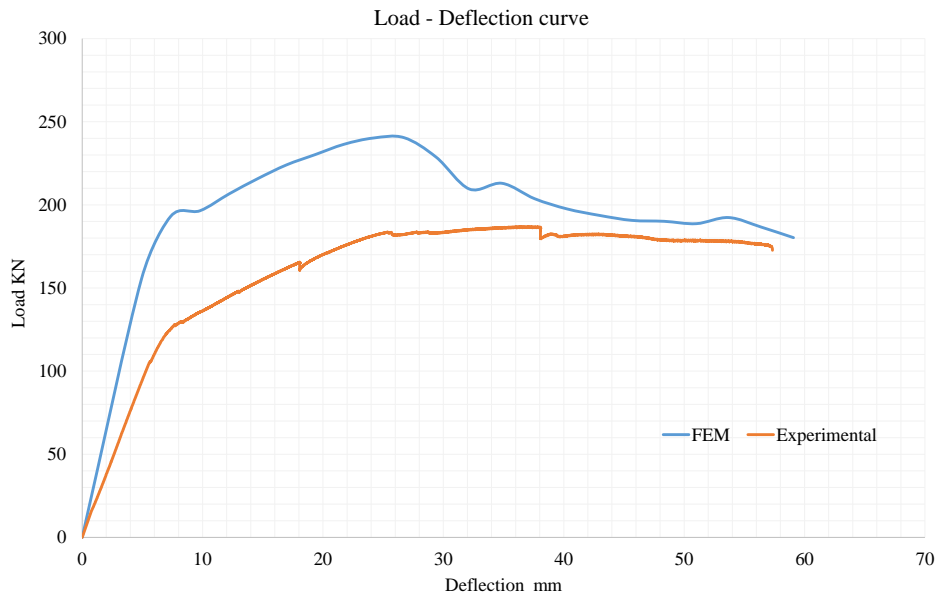


Figure 5.20: Load vs displacement (Experimental vs FEM) - C-250-5.4

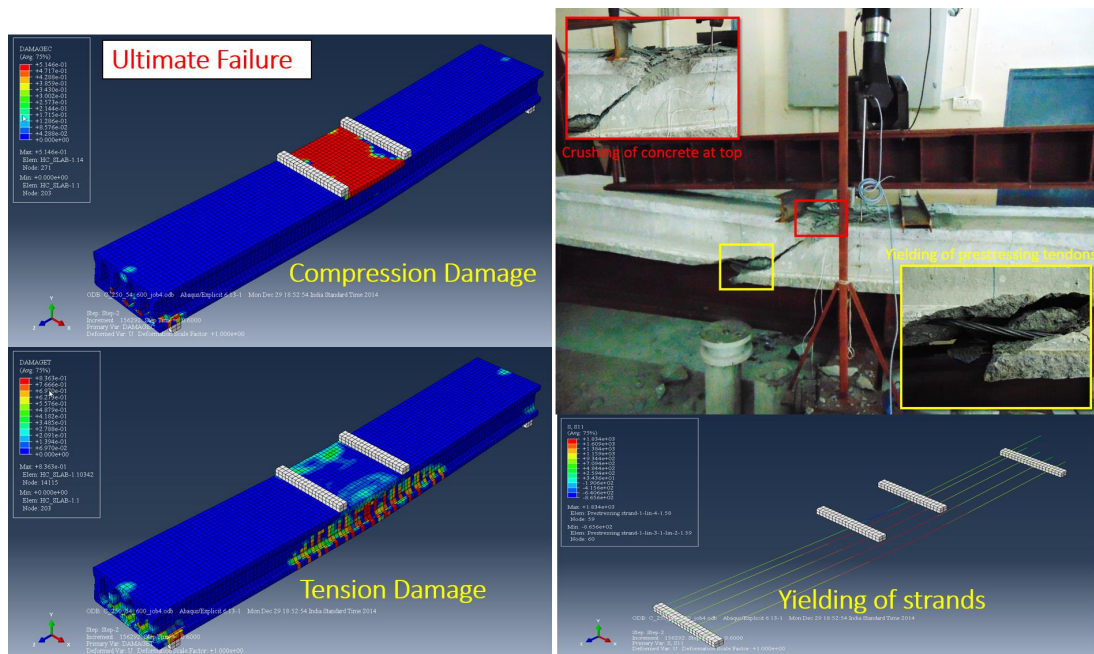


Figure 5.21: Ultimate Failure and Damage - II-C-250-5.4-0-0-0

Chapter 6

Conclusions

This research focuses on several significant strengthening concepts and failure modes of the strengthened PPHC slabs. Nine full scale slab specimens were tested to failure under a four point bending configuration. Details of test specimen are mentioned in chapter 3 of this study. The research program was primarily focused on investigating the concepts like flexure, flexure-shear behaviour of control and FRP strengthened specimens, efficiency of various FRP strengthening configurations, comparison of experimental test results with analytical predictions, finite element study, validation of FEM model.

6.0.6 Summary of key findings - Series I

Capacity and Mode of Failure

- The use of EB GFRP strengthening technique effectively enhanced the capacity of PPHC slabs by as much as 17.4%. This improvement in ultimate capacity lessened with increasing reinforcement ratio as premature debonding may govern the failure.
- As EB FRP strengthening ratio is increased, unfavourable debonding of laminates may occur which can be prevented through conscientious design of the system in terms of flexural strengthening limits.
- Having identical strengthening reinforcement ratio, the use of NSM GFRP strengthening technique showed highest enhancement in capacity of PPHC slabs by as much as 47.7%. when compared to EB GFRP technique.
- NSM technique resulted in optimum bond strength than EB technique revealing full composite action between the NSM GFRP bars and concrete.
- Increasing the strengthening reinforcement ratio can change the mode of failure form a ductile response to less ductile response.

Load-Strain Relationships

- The EB and NSM technique accommodated for the load-sharing mechanism between the internal prestressing reinforcement and FRP reinforcement thereby contributing towards load enhancement.
- In accordance with ACI 440.2R-05, all of the strengthened slabs showed service load enhancement from which having NSM technique demonstrated highest improvement in service load by as much as 49.1% making the NSM technique more attractive in serviceability governed applications.
- All of the strengthened showed service load greater than the experimental cracking load.

- By FRP strengthening, yielding can be delayed due to the reserve stiffness of the internal steel reinforcement due to load carrying contribution of FRP. Overall strengthened specimens experienced a noticeable enhancement in post-cracking stiffness, and correspondingly a significant increase in their respective yield loads.

Load-Deflection Relationships

- Strengthening of PPHC slabs with EB GFRP strips and NSM GFRP bars improved the overall load deflection response.
- FRP strengthening (EB & NSM) had very less effect on pre-cracking stiffness and cracking load when compared to control specimen.
- Pre-cracking stiffness for all the control and strengthened specimens was almost same. Different strengthening techniques demonstrated substantial influence on the slabs post-cracking response until the failure.
- Strengthening by EB GFRP strips showed decrease in ultimate deformability which is much pronounced in NSM GFRP bar strengthening technique indicating that, EB technique is much better in terms of overall ductility.
- In NSM FRP strengthened PPHC slabs, post-cracking response exhibited the highest stiffness improvement among all the tested slabs, despite its flexural-shear failure mode. This signifies that the extremely advantageous effect of increasing the NSM GFRP area when good bond is secured, should always be directed by flexural strengthening limits considerations precluding any abrupt changes in the failure mode.
- NSM strengthening technique using GFRP bars is more effective in strength governed applications than the EB GFRP laminates.

Cracking Behaviour

- Greater number of cracks developed for the slabs strengthened with EB GFRP strips and NSM GFRP bars irrespective of strengthening ratios used.
- Along the constant moment region, larger cracks were evenly spaced. crack widths decreased while the number of cracks increased for all the strengthened specimens. These cracks were not limited only to constant moment zone but also developed along the shear span.
- At certain load level, existing flexural cracks turned into flexure-shear cracks along the shear span of all the strengthened specimens.
- NSM FRP strengthened specimens exhibited high level of flexural cracking, indicating that the flexural strengthening limit was marginally violated.

6.0.7 Summary of key findings - Series II

Capacity and Mode of Failure

- The use of EB GFRP strengthening technique effectively enhanced the flexure-shear capacity of PPHC slabs by as much as 25.3% without any compromise in deflection ductility.
- As EB FRP strengthening ratio is increased, unfavourable debonding of laminates may occur which can be prevented through conscientious design of the system in terms of flexural strengthening limits.
- NSM technique resulted in optimum bond strength than EB technique revealing full composite action between the NSM GFRP bars and concrete.
- Increasing the strengthening reinforcement ratio can change the mode of failure from a ductile response to less ductile response.
- Shear strengthening with U-wrap layers acted as an anchorage and prevented premature debonding failure mode.

Load-Deflection Relationships

- Strengthening of PPHC slabs with EB GFRP strips and NSM GFRP bars improved the overall load deflection response.
- Prior to cracking the load-deflection behaviour of unstrengthened and strengthened specimens was near identical. In case of EB FRP specimens, addition of thin EB FRP laminates slightly increased the section moment of inertia thereby cracking load was marginally increased. In case of NSM FRP specimens cracking loads slightly decreased to accommodate the redistribution of stresses caused by removing the concrete material during grooving.
- Pre-cracking stiffness for all the control and strengthened specimens was almost same. Different strengthening techniques demonstrated substantial influence on the slabs post-cracking response until the failure.
- By FRP strengthening, yielding can be delayed due to the reserve stiffness of the internal steel reinforcement due to load carrying contribution of FRP. Overall strengthened specimens experienced a noticeable enhancement in post-cracking stiffness, and correspondingly a significant increase in their respective yield loads.
- Strengthening by EB GFRP strips showed decrease in ultimate deformability which is much pronounced in NSM GFRP bar strengthening technique indicating that, EB technique is much better in terms of overall ductility.
- Addition of flexural laminates increased the deflection ductility for lower strengthening ratios as their failure modes were not significantly altered.
- Flexural GFRP strengthening (high ratio) effectively enhanced the capacity up to 26%. Post-cracking stiffness also increased significantly due to the beneficial effect of anchorage effect provided by U-wrapping.
- Low FRP ratio resulted in earlier debonding followed by rupture of FRP sheet and did not produce significant increase in the ultimate capacity. Marginal im-

provement in post-cracking stiffness was observed. However, it degraded to the stiffness of control slab after rupture of FRP sheets.

- High FRP ratio resulted in good improvement in ultimate strength, post-cracking stiffness. However, there was decrease in displacement at failure indicating reduction in ductility due to FRP strengthening.
- In high shear conditions, shear strengthening improved the deflection ductility of PPHC slabs
- NSM strengthening changed the failure from flexure dominant to more shear dominant behaviour. Due to change in the failure mode, NSM slabs failed in a brittle manner leading to no increase in strength. Future work should focus on improving the efficiency of NSM strengthening on behaviour of hollow core slabs at low a/d ratios.
- For lower a/d ratio (shear dominant), EB GFRP strengthening in terms of flexure and shear strengthening increased the capacity of PPHC slabs as well as improved the deflection ductility making it more attractive for strength and seismic governed applications

Cracking Behaviour

- Greater number of cracks developed for the slabs strengthened with EB GFRP strips and NSM GFRP bars irrespective of strengthening ratios used.
- Along the constant moment region, larger cracks were evenly spaced. crack widths decreased while the number of cracks increased for all the strengthened specimens. These cracks were not limited only to constant moment zone but also developed along the shear span.
- At certain load level, existing flexural cracks turned into flexure-shear cracks along the shear span of all the strengthened specimens.

- GFRP strengthening by EB strips and NSM bars resulted in uniform distribution of cracks relative to control PHC slab which failed by few major cracks.
- EB GFRP strengthened specimens exhibited high level of flexural cracking, making the ultimate flexure shear failure mode more ductile.

6.0.8 Concluding Remarks

Capacity and Mode of Failure

- For higher a/d ratio (flexure dominant), having identical strengthening reinforcement ratio, the use of NSM GFRP strengthening technique showed highest enhancement in capacity of PPHC slabs by as much as 47.7% when compared to EB GFRP technique.
- For lower a/d ratio (shear dominant), the use of EB GFRP strengthening technique effectively enhanced the flexure-shear capacity of PPHC slabs by as much as 25.3% without any compromise in deflection ductility.
- NSM technique resulted in optimum bond strength than EB technique revealing full composite action between the NSM GFRP bars and concrete.
- Increasing the strengthening reinforcement ratio can change the mode of failure from a ductile response to less ductile response.

Load Deflection Relationships

- Strengthening of PPHC slabs with EB GFRP strips and NSM GFRP bars improved the overall load deflection response.
- FRP strengthening (EB & NSM) had very less effect on pre-cracking stiffness and cracking load when compared to control specimen.
- For higher a/d ratio (flexure dominant) NSM strengthening showed highest post-cracking stiffness than EB technique, due to good bond which raises the impor-

tance of flexure Strengthening limit considerations.

- For Lower a/d ratio (shear dominant) EB strengthening showed highest post-cracking stiffness than NSM technique, due to Anchorage effect by shear strengthening by which good bond was observed.
- For higher a/d ratio (flexure dominant) NSM strengthening using GFRP bars is more effective in strength governed applications than EB GFRP strips.
- For lower a/d ratio (shear dominant), EB GFRP strengthening in terms of flexure and shear strengthening increased the capacity of PPHC slabs as well as improved the deflection ductility making it more attractive for strength governed applications.

Load-Strain Relationships

- In accordance with ACI 440.2R-05, (In Flexure dominant) among all, NSM slabs showed maximum service load enhancement, pointing that NSM technique can be more attractive for serviceability governed applications. (In Shear dominant) among all, EB slab (high ratio) showed maximum service load enhancement, indicating its use in serviceability governed applications.
- By FRP strengthening, yielding can be delayed due to the reserve stiffness of the internal steel reinforcement due to load carrying contribution of FRP.

Cracking Behaviour

- Greater number of cracks developed for the slabs strengthened with EB GFRP strips and NSM GFRP bars irrespective of strengthening ratios used.
- Crack widths decreased while the number of cracks increased for all the strengthened specimens.

- NSM FRP strengthened specimens exhibited high level of flexural cracking, indicating that the flexural strengthening limit was marginally violated.

Analytical Study

- Flexure dominant (Series I) – Very good correlation was observed between the analytical and experimental capacities and failure modes.
- Shear dominant (Series II) – Predicted failure modes matching with experimental but capacity significantly under-predicted.
- Indicating that the ACI code equations for shear, needs to be modified in order to predict the ultimate load capacity accurately.

FEM Study

- Failure progression and Failure mode is matching but over estimated capacity and stiffness.
- There is a need of further refinement, calibration and validation of model.

6.0.9 Further Work

- Experimental test NSM strengthened slabs again (I-S-150-7.5-NSM-0.36-0.564) & (II-S-250-5.4-NSM-0.372-0.62) for further verification.
- Experimentally evaluate the efficiency of EB anchorage system to prevent premature debonding.
- Calibration of FEM model and run parametric studies.

References

- [1] T. C. Triantafillou and N. Plevris. Strengthening of RC beams with epoxy-bonded fibre-composite materials. *Materials and Structures* 25, (1992) 201–211.
- [2] H. Rahimi and A. Hutchinson. Concrete beams strengthened with externally bonded FRP plates. *Journal of Composites for Construction* 5, (2001) 44–56.
- [3] A. Belarbi, S. Bae, D. Kuchma, A. Mirmiran, and A. Okeil. Design of FRP Systems for Strengthening Concrete Girders in Shear, NCHRP Report 678. *Transportation Research Board, Washington, DC* .
- [4] M. Murphy, A. Belarbi, and S.-W. Bae. Behavior of prestressed concrete I-girders strengthened in shear with externally bonded fiber-reinforced-polymer sheets. *PCI journal* 57, (2012) 63–82.
- [5] D. R. Buettner and R. J. Becker. PCI manual for the design of hollow core slabs. Prestressed Concrete Institute, 1985.
- [6] L. Yang. Design of prestressed hollow core slabs with reference to web shear failure. *Journal of Structural Engineering* 120, (1994) 2675–2696.
- [7] ACI-440.2R-08. Guide for the Design and Construction of Externally Bonded FRP Systems for Strengthening Concrete Structures 2008.
- [8] J. G. MacGregor, J. K. Wight, S. Teng, and P. Irawan. Reinforced concrete: mechanics and design, volume 3. Prentice Hall Upper Saddle River, NJ, 1997.
- [9] O. A. Rosenboom. Behavior of FRP repair/strengthening systems for prestressed concrete. Ph.D. thesis 2006.
- [10] M. P. Collins and D. Mitchell. Prestressed concrete structures. Response Publications, 1997.
- [11] ACI. Building code requirements for structural concrete (ACI 318-05) and commentary (ACI 318R-05) 2005.

- [12] M. Pajari. Design of prestressed hollow core slabs. Technical Research Centre of Finland, 1989.
- [13] C. Bakis, L. C. Bank, V. Brown, E. Cosenza, J. Davalos, J. Lesko, A. Machida, S. Rizkalla, and T. Triantafillou. Fiber-reinforced polymer composites for construction-state-of-the-art review. *Journal of Composites for Construction* 6, (2002) 73–87.
- [14] H. V. GangaRao, N. Taly, and P. Vijay. Reinforced concrete design with FRP composites. CRC press, 2006.
- [15] L. De Lorenzis and J. Teng. Near-surface mounted FRP reinforcement: An emerging technique for strengthening structures. *Composites Part B: Engineering* 38, (2007) 119–143.
- [16] H. V. GangaRao and P. Vijay. Bending behavior of concrete beams wrapped with carbon fabric. *Journal of Structural Engineering* 124, (1998) 3–10.
- [17] N. Attari, S. Amziane, and M. Chemrouk. Flexural strengthening of concrete beams using CFRP, GFRP and hybrid FRP sheets. *Construction and Building Materials* 37, (2012) 746–757.
- [18] U. Ebead and H. Marzouk. Fiber-reinforced polymer strengthening of two-way slabs. *ACI Structural Journal* 101.
- [19] O. Chaallal, M. Shahawy, and M. Hassan. Performance of reinforced concrete T-girders strengthened in shear with carbon fiber-reinforced polymer fabric. *ACI Structural Journal* 99.
- [20] M. I. Ary and T. H.-K. Kang. Shear-strengthening of reinforced & prestressed concrete beams using FRP: Part I—Review of previous research. *International Journal of Concrete Structures and Materials* 6, (2012) 41–47.
- [21] T. H.-K. Kang and M. I. Ary. Shear-strengthening of reinforced & prestressed concrete beams using FRP: Part II—Experimental investigation. *International Journal of Concrete Structures and Materials* 6, (2012) 49–57.
- [22] R. El-Hacha and S. H. Rizkalla. Near-surface-mounted fiber-reinforced polymer reinforcements for flexural strengthening of concrete structures. *ACI Structural Journal* 101.
- [23] T. Hassan and S. Rizkalla. Flexural strengthening of prestressed bridge slabs with FRP systems. *PCI journal* 47, (2002) 76–93.

- [24] L. De Lorenzis, A. Nanni, and A. La Tegola. Strengthening of reinforced concrete structures with near surface mounted FRP rods. In *International Meeting on Composite Materials, PLAST 2000, Proceedings, Advancing with Composites*. 2000 9–11.
- [25] D. Lee and L. Cheng. Assessing the strengthening effect of various near-surface-mounted FRP reinforcements on concrete bridge slab overhangs. *Journal of Composites for Construction* 15, (2010) 615–624.
- [26] L. De Lorenzis and A. Nanni. Shear strengthening of reinforced concrete beams with near-surface mounted fiber-reinforced polymer rods. *ACI Structural Journal* 98.
- [27] S. Dias and J. Barros. Shear strengthening of RC T-section beams with low strength concrete using NSM CFRP laminates. *Cement and Concrete Composites* 33, (2011) 334–345.
- [28] T. K. Hassan and S. H. Rizkalla. Bond mechanism of near-surface-mounted fiber-reinforced polymer bars for flexural strengthening of concrete structures. *ACI Structural Journal* 101.
- [29] D. Lee, L. Cheng, and J. Yan-Gee Hui. Bond characteristics of various NSM FRP reinforcements in concrete. *Journal of Composites for Construction* 17, (2012) 117–129.
- [30] N. Wahab, K. A. Soudki, and T. Topper. Mechanism of bond behavior of concrete beams strengthened with near-surface-mounted CFRP rods. *Journal of Composites for Construction* 15, (2010) 85–92.
- [31] P. Kmiecik and M. Kamiński. Modelling of reinforced concrete structures and composite structures with concrete strength degradation taken into consideration. *Archives of civil and mechanical engineering* 11, (2011) 623–636.
- [32] T. Wang and T. T. Hsu. Nonlinear finite element analysis of concrete structures using new constitutive models. *Computers & Structures* 79, (2001) 2781–2791.
- [33] S. Pul. Experimental investigation of tensile behaviour of high strength concrete. *Indian Journal of Engineering and Materials Sciences* 15, (2008) 467.
- [34] R. Al-Rousan, M. Issa, and H. Shabila. Performance of reinforced concrete slabs strengthened with different types and configurations of CFRP. *Composites Part B: Engineering* 43, (2012) 510–521.

- [35] F. Elgabbas, A. El-Ghandour, A. Abdelrahman, and A. El-Dieb. Different CFRP strengthening techniques for prestressed hollow core concrete slabs: Experimental study and analytical investigation. *Composite Structures* 92, (2010) 401–411.
- [36] T. Y. Lin and N. H. Burns. Design of prestressed concrete structures. 1981.
- [37] S. Foubert. Flexural strengthening of prestressed hollow-core slabs using near-surface mounted (NSM) CFRP reinforcement. Ph.D. thesis, University of Manitoba 2014.
- [38] T. Jankowiak and T. Lodygowski. Identification of parameters of concrete damage plasticity constitutive model. *Foundations of civil and environmental engineering* 6, (2005) 53–69.